Università degli Studi di Padova

Facoltà di Ingegneria

Corso di Laurea in Ingegneria delle Telecomunicazioni

Tesi di Laurea Specialistica

Data decoding aided channel estimation techniques for OFDM systems in vehicular environment

Relatore: Ch.mo Prof. Silvano Pupolin

Correlatori: Massimiliano Siti, Antonio Assalini

Laureando: Andrea Agnoletto

Padova, 8 Marzo 2010

e-mail: andrea.agno@gmail.com

Prefazione

L'oggetto del presente lavoro di tesi è costituito dallo studio e sviluppo di algoritmi di inseguimento di canale per sistemi basati su una modulazione di tipo Orthogonal Frequency Division Multiplexing (OFDM), con riferimento allo standard IEEE802.11p per comunicazioni mobili di tipo Wireless Local Area Network (WLAN), tra veicolo e veicolo e tra veicolo e infrastruttura. La caratteristica principale dei sistemi wireless in ambiente veicolare è la presenza dell'effetto Doppler dovuto alla velocità relativa tra trasmettitore e ricevitore che rende il canale wireless tempo variante.

I primi capitoli della presente tesi sono dedicati all'analisi delle caratteristiche e della modellizzazione del canale wireless in ambiente veicolare, del sistema OFDM, dello standard IEEE 802.11p proposto per comunicazioni wireless in ambiente veicolare. I capitoli conclusivi invece presentano rispettivamente il lavoro compiuto riguardo alcune differenti opzioni di algoritmi di stima di canale per sistemi OFDM, e l'analisi e implementazione di tecniche di stima dell'effetto Doppler presente negli ambienti veicolari.

I due principali schemi di stima e inseguimento di canale investigati sono basati sull'utilizzo del decodificatore di Viterbi per ricostruire il simbolo OFDM ricevuto e utilizzarlo nella stima di canale. Il primo schema, di tipo iterativo, è più complesso dal punto di vista computazionale e implementativo rispetto a schemi di stima e inseguimento di canale che non utilizzano il decodificatore: per ogni simbolo OFDM ricevuto sono effettuate due iterazioni del decodificatore di Viterbi (che è il blocco computazionalmente più oneroso): in tale schema, i dati in uscita dalla prima iterazione di decodifica di Viterbi sono utilizzati per ricostruire la sequenza di simboli complessi trasmessa, i quali a loro volta servono per ripetere la stima di canale da utilizzare per una successiva e finale equalizzazione e decodifica (seconda passata di Viterbi) del simbolo OFDM in oggetto.

Il secondo schema proposto è di tipo non iterativo, ovvero prevede una sola iterazione del decodificatore di Viterbi. per decodificare i bit di informazione corrispondenti al simbolo OFDM ricevuto all'istante sotto osservazione, e al tempo stesso per ricostruire la sequenza di simboli complessi trasmessi da utilizzare per raffinare la stima di canale, che sara' utilizzata per l'equalizzazione del simbolo OFDM successivo. Ne risulta uno schema con impatto di complessità computazionale confrontabile con gli schemi che non utilizzano il decodificatore di Viterbi nella stima di canale.

Le simulazioni di prestazione ottenute con i due schemi mostrano che lo schema

non iterativo produce risultati confrontabili con gli stessi ottenuti nel caso iterativo, peggioramenti maggiori di 1 dB di rapporto segnale-rumore si osservano solo negli scenari simulati con velocità relative tra trasmettitore e ricevitore molto elevate. Dai risultati ottenuti si osserva in particolare che entrambi gli schemi inseguono molto bene il canale e significative perdite in termini di rapporto segnale-rumore rispetto al caso di conoscenza ideale del canale si notano solo in un ristretto numero di scenari simulati, caratterizzati da alti bitrate e alte velocità relative.

A completamento del capitolo in oggetto sono state descritte ulteriori analisi sugli errori residui in uscita dal decodificatore di Viterbi. In entrambi gli algoritmi menzionati, la equalizzazione di partenza del simbolo OFDM in oggetto è effettuata a partire dalla stima di canale derivata all'istante di tempo precedente, e perciò generalmente affetta da degradazione dovuta all'effetto Doppler. Questa considerazione ha motivato l'ultimo argomento del capitolo in esame, ovvero la analisi e simulazione di metodi di predizione della stima di canale per compensare la degradazione dello stesso dovuta all'effetto Doppler.

Negli algoritmi di inseguimento di canale citati sopra, la stima di canale viene ripetuta per ogni simbolo OFDM ricevuto. Con l'obiettivo di ridurre il consumo di energia, è stato analizzata la possibilità di ridurre la frequenza di aggiornamento della stima di canale senza degradare significativamente le prestazioni. L'ultimo capitolo è pertanto dedicato alla presentazione di metodi per la derivazione di un valore di frequenza di aggiornamento in funzione della velocità relativa, per una massima degradazione tollerabile delle prestazioni, imposta a priori. Prerequisito per l'applicabilita' di tale idea è la conoscenza al ricevitore della velocità relativa tra trasmettitore e ricevitore. Allo scopo, due differenti algoritmi di stima della velocità in banda base sono stati modellati con applicazione ai sistemi veicolari, e confrontati. Previa l'introduzione di una opportuna modifica rispetto a quanto presentato in letteratura, simulazioni di stima della velocita' relativa hanno mostrato che uno dei due metodi analizzati e' potenzialmente adeguato allo scopo. A conclusione del capitolo sono riportate le curve di prestazione in termini di tasso di errore di pacchetto WLAN verso rapporto segnale-rumore, in cui la frequenza di aggiornamento della stima di canale è determinata a partire dalla stima di velocità ottenuta utilizzando lo stimatore di velocità ritenuto più idoneo all'utilizzo in ambiente veicolare.

Contents

Introduction

During the last two decades wireless communications have become one of the key sectors in worldwide economy and everyday life. Examples of this arise from wireless local area networks (WLANs) to mobile phones, Bluetooth personal devices and satellite television broadcasting; all these technologies have become fundamental and new fields of application for wireless communications are continuously emerging.

Providing wireless communications in high mobility scenarios is the new challenge derived from the necessity to guarantee wireless access in the most practical real situations.

In this contest Wireless Access in Vehicular Environment (WAVE) is a technology that provides connectivity in the Dedicated Short Range Communications (DSRC) frequencies for applications suitable in the area of the Intelligent Transport System (ITS). An official classification of ITS applications does not exist. However, potentially a vast set of applications can be provided, ranging from driver safety increase, which is the main purpose of these networks, to traffic flow monitoring and congestion mitigation, or electronic tolling collection. The grant of WAVE is to provide wireless low latency, geographically local, high data rate, and high mobility communications whose typical applications are in the area of ITS.

This kind of applications are considered critical for the next future: during the last years safety in vehicular context has been greatly improved with new technologies including various kind of sensors that continuously monitor the road to prevent accidents. The continuous increase of the number of vehicles, and consequently of collisions, underlines the importance of inter-vehicle communications, considered a key-factor in future preventing accidents and increasing safety.

A contextualization to the vehicular environment in the sense of wireless communications is given by wireless local area networks (WLANs). Typical scenarios in which WAVE is supposed to focus are small aggregates of vehicles. In this context the IEEE 802.11 set of Standards for WLANs has been extended with IEEE 802.11p

that is a proposed enhancement to IEEE 802.11 in order to guarantee reliable data exchange between high-speed vehicles and between vehicles and the roadside infrastructure in the licensed ITS band of 5.9 GHz (5.85-5.925 GHz). Based on the Orthogonal Frequency Division Multiplexing (OFDM) system, IEEE 802.11p provides physical and Medium Access Control (MAC) layers specifications.

Aim of this thesis is the study of the issues related to the wireless channel estimation in a time-varying frequency-selective contest for OFDM systems. Starting from the pre-existent work, the focus will be on the decision-directed channel estimation (DD-CE) techniques. After a review on the existent work, DD-CE algorithms with forward error correction (FEC) will be investigated by a comparison in terms of performance and complexity. DD-CE with FEC shows great improvements in performance even in high-mobility scenarios with respect to the DD-CE schemes without FEC, but at the cost of higher system complexity.

Despite that, two further improvements to the investigated channel tracking algorithms have been evaluated. The first, is motivated by the performance gap still observable compared to the ideal case for very challenging scenarios like high relative speed ($\geq$ 120 Km/h), long WLAN packets ($\geq$ 400 byte), high modulation orders (64-QAM). Linear prediction of the channel estimate is considered in order to compensate the degradation of the channel estimation due to the Doppler effect with comparisons between optimal and sub-optimal well-known algorithms.

As a second improvement to the data decoding-aided DD-CE scheme, the selection of the CE occurrence as a function of the estimated relative speed between transmitter and receiver is discussed. This may be useful in practical portable systems to reduce processing time and/or power consumption. In particular it will be presented a strategy to select the CE occurrence based on the relative speed between transmitter and receiver and a maximum (set a-priori by the designer) tolerable degradation of the SNR seen at the receiver, due to the Doppler effect.

The relative speed between transmitter and receiver is a function of the Doppler spread; this motivates the assessment of the state-of-the-art Doppler spread estimation algorithms and their application to vehicular systems. The most effective in vehicular environment will be then taken into account. Finally, the performance results obtained with decreased CE occurrence based on the estimated relative speed, obtained with the selected Doppler spread estimator, will be presented.

This thesis is organized as follows.

Chapter 1. This chapter deals with the description of the time-varying frequency selective wireless channel. The concepts of path loss, shadowing effect, Doppler shift and multipath fading are investigated. The modeling of the discrete-time wireless channel is presented. Finally, wireless channel models suitable for vehicular environment are presented.

Chapter 2. In this chapter Orthogonal Frequency Division Multiplexing (ODFM) system is analyzed: the general OFDM system and a simplified model employing prototype filters are presented. The filterless OFDM system with cyclic prefix is described: under the assumption of absence of noise, it guarantees the reconstruction of the transmitted symbol with a simple zero-forcing equalization even for frequency-selective channels.

Chapter 3. This chapter describes the Wireless Access in Vehicular Environment technology as the system considered to provide wireless connectivity in vehicular environment. In this chapter the description of the IEEE 802.11p physical layer is also included together with the generation procedure of the physical layer data unit.

Chapter 4. Chaper 4 deals with channel estimation (CE) techniques. First a brief general subdivision of the various CE techniques is given. Then various CE techniques suitable for IEEE 802.11p are presented together with the evaluation of the relative CE error. The eviewed approaches are reported in increasing order of complexity.

Chapter 5. This chapter deals with DD-CE techniques with particular focus on the DD-CE algorithms with forward error-correction (FEC) due to the decoder. The improvements in performance with respect to the case with no FEC are shown. Two FEC aided DD-CE algorithms are proposed and compared in terms of complexity and performance. Moreover linear prediction of the channel is studied; a comparison in terms of performance and complexity between the optimal and a sub-optimal approach is also included.

Chapter 6. In this chapter the problem of evaluating the impact of CE occurrence on link performance is presented. It is shown that the time variation of the channel due to the relative speed between transmitter and receiver is related to the Doppler

spread, and consequently to the relative speed between transmitter and receiver. A strategy to decrease the CE occurrence as a function of the relative speed between transmitter and receiver is presented, in order to reduce processing time and power consumption. Consequently two different Doppler spread estimation algorithms are studied and reviewed. The most effective in vehicular environment will be then taken into account. Finally simulation results with decreased CE occurrence, selected as a function of the estimated relative speed and a maximum tolerable degradation of the signal-to-noise ratio seen at the receiver, are presented.

Chapter 7. Chapter 7 reports a brief conclusion of this thesis.

Chapter 1

The Wireless Channel

1.1 Introduction

In wireless communications the wireless radio channel is the source of the various degradations such as attenuation, noise and interferences that afflict the signal at the receiver with respect to the transmitted signal. These elements have a nature intrinsically difficult to predict. Moreover in vehicular environment all these degradations of the signal are not static: the time-varying nature of the scenario causes a continuous variation of the wireless channel characteristics. To better understand and model the time-varying wireless channel the different aspects of attenuation, noise contribution, interference and time-varying effects will be analyzed.

The additive white Gaussian noise (AWGN) is the main source of noise in a wireless system and is the model for the thermal noise generated at the receiver. The various degradations that afflict the received signal are typical grouped in two main categories:

- *large-scale fading* takes into account the attenuation caused by the distance between the transmitter and the receiver that is usually defined *path loss* and the slow fluctuation of the receiver power due to large obstacles (with respect to the wavelength) between the receiver and the transmitter as buildings and hills, typically referred to as *shadowing*; these degradations of the received signal are usually frequency independent;
- *small-scale fading* takes into account the reflection and scattering introduced by small obstacles (with a spatial scale of the order of the wavelength) as

vehicles or small objects; these kind of interferences are typically frequency selective.

The time-varying nature of the wireless channel is given by the movement of either the transmitter or the receiver or of the reflectors in the transmission paths. The consequence is a change in the amplitude, distortion and time of arrival of the different rays seen at the receiver. This effect is known as *Doppler shift*.

In vehicular environment these non-static elements do not generally afflict the large-scale fading: the comprehensive geometry of large obstacles is almost static in the transmission time considered for the typically achievable relative speeds. On the contrary small-scale fading has a time-varying nature: the variations of the scattering and reflections generated by small obstacles is not negligible in vehicular scenarios.

Under these assumptions the wireless channel has a time-varying frequency-selective nature. In the following these aspects introduced will be investigated in order to model the wireless channel in vehicular environment.

1.1.1 Path loss

The simplest scenario for wireless communication is the free space: a transmitter and a receiver at distance d from each other with no obstacles. In this assumption the signal propagates along a straight line and no distortion occurs. The channel model associated with this transmission is called a line-of-sight (LOS) channel, and the corresponding received signal is called the LOS signal or ray. Free space path loss attenuates the transmitted signal by the factor:

$$\frac{P_r}{P_t} = G_1 G_2 \left(\frac{\lambda}{4\pi d} \right)^2 \tag{1.1}$$

where P_t [W] and P_r [W] are, respectively, the power of the transmitted and received signals, G_1 and G_2 are the gains of the transmitting and receiving antennas and λ [m] is the wavelength of the radio wave. Therefore, the received signal power falls off inversely proportional to the square of the distance d [m] between the transmit and receive antennas.

Equation (1.1) holds for non-LOS components too tacking into account that d represents the total distance covered by the ray. The received signal power is also proportional to the square of the signal wavelength, so as the carrier frequency increases, the received power decreases.

Environment	γ range
Urban macro cells	$3.7 - 6.5$
Urban micro cells	$2.7 - 3.5$
Office Building (same floor)	$1.6 - 3.5$
Office Building (multiple floors)	$2 - 6$
Store	$1.8 - 2.2$
Factory	$1.6 - 3.3$
Home	3

Table 1.1: Typical Path Loss Exponents

In cases of multipath propagation ray tracing can be useful to study the attenuation of the received power due to the combined path-loss; for example the two ray tracing model sums the effect of the LOS component with the one reflected by the ground.

A number of path loss models have been developed to describe free-space attenuation in typical wireless environments such as large urban macro cells and urban micro cells. These models are mainly based on empirical measurements over a given distance in a given frequency range and a particular geographical area or building.

The complexity of signal propagation in wireless mobile environments makes very difficult to obtain a general model that characterizes path loss accurately across different environments. However, for general trade-off analysis of various system designs it is sometimes convenient to use a simpler model such as the following:

$$a(d) = \frac{P_r}{P_t} = K_a \left(\frac{d_0}{d} \right)^{\gamma} \tag{1.2}$$

where K_a is a constant that depends on the antenna characteristics and on the average channel attenuation, d_0 [m] is a reference distance for the antenna far-field region, and γ depends on the type of environment. In table 1.1.1 are reported some examples of measured values of γ for different scenarios [2].

1.1.2 Shadowing effect

Big obstacles between the transmitter and the receiver as buildings or hills cause a random attenuation of the signal with respect to the average received power. This effect is commonly referred to as shadowing. When the attenuation is very strong,

the signal can be severely attenuated.

In order to model the shadowing effect the ratio of transmit-to-receive power is defined as $\psi(t) = P_t(t)/P_r(t)$. With this notation the power attenuation due to the shadowing effect at time t is $P_r(t)/P_t(t) = 1/\psi(t)$.

From empirical studies it turned out that the shadowing is distributed according to a log-normal distribution, and this is the most common model for this phenomenon. The distribution of these fluctuations of the power attenuation ψ is given by [2]:

$$p(\psi) = \frac{10/\ln 10}{\psi\sqrt{2\pi\sigma^2_{\psi_{dB}}}} \exp\left\{-\frac{(10\log_{10}\psi - \mu_{\psi_{dB}})^2}{2\sigma_{\psi^2_{dB}}}\right\} \quad \psi > 0 \tag{1.3}$$

where $\mu_{\psi_{dB}}$ is the expectation of $\psi_{dB} = 10\log_{10}(\psi)$ in dB and $\sigma^2_{\psi_{dB}}$ is the standard deviation of ψ, also in dB. The expectation can be based on an analytical model or empirical measurements. The expectation of $\psi(t)$ can be obtained from 1.3 as:

$$\mu_\psi = \mathrm{E}\left[\psi(t)\right] = \exp\left[\frac{\mu_{\psi_{dB}}}{10/\ln 10} + \frac{\sigma^2_{\psi_{dB}}}{2(10/\ln 10)^2}\right] \tag{1.4}$$

and the conversion from the linear mean (in dB) to the log mean is:

$$10\log_{10}\mu_\psi = \mu_{\psi_{dB}} + \frac{\sigma^2_{\psi_{dB}}}{20/\ln 10}. \tag{1.5}$$

After a change of variables it results that the distribution of the dB value of $\psi(t)$ is Gaussian with mean $\mu_{\psi_{dB}}$ and standard deviation $\sigma^2_{\psi_{dB}}$,

$$p(\psi_{dB}) = \frac{1}{\sqrt{2\pi\sigma^2_{\psi_{dB}}}} \exp\left\{-\frac{(\psi_{dB} - \mu_{\psi_{dB}})^2}{2\sigma^2_{\psi_{dB}}}\right\} \tag{1.6}$$

The combined effect of path loss and shadowing plays a fundamental role in wireless systems design. In fact, usually, there is a minimum received power level P_{min}, below which the performance becomes unacceptable. The *outage probability* $p_{outage}(P_{min}, d)$ under path loss and shadowing is defined as the probability that the received power at a given distance d, $P_r(d,t)$ is lower than P_{min}, that is $p_{outage}(P_{min}, d, t) = \mathrm{P}\left[P_r(d,t) < P_{min}\right]$. P_{min} also depends on the sensitivity of the receiver. Combining path loss and shadowing model, the outage probability becomes [2]

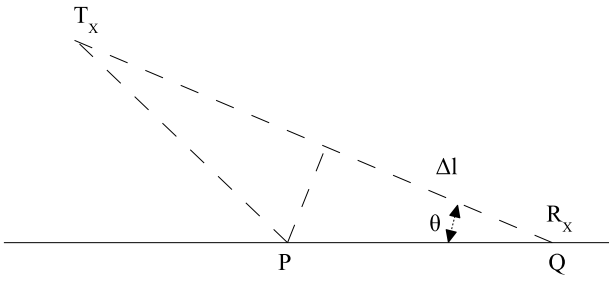

Figure 1.1: Illustration of the Doppler spread

$$p_{outage} = \mathrm{P}\left[P_r(d,t) < P_{min}\right] = 1 - Q\left(\frac{P_{min} - (P_t(t) - 10\log_{10} K_a - 10\gamma \log_{10}(d/d_0))}{\sigma_{\psi_{dB}}}\right) \quad (1.7)$$

where

$$Q(z) = p(x > z) = \int_z^{+\infty} \frac{1}{2\pi} e^{-y^2/2} dy \quad (1.8)$$

is the complementary Gaussian distribution function.

1.1.3 Doppler spread

Doppler spread, or Doppler shift, is the frequency shift that the receiver undergoes with respect to the transmitted frequency. This is caused by the relative motion between transmitter and receiver.

With reference to Figure 1.1 let T_X be the transmitter and R_X the receiver that moves from a point P to a point Q with speed v. The variation of distance between the two equipments is $\Delta l = v\Delta t \cos\theta$ where Δt is the time the receiver takes to go from P to Q, θ is the angle of incidence of the signal with respect to the direction of motion and $v\cos\theta$ is the relative speed between the transmitter and the receiver.

The phase variation due to this difference in the path length is

$$\Delta\phi = \frac{2\pi\Delta l}{\lambda} = \frac{2\pi v \Delta t \cos\theta}{\lambda} \quad (1.9)$$

where λ is the wavelength of the transmitted signal. The Doppler frequency is then given by the relation

$$f_D = \frac{1}{2\pi}\frac{\Delta\phi}{\Delta t} = \frac{v\cos\theta}{\lambda} = v\frac{f_c\cos\theta}{c} \tag{1.10}$$

being f_c the carrier frequency and c the speed of light. If the signal propagation is taking place through only one ray, the received signal undergoes only one Doppler shift. According to the equation above, the frequency shift f_D depends on the angle of arrival, and in the presence of different paths the received signal is no longer monochromatic. In this case Doppler spectrum $D(f)$ indicates the spectrum of the received signal around the central frequency f_c. A common assumption considers the Doppler spread obtained from the motion of the two vehicles moving in the same direction, for which it results $\cos\theta = 1$ and $f_D = f_c v/c$.

A model known as the Jakes model or classical Doppler spectrum is widely used; this model introduced by Clarke is given by

$$D(f) = \begin{cases} \dfrac{1}{\pi f_D\sqrt{1-(f/f_D)^2}} & |f| \le f_D \\ 0 & \text{otherwise} \end{cases} \tag{1.11}$$

where the maximum frequency f_D of the Doppler spectrum band is called Doppler spread. Another widely used model is the flat spectrum, defined as:

$$D(f) = \begin{cases} \dfrac{1}{2f_D} & |f| \le f_D \\ 0 & \text{otherwise} \end{cases} \tag{1.12}$$

Another important parameter is obtained by taking the inverse of the Doppler spread; this parameter is defined coherence time t_{coh} and it gives an approximated measure of the time interval over which the channel impulse response can be assumed to be time invariant.

Let T be the symbol period in a multi-carrier transmission system, and define the normalized factor

$$\nu_D = f_D T = \frac{v}{c} f_c T, \tag{1.13}$$

then the time varying nature of the channel is commonly assumed fast fading if $f_D T > 10^{-2}$ and the impulse response varies over a symbol period. Vice versa if $f_D T < 10^{-3}$ the impulse response is slowly time variant and it can be considered to be static over one symbol period. In a multi-carrier transmission system, the inverse of ν_D

$$N_S = \frac{1}{\nu_D} = \frac{1}{f_D T} \tag{1.14}$$

gives an approximated number of consecutive symbols where the channel can be considered time invariant.

1.1.4 Statistical multipath channels

When a pulse is transmitted over a time-dispersive channel the received signal will be viewed as a train of pulses, where a pulse corresponds to either the LOS component, or a distinct path associated with a scatterer or cluster of scatterers. A very important characteristic of a multipath environment is the time delay spread. The delay spread equals the time interval between the arrival of the first and last ray [1].

The baseband expression of a multipath channel impulse response seen at time t in response to an impulse applied at time $t - \tau$ with L_{ch} paths seen at the receiver is:

$$h(t, \tau) = \sum_{l=0}^{L_{ch}-1} h_l(t)\delta(\tau - \tau_l(t)) \tag{1.15}$$

where $\delta(\cdot)$ is the Dirac pulse, $h_l(t)$ is the complex valued gain of the $l-$th path seen at the receiver with delay $\tau_l(t)$ and $t \in \mathbb{R}$ is the observation time.

The presented path loss and shadowing models can be grouped together and then the wireless channel model becomes:

$$h(t, \tau) = \sqrt{(1/\psi(t))}\sqrt{a(d)} \sum_{l=0}^{L_{ch}-1} h_l(t)\delta(\tau - \tau_l(t)) \tag{1.16}$$

where $a(d)$ is the path loss attenuation (1.2) and d is the distance between transmitter and receiver in meters at time t. Through the model (1.16) the transmission link is modeled as a linear filter with a time-varying impulse response; the non-static behavior of the channel is caused by changes in the environment as the relative motion between transmitter and receiver.

In case time variations can be neglected for the system of interest, i.e. $h_l(t) \simeq h_l$ and $\tau_l(t) \simeq \tau_l$, the model is referred to as *slow fading*. On the other hand, the Doppler effect introduced in subsection 1.1.3 must be taken into account for vehicular systems, as shown in 3.1.

In a digital transmission system the effect of multipath depends on the duration of the symbol period compared to the length of the channel impulse response. If the duration of the channel impulse response is very low compared to the duration of the symbol period, then a model with only one path is adeguate and results in a flat fading channel. In more general conditions, a suitable model has to include several paths. A typical statistical description of the gains $h_l(t)$ is given by [1]:

$$h_l(t) = \begin{cases} C + \tilde{h}_0(t) & l = 0 \\ \tilde{h}_l(t) & l = 1, \ldots, L_{ch} - 1 \end{cases} \tag{1.17}$$

where C is a real-valued constant which takes into account the LOS component and $h_l(t)$ are complex-valued Gaussian random variables with zero mean. The phase of $\tilde{h}_l(t)$ is uniformly distributed in $[0, 2\pi)$. Therefore the first path contains a deterministic component added to a random one. The other paths are assumed to be random. The distribution of $|h_0|$ results a Rice distribution while $|h_i|$, $i = 1, \ldots, L_{ch} - 1$ have Rayleigh distribution. In particular defining

$$\tilde{h}_l(t) = \frac{h_l(t)}{\sqrt{\mathrm{E}[|h_l(t)|^2]}} \tag{1.18}$$

it turns that

$$\begin{aligned} p_{|\hat{h}_0|}(\psi) &= 2(1+K)\psi \exp[-K - (1+K)\psi^2] I_0\left(2\psi\sqrt{K(1+K)}\right) 1(\psi) \\ p_{|\hat{h}_l|}(\psi) &= 2\psi e^{-\psi^2} 1(\psi) \end{aligned} \tag{1.19}$$

where $I_0(\cdot)$ is the modified Bessel function of the first type and zero-th order and $1(\psi)$ equal to 1 for $\psi > 0$ and to 0 for $\psi < 0$. In presence of the LOS component the parameter $K = C^2 / \mathrm{E}[|\tilde{h}_0|^2]$, known as Rice factor, is equal to the ratio between the power of the LOS component and the power of the reflected component. For a model with several paths, $L_{ch} > 1$, K is defined as $K = C^2/M_c$, where M_c is the statistical power of all reflected and/or scattered components. Assuming that the power delay profile (PDP) of the channel is normalized, that is

$$\sum_{i=0}^{L_{ch}-1} \mathrm{E}[|h_i(t)|^2] = \sum_{i=0}^{L_{ch}-1} \sigma_{h_i}^2 = 1 \tag{1.20}$$

it results that $C = \sqrt{K/(K+1)}$. If the LOS component is absent, $C = 0$ and all gains have a Rayleigh distribution. Typical values of K are 3 and 10 dB, if no LOS exists then $K = 0$.

1.2 Wireless channel models

1.2.1 Tapped-delay-line channel model

In order to introduce a time-varying frequency-selective channel model in discrete time it is firstly described a continuous time channel model that takes into account all the aspects presented previously.

Assuming that signal propagation occurs through a large number of paths, it has been shown that the baseband equivalent channel impulse response can be represented with good approximation as a time-varying complex-valued Gaussian random process $h(t,\tau)$ where $h(t,\tau)$ is the output of the channel at instant t in response to an ideal impulse applied at instant $t-\tau$.

A widely used statistical model is the wide-sense stationary uncorrelated scattering (WSS-US) channel model. The WSS property implies that the second-order statistics of the channel are stationary; US model means that the paths that arrive with different delays are uncorrelated. In this way the cross-correlation of the channel evaluated for delays $\tau, \tau-\Delta\tau$ at time instants t and $t-\Delta t$ is

$$r_h(t,t-\Delta t;\tau-\Delta\tau) = \mathrm{E}[h(t,\tau)h^*(t-\Delta t,\tau-\Delta\tau)] \quad = r_h(\Delta t,\tau)\delta(\Delta\tau). \tag{1.21}$$

This means that the autocorrelation of the channel is zero for impulse responses considered at different delays. Moreover, as $h(t,\tau)$ is stationary in t, the autocorrelation depends only on the difference of the times at which the two impulse responses are evaluated. Imposing $\Delta t = 0$ the power delay profile can be defined as:

$$M(\tau) = \mathrm{E}[|h(\tau)|^2] \tag{1.22}$$

and it represents the power behavior of the channel impulse response for a given delay. In presence of multipath, another useful parameter is the root-mean square time delay spread τ_{rms}, given by

$$\tau_{rms}^2 = \frac{\int (u-\bar{\tau})^2 M(u)du}{\int M(u)du} = \frac{\int u^2 M(u)du}{\int M(u)du} - \bar{\tau}^2 \tag{1.23}$$

with

$$\bar{\tau} = \frac{\int uM(u)du}{\int M(u)du} \tag{1.24}$$

that expresses the channel dispersion in the time domain. It stands out that (1.23) expresses the average root-mean square time delay spread τ_{rms} as the squared root of

the second-order central moment of the power delay profile. For a Rayleigh channel model, typical curves for $M(\tau)$ can be Gaussian unilateral or Exponential unilateral.

The inverse of the root-mean square time delay spread τ_{rms} is proportional to the coherence bandwidth of the channel; it is often approximated as $B_{coh} \cong 1/(5\tau_{rms})$ that is a measure of the frequency selectivity of the channel. In particular, if B_{coh} is lower than the transmission rate of the system, then the channel is considered frequency selective, otherwise it is said to be a flat fading channel.

For many purposes, it is useful to approximate the continuous time wireless link by a discrete-time channel with sampling period T_c, often assumed equal to the chip period of the multicarrier transmission, that is $T_c = 1/B$ where B is the transmission bandwidth of the multicarrier system.

The discrete time model is obtained by sampling $M(\tau)$ with sampling period T_c and by truncating the channel impulse response so that it includes only a finite number of propagation paths, where the less significant paths can be neglected. For a fixed t, the time axis is divided into equal intervals of duration T_c. With reference to (1.15) the paths are restricted to lie in one of the time interval bins. If L_{ch} represents the number of significant paths, then the multipath spread of this discrete model is $(L_{ch} - 1)T_c$.

Thus, in the discrete time domain the multipath wireless channel is modeled as a time-varying discrete WSS-US channel having T_c spaced taps components as

$$h(kT_c, mT_c) = \sum_{l=0}^{L_{ch}-1} h_l(kT_c)\delta(mT_c - lT_c). \tag{1.25}$$

and the autocorrelation function of $h(kT_c, mT_c)$ for delays Δt, $\Delta\tau$ is

$$r_h(kT_c, kT_c - \Delta t; mT_c, mT_c - \Delta\tau) = r_h(\Delta t; \Delta\tau) = \sum_{l=0}^{L_{ch}-1} r_{h_l}(\Delta t)\delta(\Delta\tau - lT_c) \tag{1.26}$$

where $r_{h_l}(\Delta t)$ is the autocorrelation function of the $l-$th tap evaluated for a delay Δt. If the transmitter and the receiver are in a static position, that is $v = 0$, then all the taps are constant during the transmission. In a mobile system, if a NLOS model is considered, all the taps $h_l(kT_c)$ are complex-valued Gaussian stationary processes with zero mean. The Doppler spectrum results the Fourier transform of $r_{h_l}(\Delta t)$:

$$D(f) = \int_{-\infty}^{+\infty} r_{h_l}(\Delta t)e^{-j2\pi f\Delta t}df. \tag{1.27}$$

A widely considered Doppler spectrum in outdoor scenario is the Jakes model (1.11) that is applied independently to every tap.

The overall power is normalized to

$$\sum_{l=0}^{L_{ch}-1} \mathrm{E}[|h_l(kT_c)|^2] = \sum_{l=0}^{L_{ch}-1} \sigma_{h_l}^2 = 1 \tag{1.28}$$

where $\sigma_{h_l}^2$ is the variance of each tap.

Let the channel impulse response at time instant kT_c be defined in the $M \times 1$ vector form as $\mathbf{h}(kT_c) = [h_0(kT_c), h_1(kT_c), \ldots, h_{L_{ch}-1}(kT_c), 0, \ldots, 0]^T$, where the first L_{ch} entries corresponds to the non-zero taps and the last $M - L_{ch}$ are set to zero. Let $\mathbf{F}_M$ be the $M \times M$ discrete Fourier transform (DFT) matrix, with the (m, n)th entry equals to $[\mathbf{F}_M]_{m,n} = \exp(-j2\pi mn/M)$. Then, the channel frequency response (CFR), in vector form, is given by

$$\mathbf{H}(kT_c) = \mathbf{F}_M \mathbf{h}(kT_c) \tag{1.29}$$

From equation (1.29), the $M \times 1$ vector $\mathbf{H}(kT_c)$ must be interpreted as the CFR of the channel observed at time kT_c. For any $m = 0, 1, \ldots, M-1$ the $m-$th component of $\mathbf{H}$ can be modeled with a complex Gaussian random variable with zero mean and variance

$$\sigma_H^2 = \sum_{l=0}^{L_{ch}-1} \sigma_{h_l}^2 = 1 \tag{1.30}$$

and this implies that the channel frequency response samples H_m, $m = 0, \ldots, M-1$, are identically distributed, Gaussian, with zero mean and variance σ_H^2.

1.2.2 Wireless channel models for Vehicular Environment

In literature various channel models suitable for vehicular environment have been proposed, some of them are based on extensive measurements taken in outdoor environment. In [5] six small-scale fading channel models for wireless communication systems in vehicular environment are proposed from Georgia Tech university and are characterized by LOS scenarios. These models have been cited in IEEE 802.11p as informative examples but not as official reference models for the standard.

Nevertheless, in vehicular environment there may be conditions in which a LOS component is not present, which are also the most critical for the physical layer

performance. Therefore, it is important to take into account also non-LOS (NLOS) scenarios when evaluating the communication system performance.

For this reason in the following evaluations indoor NLOS scenarios proposed by ETSI have been taken into account.

ETSI channel models As an example of propagation scenarios with NLOS component the channel models by ETSI [6], [7] have been considered. Those models are of reference for indoor wireless local area networks and imply an independent Jakes Doppler spectrum on each tap. Summarizing, they and are characterized by:

- ETSI A: NLOS conditions and 50 ns average rms delay spread, corresponding to a typical office environment;
- ETSI B: NLOS conditions and 100 ns average rms delay spread, corresponding to a typical large open space and office environment;
- ETSI C: NLOS conditions and 150 ns average rms delay spread, corresponding to a typical large open space;
- ETSI D: LOS conditions, same as ETSI C but with a 10 dB spike at zero delay and 140 ns average rms delay spread;
- ETSI E: NLOS conditions and 250 ns average rms delay spread, corresponding to a typical large open space.

The corresponding power delay profiles are reported in tables 1.2 to 1.6.

Tap number	Delay (ns)	Average relative Power (dB)	Ricean K factor
1	0	0.0	0
2	10	-0.9	0
3	20	-1.7	0
4	30	-2.6	0
5	40	-3.5	0
6	50	-4.3	0
7	60	-5.2	0
8	70	-6.1	0
9	80	-6.9	0
10	90	-7.8	0
11	110	-4.7	0
12	140	-7.3	0
13	170	-9.9	0
14	200	-12.5	0
15	240	-13.7	0
16	290	-18.0	0
17	340	-22.4	0
18	390	-26.7	0

Table 1.2: Power Delay Profile for ETSI A

Tap number	Delay (ns)	Average relative Power (dB)	Ricean K factor
1	0	-2.6	0
2	10	-3.0	0
3	20	-3.5	0
4	30	-3.9	0
5	50	0.0	0
6	80	-1.3	0
7	110	-2.6	0
8	140	-3.9	0
9	180	-3.4	0
10	230	-5.6	0
11	280	-7.7	0
12	330	-9.9	0
13	380	-12.1	0
14	430	-14.3	0
15	490	-15.4	0
16	560	-18.4	0
17	640	-20.7	0
18	730	-24.6	0

Table 1.3: Power Delay Profile for ETSI B

Tap number	Delay (ns)	Average relative Power (dB)	Ricean K factor
1	0	-3.3	0
2	10	-3.6	0
3	20	-3.9	0
4	30	-4.2	0
5	50	0.0	0
6	80	-0.9	0
7	110	-1.7	0
8	140	-2.6	0
9	180	-1.5	0
10	230	-3.0	0
11	280	-4.4	0
12	330	-5.9	0
13	400	-5.3	0
14	490	-7.9	0
15	600	-9.4	0
16	730	-13.2	0
17	880	-16.3	0
18	1050	-21.2	0

Table 1.4: Power Delay Profile for ETSI C

Tap number	Delay (ns)	Average relative Power (dB)	Ricean K factor
1	0	0.0	10
2	10	-10.0	0
3	20	-10.3	0
4	30	-10.6	0
5	50	-6.4	0
6	80	-7.2	0
7	110	-8.1	0
8	140	-9.0	0
9	180	-7.9	0
10	230	-9.4	0
11	280	-10.8	0
12	330	-12.3	0
13	400	-11.7	0
14	490	-14.3	0
15	600	-15.8	0
16	730	-19.6	0
17	880	-22.7	0
18	1050	-27.6	0

Table 1.5: Power Delay Profile for ETSI D

Tap number	Delay (ns)	Average relative Power (dB)	Ricean K factor
1	0	-4.9	0
2	10	-5.1	0
3	20	-5.2	0
4	40	-0.8	0
5	70	-1.3	0
6	100	-1.9	0
7	140	-0.3	0
8	190	-1.2	0
9	240	-2.1	0
10	320	0.0	0
11	430	-1.9	0
12	560	-2.8	0
13	710	-5.4	0
14	880	-7.3	0
15	1070	-10.6	0
16	1280	-13.4	0
17	1510	-17.4	0
18	1760	-20.9	0

Table 1.6: Power Delay Profile for ETSI E

Chapter 2

Orthogonal Frequency Division Multiplexing

2.1 OFDM systems

Wireless channels in vehicular environment can exhibit high signal attenuation during transmission and have a frequency-selective nature. In this scenario, if a single carrier modulation system is used, channel equalization and data detection become difficult tasks.

A popular wireless modulation technique is represented by orthogonal frequency division multiplexing (OFDM). OFDM systems correspond to dividing the overall information stream to be transmitted into many lower data rate streams, each one modulating a different sub-carrier of the main frequency carrier. Equivalently, the overall bandwidth is divided into many sub-bands centered on the sub-carriers. This operation makes data communication more robust under wireless multi-path fading channel and simplifies frequency equalization operations.

In the present chapter the filterless OFDM system with cyclic prefix extension will also be introduced, which is used by many digital communication systems as some standards of the IEEE 802.11 family, WiMax and the DVB Standard. The particularity of this OFDM system is the efficient implementation and the simplicity of equalization of the received symbol under frequency-selective wireless channel. A complete treatment of OFDM systems can be found in [1].

An example of typical OFDM transmitter and receiver block diagrams are reported in chapter 3, figures 3.4 and 3.5.

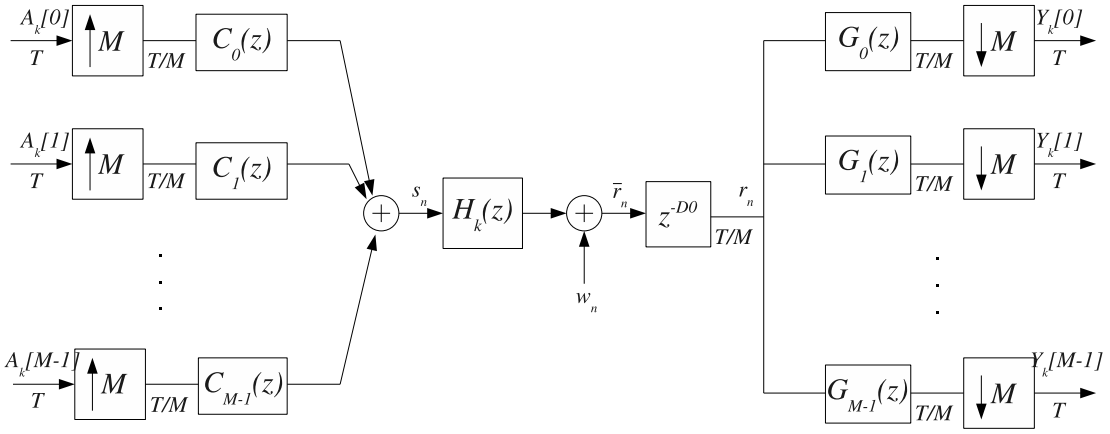

Figure 2.1: Block diagram of an OFDM system.

2.1.1 System model

In a OFDM system blocks of M complex symbols are transmitted in parallel over M distinct sub-channels. The system block diagram is reported in figure 2.1. Let the block of M symbols that are simultaneously transmitted at the given discrete time instant kT be defined as

$$\mathbf{A}_k = [A_k[0], A_k[1], \ldots, A_k[M-1]]^T \tag{2.1}$$

where each symbol $A_k[i]$, $i = 0, 1, \ldots, M-1$, belongs to a two dimensional M-PSK or M-QAM constellation $\mathcal{A}_i$. The constellation cardinality could be different for each sub-channel. Let the symbols $\mathbf{A}_k$ be zero mean and independent identically distributed (i.i.d.). Moreover the constellation symbols are normalized in order to get $E\left[|A[i]|^2\right] = 1$, $i = 0, 1, \ldots, M-1$. The modulation rate is defined as $F = 1/T$ where T is the transmission period of the OFDM symbol $\mathbf{A}_k$.

The $i-$th information data flow is zero padding interpolated by a factor M. The time-resolution of the interpolated data-flow is $T_c = T/M$. Then the $i-$th branch is filtered with a modulation filter $c_n[i]$ having impulse response given by $c_n[i]$, $n = 0, 1, \ldots, Mq-1$ and transfer function and frequency response respectively:

$$C_i(z) = \sum_{n=-\infty}^{+\infty} c_n[i] z^{-n} = \sum_{n=0}^{Mq-1} c_n[i] z^{-n} \tag{2.2}$$

$$C_i(f) = C_i(z)|_{z=e^{j2\pi fT/M}}, \quad i = 0, 1, \ldots, M-1. \tag{2.3}$$

The filters used on the different sub-channels act as shaping filters for the M upsampled branches. Note that the filters $c_n[i]$ work in parallel at rate $F_c = 1/T_c = M/T$, where $T_c = T/M$ is called *transmission rate*. The transmission bandwidth of the system is given by $B = 1/T_c = 1/(T/M) = M/T$. The OFDM modulated signal s_n, that is transmitted over the wireless channel, is obtained by summing all the resulting data flows

$$s_n = \sum_{i=0}^{M-1} \sum_{k=-\infty}^{+\infty} A_k[i] c_{n-kM}[i] \tag{2.4}$$

With reference to the system shown in figure 2.1, the signal s_n is transmitted over the wireless channel that has impulse response given by

$$\mathbf{h}_k = [h_{k,0}, h_{k,1}, \ldots, h_{k,L_{ch}-1}]^T \tag{2.5}$$

and transfer function $H_k(z)$ defined as

$$H_k(z) = \sum_{n=-\infty}^{+\infty} h_{k,n} z^{-n} = \sum_{n=0}^{L_{ch}-1} h_{k,n} z^{-n}. \tag{2.6}$$

The compact notation of the channel impulse response $\mathbf{h}_k = \mathbf{h}(kT)$ takes into account that, as furtherly discussed in section 3.1, in vehicular environment the wireless channel can be considered static within one OFDM symbol time.

The AWGN noise w_n has variance N_0 and is the model for the thermal noise generated ad the receiver. The block delay that introduces a delay of D_0 time instants, i.e. a delay time of $D_0 T_c$ seconds, guarantes the proper synchronization at the receiver side.

In case of ideal and noiseless channel, i.e. $\mathbf{h}_k = [1, 0, 0, \ldots, 0]^T$ and $w_n = 0$, it results $\bar{r}_n = s_n$.

At the receiver the received signal r_n is filtered by M filters having impulse responses given by $g_n[i]$ with support $\{0, 1, \ldots, Mq-1\}$ and transfer function given by

$$G_i(z) = \sum_{n=-\infty}^{+\infty} g_n[i] z^{-n} = \sum_{n=0}^{Mq-1} g_n[i] z^{-n} \tag{2.7}$$

for every $i-$th branch, $i = 0, 1, \ldots, M-1$. The M filters used by the demodulator work in parallel at the transmission rate F_c. The output data flows are then downsampled to the rate $F = 1/T$ in order to achieve the reconstructed symbols

$Y_k[i]$, $i = 0, 1, \ldots, M-1$. If the system composed by the cascade of modulator and demodulator introduces a delay D_0 in the signal reception, then the received vector

$$\mathbf{Y}_k = [Y_k[0], Y_k[1], \ldots, Y_k[M-1]]^T \tag{2.8}$$

corresponds to the reconstruction of the OFDM symbol A_{k-D_0} transmitted D_0 modulation intervals before.

Orthogonality Conditions With the assumption that the transmission is over an ideal and noiseless channel, i.e. $\bar{r}_n = s_n$, the transmission and reception filters $c_n[i]$ and $g_n[i]$ are usually designed to satisfy a perfect reconstruction condition. This mean that the designed filters have to guarantee:

- absence of inter-carrier interference (ICI); this means that no interference between symbols transmitted at the same time-instant on different sub-carriers occurs;
- absence of inter-symbol interference (ISI); this means that no interference between symbols transmitted on the same sub-channel at different time-instants occurs.

The support, in the time domain, of the filter $c_n[i]$ is indicated as $\{0, 1, \ldots, Mq-1\}$. Assuming matched filters are used at the receiver, i.e. $g_n[i] = c^*_{Mq-n}[i]$, the perfect reconstruction condition becomes [1]

$$\begin{aligned} \sum_{p=0}^{Mq-1} c_p[i] g_{n-p}[j] &= \sum_{p=0}^{Mq-1} c_p[i] c^*_{Mq+p-n}[j] = \\ &= \sum_{p=0}^{Mq-1} c_p[i] c^*_{p+M(q-k)}[j] = \\ &= \delta_{i-j}\delta_{k-q}, \quad i, j = 0, 1, \ldots, M-1, \end{aligned} \tag{2.9}$$

where $\delta_{i,j}$ is the Kronecker delta and $n = Mq$.

2.2 OFDM System with cyclic prefix

A simplified OFDM system implementation is now considered in which only one *prototype filter* c_n and g_n is used for all sub-carriers respectively at the transmitter and the receiver [1].

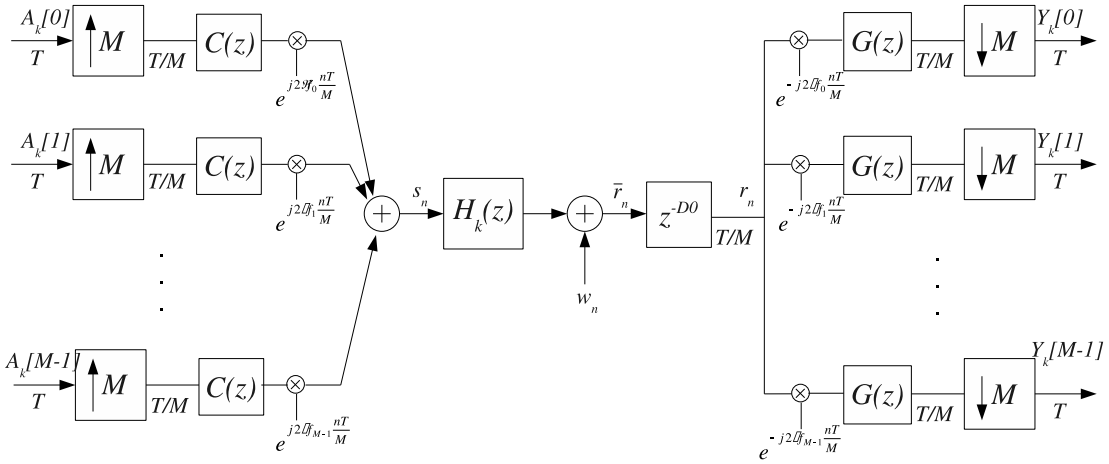

Figure 2.2: Block diagram of an OFDM system with uniform filter banks.

The shaping filters of the sub-channels used by the modulator are obtained by shifting the frequency response of the prototype filter c_n with support $\{0, 1, \ldots, Mq-1\}$ and transfer function $C(z)$ around equally spaced sub-carriers $f_i = i/T$, $i = 0, 1, \ldots, M-1$.

At the receiver side, the incoming signal $r_n[i]$, on each branch of the demodulator is shifted taking back each $i-$th sub-channel in the baseband. The signal is then shaped using a prototype filter g_n matched to that used in transmission, i.e. $g_n = c^*_{Mq-n}$.

A basic scheme of an OFDM system with a prototype filter and complex exponential modulators is shown in figure 2.2. In this architecture the equivalent shaping filters can be written as

$$c_n[i] = c_n e^{j2\pi f_i n \frac{T}{M}} = c_n e^{j2\pi \frac{in}{M}}, \quad i = 0, 1, \ldots, M-1, \tag{2.10}$$

$$g_n[i] = g_n e^{-j2\pi f_i n \frac{T}{M}} = g_n e^{-j2\pi \frac{in}{M}}, \quad i = 0, 1, \ldots, M-1. \tag{2.11}$$

This realization is a particular case of the general OFDM scheme; in the following an efficient implementation that uses the Discrete Fourier Transform (DFT) and a polyphase filtering network is derived.

The i-th sub-channel signal at the transmitter is:

$$s_n[i] = e^{j2\pi\frac{in}{M}} \sum_{k=-\infty}^{+\infty} A_k[i] c_{n-kM} \tag{2.12}$$

and the overall signal s_n:

$$s_n = \sum_{i=0}^{M-1} e^{j2\pi\frac{in}{M}} \sum_{k=-\infty}^{+\infty} c_{n-kM} A_k[i]. \tag{2.13}$$

With the change of variables $n = mM + l$ with $l = 0, \ldots, M-1$, it turns that:

$$s_{mM+l} = \sum_{i=0}^{M-1} e^{j2\pi\frac{i}{M}(mM+l)} \sum_{k=-\infty}^{+\infty} c_{(m-k)M+l} A_k[i]. \tag{2.14}$$

It should be noted that $e^{j2\pi im} = 1$. By expressing the $l-$th polyphase components of s_{mM+l} and c_{mM+l} as

$$s_m^{(l)} = s_{mM+l} \tag{2.15}$$

and

$$c_m^{(l)} = c_{mM+l}, \tag{2.16}$$

the l-th polyphase component of $\{s_n\}$ results:

$$s_m^{(l)} = \sum_{k=-\infty}^{+\infty} c_{m-k}^{(l)} \sum_{i=0}^{M-1} W_M^{-il} A_k[i] \tag{2.17}$$

where $c_m^{(l)}$, $l = 0, 1, \ldots, M-1$ denotes the polyphase component of the prototype filter impulse response with related transfer function defined as $C^{(l)}(z)$ and $W_M = e^{-j\frac{2\pi}{M}}$.

The inner summation in (2.17) is:

$$\sum_{i=0}^{M-1} W_M^{-il} A_k[i] = a_k[l], \quad l = 0, 1, \ldots, M-1 \tag{2.18}$$

being $a_k[l]$ the $l-$th element of the IDFT of $\mathbf{A}_k \in \mathbb{C}^{M\times 1}$, defined as $\mathbf{a}_k = \mathbf{F}_M^{-1}\mathbf{A}_k$, with $l = 0, 1, \ldots, M-1$.

Finally the l-th polyphase component of $\{s_n\}$ can be expressed as:

$$s_n^{(l)} = \sum_{k=-\infty}^{+\infty} c_{n-k}^{(l)} a_k[l] = \sum_{p=-\infty}^{+\infty} c_p^{(l)} a_{n-p}[l]. \tag{2.19}$$

From this relation it follows that each sample of the signal s_n can be obtained by the convolution of the signal at the $l-$th output of the IDFT block with the $l-$th polyphase component of the prototype filter $c_n^{(l)}$.

With reference to the figure 2.2, at the receiver side the relation between the received sequence $r_n = \bar{r}_{n-D0}$ and the output of the i-th sub-channel $Y_k[i]$ is:

$$Y_k[i] = \sum_{n=-\infty}^{+\infty} r_n g_{kM-n} e^{-j2\pi f_i n \frac{T}{M}} = \sum_{n=-\infty}^{+\infty} r_n g_{kM-n} e^{-j2\pi \frac{in}{M}}. \tag{2.20}$$

With the change of variables $n = mM + l$, $l = 0, 1, \ldots, M-1$ and recalling the definition of matched filter $g_n = c^*_{Mq-n}$, it reads

$$Y_k[i] = \sum_{l=0}^{M-1} \sum_{m=-\infty}^{+\infty} c^*_{(q-k+m)M+l} e^{-j2\pi \frac{i}{M}(mM+l)} r_{mM+l}. \tag{2.21}$$

We further note that $e^{-j2\pi im} = 1$ and set $r_m^{(l)} = r_{mM+l}$, $c_m^{(l)*} = c^*_{mM+l}$, so the output signal can be written as:

$$Y_k[i] = \sum_{l=0}^{M-1} e^{-j\frac{2\pi}{M}il} \sum_{m=-\infty}^{+\infty} c^{(l)*}_{q+m-k} r_m^{(l)} \tag{2.22}$$

that finally becomes, employing the relation $e^{-j\frac{2\pi}{M}il} = W_M^{il}$,

$$Y_k[i] = \sum_{l=0}^{M-1} W_M^{il} \sum_{m=-\infty}^{+\infty} c^{(l)*}_{q+m-k} r_m^{(l)}. \tag{2.23}$$

The demodulator can be implemented using a bank of polyphase filters, where for each $l-$th branch, $l = 0, 1, \ldots, M-1$, the content of the delay line is convolved with the $l-$th polyphase component $g_m^{(l)}$ of the matched filter g_k.

The resulting scheme comprising a inverse DFT (IDFT) operation at the transmitter and a DFT operation at the receiver is shown in figure 2.3. It should be noted that the rate of the equivalent shaping filters $c_m^{(l)}$ and $g_m^{(l)}$ is T and the upsampling operation to the transmission rate $T_c = T/M$ is obtained with the P/S operation on the M polyphase components $s_m^{(l)}$ of the output signal s_n. Moreover, as matched filters $g_m^{(l)}$ are used, their respective transfer functions read $G^{(l)}(z) = C^{(l)*}(1/z^*)$.

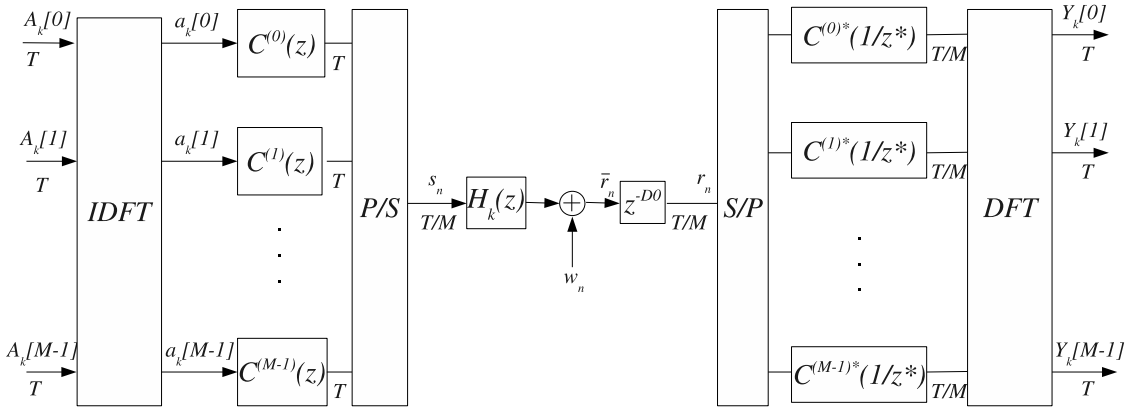

Figure 2.3: Block diagram of an OFDM system with efficient implementation.

2.2.1 Equalization in OFDM systems

In the present section the filterless OFDM system implementation is derived. The filterless OFDM system is a system where the prototype filters used at transmitter and receiver are given by

$$c_n = \begin{cases} 1 & 0 \leq n \leq M-1 \\ 0 & \text{otherwise} \end{cases} \tag{2.24}$$

The impulse response of the polyphase components of the prototype filter are:

$$\left\{c_n^{(l)}\right\} = \{\delta_n\} \quad l = 0, 1, \ldots\ M-1. \tag{2.25}$$

This assumption satisfies the orthogonality conditions (2.9). It results that the transmitted signal can be obtained by directly applying the P/S conversion at the output of the IDFT.

Under the condition of ideal and noiseless channel, at the receiver the S/P converter creates block of M samples so that the output of the IDFT goes unchanged to the input of the DFT and the output produces the transmitted signal without distortion.

A channel having impulse response $\mathbf{h}_k$, transfer function $H_k(z)$ and support $\{0, 1, \ldots, L_{ch}-1\}$, with $L_{ch} > 1$ is considered. The equalization technique is simplified if the concept of circular convolution can be applied, that allows expressing the convolution between two discrete-time sequences in the time domain as the product of finite length between the DFT of the same sequences [1].

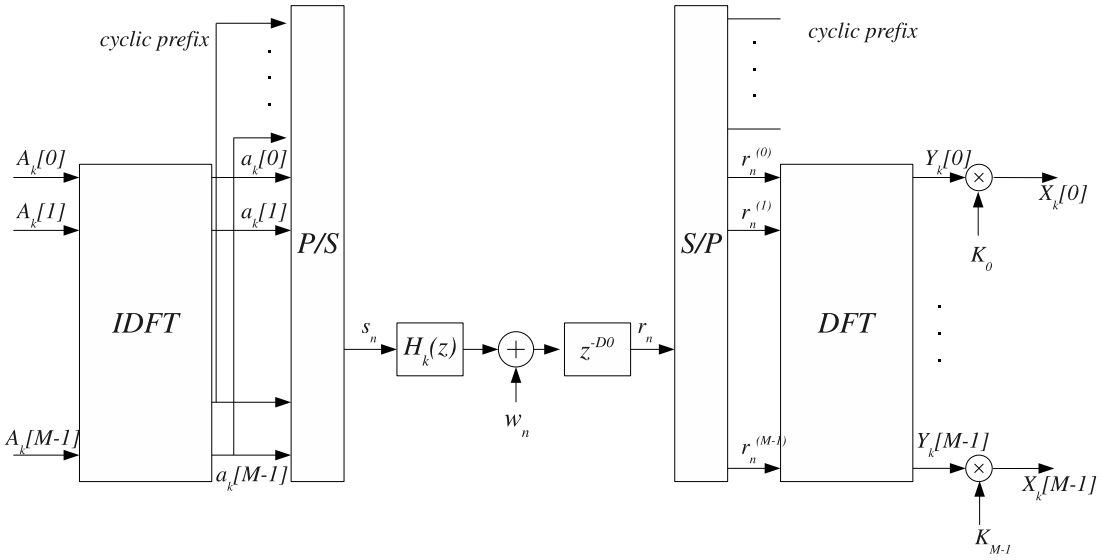

Figure 2.4: Block diagram of a filterless OFDM system with cyclic prefix and frequency-domain equalizer.

In order to enable circular convolutions, with reference to figure 2.4, the block of symbols $\mathbf{a}_k$ is extended appending the last $L_{cp} - 1 = L_{ch} - 1$ elements at the beginning of the sequence. In this way for the same transmission rate M/T the IDFT must work at the rate $\frac{1}{T'} = \frac{M}{(M+L_{cp}-1)T} < \frac{1}{T}$. After the P/S conversion, the $L_{cp} - 1 + M$ samples are transmitted over the channel. At the receiver the blocks of $L_{cp} - 1 + M$ samples are obtained after the S/P conversion; the first $L_{cp} - 1$ samples are discarded prior to DFT operations.

Beware of the properties of circular convolution, the vector $\mathbf{r}_k$ of the last M samples of the block received at time instant kT is given by:

$$\mathbf{r}_k = \mathbf{\Lambda}_k \mathbf{h}_k + \mathbf{w}_k \tag{2.26}$$

where $\mathbf{h}_k = [h_{k,0}, \ldots, h_{k,L_{ch}-1}, 0, \ldots, 0]^T$ is the M-component vector of the channel impulse response extended with $M - L_{ch}$ zeros, $\mathbf{w}_k$ is the AWGN vector and $\mathbf{\Lambda}_k$ is the $M \times M$ circulant matrix of the transmitted symbol, defined as:

$$\mathbf{\Lambda}_k = \begin{bmatrix} a_k[0] & a_k[M-1] & \cdots & a_k[1] \\ a_k[1] & a_k[0] & \cdots & a_k[2] \\ \vdots & \vdots & \ddots & \vdots \\ a_k[M-1] & a_k[M-2] & \cdots & a_k[0] \end{bmatrix}. \tag{2.27}$$

The matrix $\mathbf{\Lambda}_k$ is circulant and satisfies the relation:

$$\mathbf{F}_M \mathbf{\Lambda}_k \mathbf{F}_M^{-1} = \begin{bmatrix} A_k[0] & 0 & \cdots & 0 \\ 0 & A_k[1] & \cdots & 0 \\ \vdots & \vdots & \ddots & \vdots \\ 0 & 0 & \cdots & A_k[M-1] \end{bmatrix} = \text{diag}\{\mathbf{A}_k\} \tag{2.28}$$

where $\mathbf{F}_M$ is the $M \times M$ DFT matrix defined in 1.2.1. In frequency domain the DFT of the channel impulse response $\mathbf{h}$ is

$$\mathbf{H}_k = [H_{k,0}, \ldots, H_{k,M-1}]^T = \mathbf{F}_M \mathbf{h}_k. \tag{2.29}$$

Using (2.26) and (2.29), with reference to figure 2.4, the demodulator output can be written as:

$$\mathbf{Y}_k = \mathbf{F}_M \mathbf{r}_k = \mathbf{F}_M \mathbf{\Lambda}_k (\mathbf{F}_M^{-1} \mathbf{F}_M) \mathbf{h}_k + \mathbf{F}_M \mathbf{w}_k = \text{diag}\{\mathbf{A}_k\} \mathbf{H}_k + \mathbf{W}_k \tag{2.30}$$

where $\mathbf{W}_k = \mathbf{F}_M \mathbf{w}_k$ is the DFT of the AWGN vector.

The channel equalization process can thus be simply performed through zero-forcing, i.e. by multipling the vector $\mathbf{Y}_k$ with the diagonal matrix $\mathbf{K}$ having entries:

$$K_i = [\mathbf{K}]_{i,i} = \frac{1}{H_{k,i}} \quad i = 0, 1, \ldots, M-1. \tag{2.31}$$

Therefore the output symbol estimate vector is given by:

$$\mathbf{X}_k = \mathbf{K}\mathbf{Y}_k = \mathbf{A}_k + \mathbf{K}\mathbf{W}_k. \tag{2.32}$$

It is important to notice that with the cyclic prefix extension there is a reduction in the modulation rate by a factor $\frac{M+L_{cp}-1}{M}$.

Instead if the time duration of the channel impulse response is greater than the cyclic prefix (in other words, if the energy of the channel that falls out of the cyclic prefix can not be neglected), that is if $L_{ch} > L_{cp}$, then ISI arises.

Summarizing, the OFDM modulation scheme can be efficiently realized with the followings steps:

- Inverse Fast Fourier Transform (IFFT) performed at sampling time $T' = \frac{(M+L_{cp}-1)T}{M}$ on the M data flows $A_k[i]$, $i = 0, 1, \ldots, M-1$;

- appending the last $L_{cp} - 1$ samples of the data block at the beginning of the block as cyclic prefix;
- parallel to serial conversion (P/S) of the resulting M data flows, which is essentially a time division multiplexer.

Moreover an efficient digital implementation of the OFDM demodulator consists of:

- a serial to parallel (S/P) block that let a sequence of $M + L_{cp} - 1$ consecutive samples of the received signal be input on $M + L_{cp} - 1$ lines;
- the cyclic prefix removal obtained by eliminating the first $L_{cp} - 1$ symbols of every data block.
- a Fast Fourier Transform (FFT) performed at sampling time T to the symbols $r_n[i]$, $i = 0, 1, \ldots, M - 1$ to obtain the demodulated symbols $Y_k[i]$, $i = 0, 1, \ldots, M - 1$;
- a zero-forcing equalization of the demodulated symbols $Y_k[i]$ as reported in (2.31) and (2.32) to obtain the symbol estimates to be used for the data detection.

Chapter 3

IEEE 802.11p Standard for WLAN in Vehicular Environment

3.1 Introduction

Vehicle to vehicle (V2V) and vehicle to roadside-unit (RSU) communications (known as vehicle to infrastructure, V2I) represent a promising technology to support Intelligent Transportation Systems (ITS) applications. An official classification of ITS applications does not exist. However, potentially a vast set of applications can be provided, ranging from driver safety increase, which is the main purpose of these networks, to traffic flow monitoring and congestion mitigation, or electronic tolling collection. A possible scenario is shown in figure 3.1.

Dedicated Short Range Communications (DSRC) is the communication standard for general purpose V2V and V2I RF communication links. More specifically, it is a short to medium range communication service that supports several applications (like public safety, or electronic toll collection) requiring very low latency and high data rate. Concerning the physical layer (PHY) of DSRC technologies, most standards under development in different countries worldwide will be based on IEEE 802.11p [3], which is an amendment of the family of IEEE 802.11 standards for wireless local area network (WLAN) communications, both for physical layer and medium access control (MAC) layer, that introduces a set of specifications to enable Wireless Access in Vehicular Environment (in short, WAVE).

WAVE technology aims to guarantee wireless connectivity to IEEE 802.11 devices in vehicular environments where the physical layer properties are rapidly changing

and where very short-duration communications exchanges are required. The purpose of IEEE 802.11p is then to provide the minimum set of specifications required to ensure interoperability between wireless devices attempting to communicate in potentially rapidly changing communication environments and in situations where transactions must be completed in time frames much shorter than the minimum possible with infrastructure or ad hoc 802.11 networks. At the time of writing the standard is nearly finalized and final approval is expected by the end of 2010.

IEEE 802.11p physical layer is very similar to the popular IEEE 802.11a/g standards, OFDM-based, with the main differences being represented by the use of 5.9 GHz range (5.85-5.925 GHz) instead of 5.2 of the latter, and by the addition of a reduced bandwidth (10 MHz instead of 20 MHz).

There are however some difficulties, from a PHY perspective, of applying IEEE 802.11 to mobile communications systems, related to the perturbation of the signal due to the radio channel.

The outdoor propagation environment is generally characterized by longer delay spreads than indoor channels because the propagating radio signal is subject to obstacles such as buildings and trees, which can lead to strong reflective and/or diffractive multi-path effects placed at larger distances among them than in indoor environment. As a result, interference from the previously transmitted OFDM symbol, i.e. ISI can more easily arise for an outdoor environment than for indoor environments. It should be noticed that the bandwidth reduction of IEEE 802.11p compared to IEEE 802.11 a/g translates in a longer guard interval (GI) duration so to cope with the higher multi-path effect of urban environments.

3.2 IEEE 802.11p Physical layer

3.2.1 General description

IEEE 802.11p operates in the Dedicated Short Range Communications band allocated for Intelligent Transportation Systems (ITS) applications. They can occur between mobile stations and fixed information sources, between mobile units, and between portable units and mobile units. Transmissions have to be guaranteed over line-of-sight (LOS) between fixed and mostly high-speed units. They can also occur between stopped and slow moving vehicles, or between high-speed vehicles.

IEEE 802.11p standard specifications [3] include:

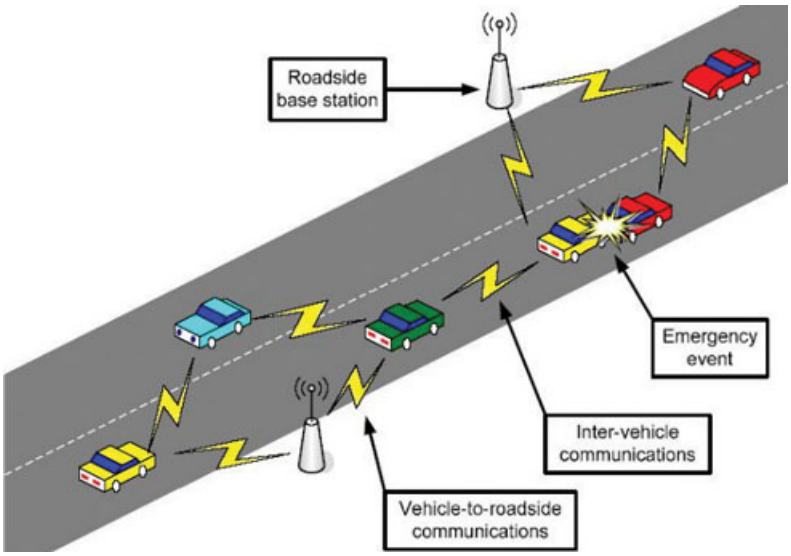

Figure 3.1: Example of V2V and V2I communications

- description of the functions and services required by WAVE-conformant stations in order to operate in vehicular environment and exchange messages without having to join a set of station clients (STAs) controlled by an Access Point (AP);

- definition of the WAVE signalling technique and interface functions that are controlled by the IEEE 802.11 Medium Access Control (MAC).

Physical layer specifications WAVE PHY is based on OFDM modulation. The radio frequency LAN system operates in the [5.850- 5.925] GHz frequency band, and 7 channels each 10 MHz wide are provided. In particular, one of them is dedicate to control functions, while the others are service channels. Optionally, 2 pairs of adjacent channels may be merged together in order to obtain two channels of 20 MHz.

The OFDM system provides a WLAN with 10 MHz bandwidth and data payload communication capabilities of 3, 4.5, 6, 9, 12, 18, 24 and 27 Mbit/s. In particular the support to transmitting and receiving data rates of 3, 6 and 12 Mbit/s is mandatory. Optionally, support for 20 MHz bandwidth can be granted and related data rates of 6, 9, 12, 18, 24, 36, 48 and 54 Mbit/s are provided. The OFDM system uses 52 sub-carriers that are modulated using binary or quadrature phase shift keying (BPSK,QPSK), 16-quadrature amplitude modulation (QAM), and 64-QAM. More-

Transmission rate [MHz]	Modulation	Coding rate	Coded bits per sub-carrier (N_{BPSC})	Coded bits per ODFM symb. (N_{CPSC})	Data bits per OFDM symb. (N_{DPSC})
3	BPSK	1/2	1	48	24
4.5	BPSK	3/4	1	48	36
6	QPSK	1/2	2	96	48
9	QPSK	3/4	2	96	72
12	16-QAM	1/2	4	192	96
18	16-QAM	3/4	4	192	144
24	64-QAM	2/3	6	288	192
27	64-QAM	3/4	6	288	216

Table 3.1: Transmission rates, B = 10 MHz

over forward error correction coding with 64-state convolutional code is used with code rates of 1/2, 2/3, or 3/4, as it is shown in tables 3.1 and 3.2.

3.2.2 OFDM parameters

In the following the main OFDM parameters of IEEE 802.11p are recalled. Table 3.3 reports the main parameters of the OFDM system for the two configurations of 10 and 20 MHz. The parameters reported in table 3.3 are defined as:

- T: OFDM symbol period (after cyclic prefix extension);
- T_c: chip time, corresponding to the discrete sampling time after the OFDM modulation;
- T_s: block symbol period, corresponding to the OFDM symbol duration without cyclic prefix;
- T_{cp}: cyclic prefix duration;
- L_{cp}: cyclic prefix length, expressed in number of modulated symbols.

Table 3.4 reports the sub-carriers repartition between data, virtual and pilot sub-carriers: data sub-carriers modulate the transmitted data, virtual sub-carriers are not used in the data transmission to achieve better out-of band signal reduction and

Transmission rate [MHz]	Modulation	Coding rate	Coded bits per sub-carrier (N_{BPSC})	Coded bits per ODFM symb. (N_{CPSC})	Data bits per OFDM symb. (N_{DPSC})
6	BPSK	1/2	1	48	24
9	BPSK	3/4	1	48	36
12	QPSK	1/2	2	96	48
18	QPSK	3/4	2	96	72
24	16-QAM	1/2	4	192	96
36	16-QAM	3/4	4	192	144
48	64-QAM	2/3	6	288	192
54	64-QAM	3/4	6	288	216

Table 3.2: Transmission rates, B = 20 MHz

Parameter	B = 10 MHz	B = 20 MHz
Sampling time	100 ns	50 ns
Frequency spacing between sub-carriers	156.25 kHz	312.5 kHz
T	$8\,\mu s$	$4\,\mu s$
T_c	$0.1\,\mu s$	$0.05\,\mu s$
T_s	$6.4\,\mu s$	$3.2\,\mu s$
T_{cp}	$1.6\,\mu s$	$0.8\,\mu s$
L_{cp}	16	16

Table 3.3: Parameters of the OFDM system in IEEE 802.11p

pilot sub-carriers modulate symbols known at the receiver in order to perform the CE tasks (see section 5.2).

3.2.3 Frame structure

The PHY layer consists of two sub-layers:

1. the physical layer convergence procedure (PLCP) sub-layer defines a method of mapping the IEEE 802.11 PHY sub-layer service data units (PSDU) into a PHY packet, of a format suitable for sending and receiving user data and management information between two or more stations using the associated

Type of sub-carriers	n.	index
Total	64	1,. . . ,64
Virtual sub-carriers	12	1, 28, . . . , 38
Pilot sub-carriers	4	8, 22, 44, 58
Data sub-carriers	48	2, . . . , 7, 9, . . . , 21, 23, . . . , 27, 39, . . . , 43, 45, . . . , 57, 59, . . . , 64

Table 3.4: Sub-carrier indexes for IEEE 802.11p

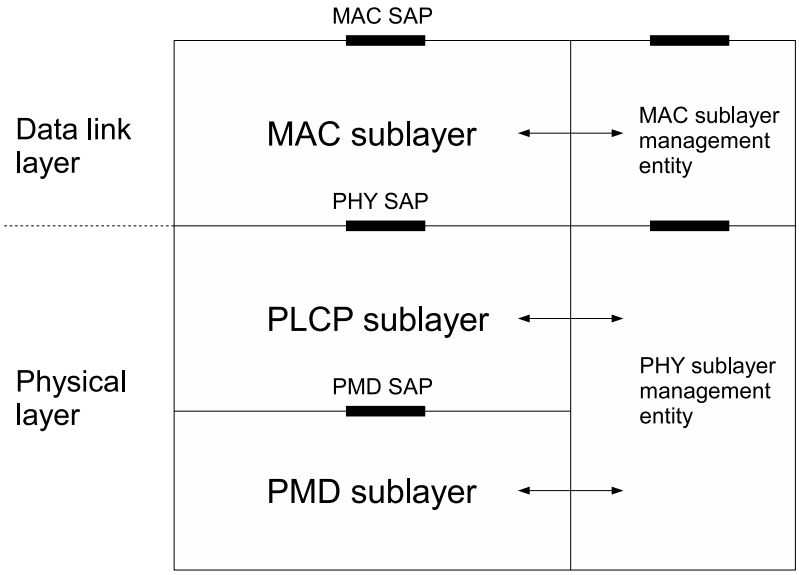

Figure 3.2: Schematic representation of PHY and MAC layers of IEEE 802.11p

physical medium dependent (PMD) system. This procedure is called the PHY convergence function, offered by the PHY layer. In this way the IEEE 802.11 MAC layer operates with minimum dependence on the PMD sub-layer;

2. a PMD system whose function defines the characteristics and methods of transmitting and receiving data through a wireless medium between two or more stations. The service of a layer or sub-layer is the set of capabilities that it offers to a user in the next higher layer. In this case the PHY services are offered to the MAC sub-layer, which is intended to be PHY independent.

The PLCP sub-layer converts a PHY sub-layer service data unit (PSDU) to a PLCP protocol data unit (PPDU), and a PPDU to a PSDU. In transmission, the PSDU received from the MAC sub-layer shall be provided with a PLCP preamble

and header to create the PPDU. At the receiver, the PLCP preamble and header of the PPDU are processed to aid the demodulation and the delivery of the PSDU. The structure of the PHY layer is shown in figure 3.2.

PLCP frame format The PLCP frame is composed of the OFDM PLCP preamble, the OFDM PLCP header, the PSDU provided by the MAC, tail bits, and pad bits as shown in figure 3.3. The PLCP preamble is used for synchronization, the PLCP header contains informations used for the correct interpretation of data as the fields LENGTH and RATE, the PSDU unit contains the transmitted data payload.

PLCP preamble At the receiver, the preamble is used for the synchronization task. In IEEE 802.11p the PLCP preamble is composed of a short training sequence (STS) composed of 10 short training symbols $t_1, \cdots, t_{10}$ and a long training sequence (LTS) composed by two OFDM symbols. Both STS and LTS are known at the receiver. The total training length is $16\mu s$ and $32\mu s$ respectively if the bandwidth is B = 20 MHz or B = 10 MHz.

During STS reception Automatic gain control (AGC) and signal detection are performed, they are usually completed after a random time. Then, the STS can be only partially exploited for the synchronization task. Typically the first 4 or 5 short training symbols are not available for the system synchronization. A short OFDM training symbol consists of 12 sub-carriers, which are modulated by the elements of the sequence S, given by

$$\begin{aligned} S_{1,52} = \sqrt{13/6}\{&0,0,1+j,0,0,0,-1-j,0,0,0,1+j,0,0,0,-1-j,\\ &0,0,0,-1-j,0,0,0,1+j,0,0,0,0,0,0,0,-1-j,0,0,0,-1-j,0,\\ &0,0,1+j,0,0,0,1+j,0,0,0,1+j,0,0,0,1+j,0,0\} \end{aligned} \quad (3.1)$$

where the factor $\sqrt{13/6}$ is used to normalize the average power of the resulting OFDM symbol, which utilizes 12 out of 52 sub-carriers. Each short training symbol has a duration of $0.8\mu s$ if the bandwidth is B = 20 MHz or $1.6\mu s$ if the bandwidth is B = 10 MHz.

The two OFDM training symbols that compose the LTS are used to perform CE and to improve synchronization accuracy. The two long training symbols are

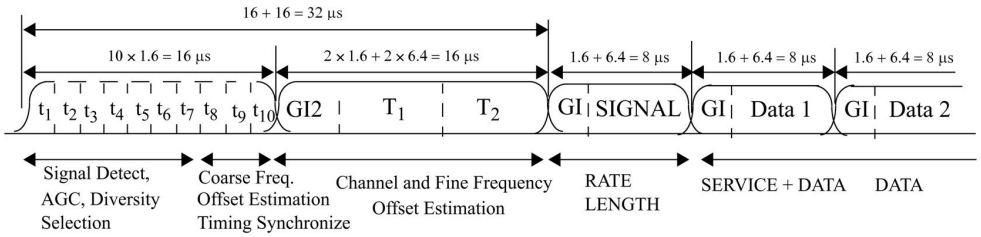

Figure 3.3: IEEE 802.11p packet frame, ©IEEE 1999.

obtained using all 52 data sub-carriers, which are modulated by the elements of the sequence L, given by

$$\begin{aligned} L_{1,52} = \{&1,1,-1,-1,1,1,-1,1,-1,1,1,1,1,1,1,-1,-1,1,1,-1,\\ &1,-1,1,1,1,1,1,-1,-1,1,1,-1,1,-1,1,-1,-1,-1,-1,-1,1,1,-1,\\ &-1,1,-1,1,-1,1,1,1,1\} \end{aligned} \quad (3.2)$$

The total duration of the LTS is $T_{LTS} = 2 * 1.6 + 2 * 6.4 = 16\mu s$ if the bandwidth is B = 10 MHz, where $1.6\mu s$ is the duration of the GI added to the LTS symbols as shown in figure 3.3.

PLCP header and PSDU structure In the PLCP header are included several fields to be used for the correct interpretation of data. It contains the following fields: LENGTH, RATE, a reserved bit, an even parity bit, and the SERVICE field. The RATE and LENGTH fields, reserved bit, and parity bit (with 6 zero tail bits appended) constitute the symbol called SIGNAL. It is one OFDM symbol of length $M = 64$ that is cyclically extended with a GI of length $L_{cp} = 16$, and it is transmitted with the most robust combination of BPSK modulation and a coding rate of 1/2.

The SERVICE field and the PSDU, which are denoted as DATA, are transmitted at the data rate described in the RATE field. They may be composed by multiple OFDM consecutive symbols, and each symbol is cyclically extended with a guard interval. SERVICE is a 16 bit field. The first six bits are set to zero, and they are used to synchronize the descrambler at receiver. The remaining 9 bits shall be reserved for future use.

The PPDU tail bit field contains six zero bits. With this field the convolutional encoder can return to the zero state. This procedure can improve the error prob-

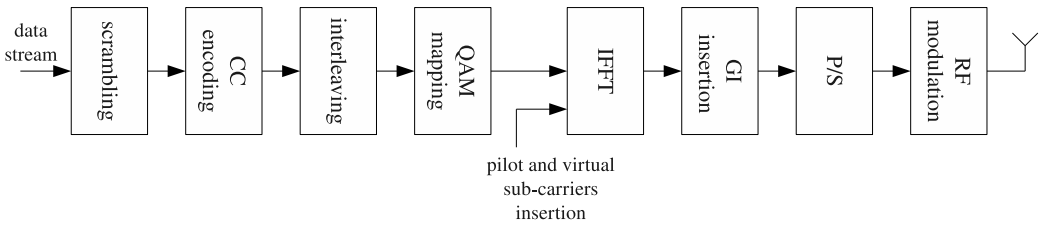

Figure 3.4: Block diagram of the IEEE 802.11p transmitter

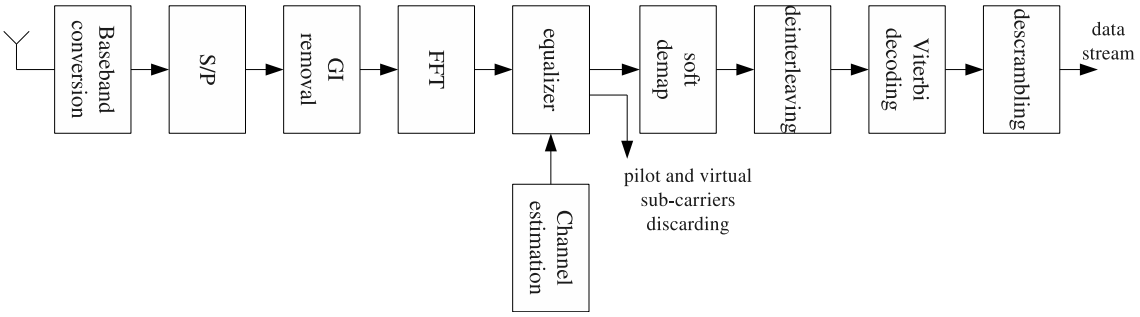

Figure 3.5: Block diagram of the IEEE 802.11p receiver

ability of the convolutional decoder, which relies on future bits when decoding and which may be not be available past the end of the message [3].

The number of bits in the DATA field has to be a multiple of the number of coded bits in an OFDM symbol, that is 48, 96, 192, or 288 bits as shown in tables 3.1 and 3.2. The length of the message is then extended in order to become a multiple of the number of data bits per OFDM symbol. The tail bits are always appended to the message, and thus and the number of padding bits are computed taking into account the PSDU length.

PPDU generation process The PPDU generation process is summarized below through the following steps as described in [4]. The transmitter and receiver block diagrams are shown in figures 3.4 and 3.5.

(a) Produce the PLCP preamble made of the ten repetitions of the STS and two repetitions of the LTS preceded by a GI as described above.

(b) Generate the PLCP header field with the RATE, LENGTH, and SERVICE fields. Encode the SIGNAL field with the convolutional encoder with rare 1/2, perform interleaving, BPSK modulation, pilot insertion, Fourier transform, and pre-pending a GI. The content of the SIGNAL field is not scrambled.

(c) Calculate, from the data rate, the number of data bits per OFDM symbol, the coding rate, the number of bits in each OFDM sub-carrier N_{BPSC} and the number of coded bits per OFDM symbol N_{CBPS}.

(d) Append the PSDU to the SERVICE field. Append to the resulting bit sequence zero bits so that the resulting length will be a multiple of the number of data bits per OFDM symbol. The resulting sequence represents the DATA part of the packet.

(e) Initiate the scrambler with a pseudo-random non-zero seed. Generate a scrambling sequence, and XOR it with the data bits obtained from the previous step.

(f) Replace the six scrambled zero bits following the data with six non scrambled zero bits; this allow the convolutional encoder to return to the zero state.

(g) Encode the scrambled data bits with a convolutional encoder with coding rate 1/2. Some of the encoder output bits are omitted to reach the desired code rate. They are chosen according to a given puncturing pattern.

(h) Divide the encoded bit sequence into blocks of N_{CBPS} bits. Perform for each group an interleaving, or permutation, of the bits according to a rule corresponding to the desired RATE.

(i) Convert each group of N_{CBPS} bits into a complex symbol according to the modulation maps (see figure 3.10) .

(j) Divide the complex symbols obtained into groups of 48 elements. Each of such groups is associated with one OFDM symbol, and in each group, the complex symbols are numbered 0 to 47 and mapped into OFDM sub-carriers numbered 2 to 7, 9 to 21, 23 to 27, 39 to 43, 45 to 57, and 59 to 64.

(k) Four sub-carriers with indexes 8, 22, 44, and 58 are used for inserting pilot symbols so that the total number of sub-carriers is then 52.

(l) Convert the symbols loaded on data and pilot sub-carriers to time domain using inverse Fourier transform. It is prepended to the Fourier-transformed waveform a circular extension of itself thus forming a GI, and truncate the resulting periodic waveform to a single OFDM symbol length by applying time domain windowing.

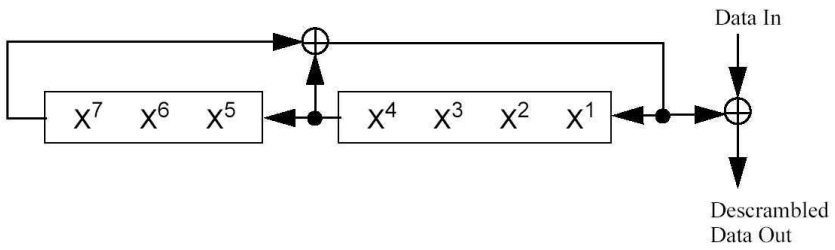

Figure 3.6: Data scrambler

(m) Concatenate the OFDM data symbols one after the other, starting after the SIGNAL symbol describing the RATE and LENGTH.

(n) Up-convert the complex baseband waveform obtained to an RF frequency according to the center frequency of the desired channel and transmit.

3.2.4 Scrambling, coding, interleaving and mapping

In the following the procedures of scrambling, encoding, interleaving and mapping for the SIGNAL and DATA symbols for IEEE 802.11p will be described.

Scrambler A scrambler is a device that transposes or inverts bits, or, otherwise, encodes a bit sequence, at the transmitter to make the message unintelligible at any receiver that is not equipped with the appropriately descrambling device.

The DATA field of the PHY packet shall be scrambled with a length-127 frame-synchronous scrambler [3]. Octets of the PSDU are placed in the transmit serial bit stream, bit 0 in the first position and bit 7 as last. The frame synchronous scrambler uses the following generator polynomial

$$S(x) = x^7 + x^4 + 1 \tag{3.3}$$

and the 127-bit sequence cyclically generated shall be (leftmost used first)

00001110 11110010 11001001 00000010 00100110 00101110 10110110 00001100
11010100 11100111 10110100 00101010 11111010 01010001 10111000 1111111, (3.4)

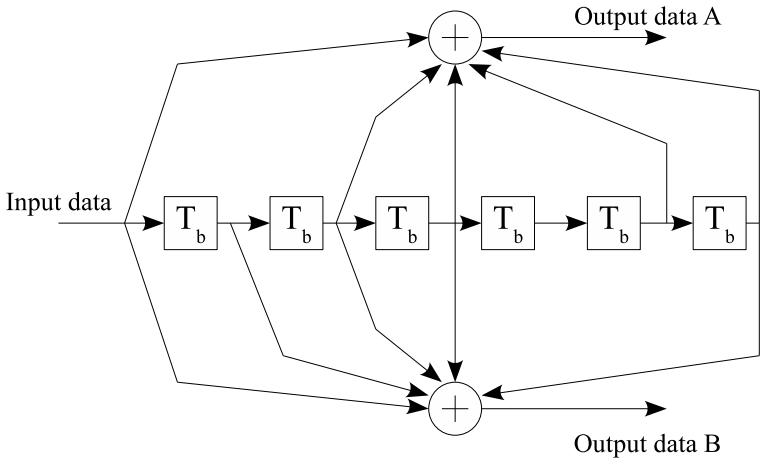

Figure 3.7: Convolutional encoder

when an initial state with all ones is used.

The data scrambler structure is showed in figure 3.6. When a transmission occurs, the initial state of the scrambler is set to a pseudo random non-zero state. The first seven bits of the SERVICE field are set to all zeros, prior to scrambling, in order to enable an estimation of the initial state of the scrambler at the receiver side.

Convolutional encoder The DATA field in the PHY packet is coded with a convolutional encoder of coding rate 1/2, 2/3, or 3/4, corresponding to the desired data rate. The convolutional encoder is showed in Figure 3.7. It uses the industry-standard generator polynomials $g_0 = 1011011$ and $g_1 = 1111001$, or, in octal representation, $g_0 = 133_8$ and $g_1 = 171_8$, of rate 1/2. The bit denoted as 'A' shall be output from the encoder before the bit denoted as 'B'.

Starting from a coding rate of 1/2, higher rates as 2/3 and 3/4 can be obtained by transmitting only some of the encoded bits. This procedure, called puncturing, is performed according to a specific puncturing matrix. At the receiver, dummy zeros are inserted into the convolutional decoder in place of the deleted bits. An example of the bit-stealing and bit-insertion procedure, in order to obtain a code rate of 2/3 and 3/4, is provided in [4] and shown in figures 3.8 and 3.9. At the receiver decoding using the Viterbi algorithm is a widely adopted technique.

Interleaver Interleaving is a widely used technique to protect transmissions against burst errors. Independently from the interleaving, the data flow is transmitted

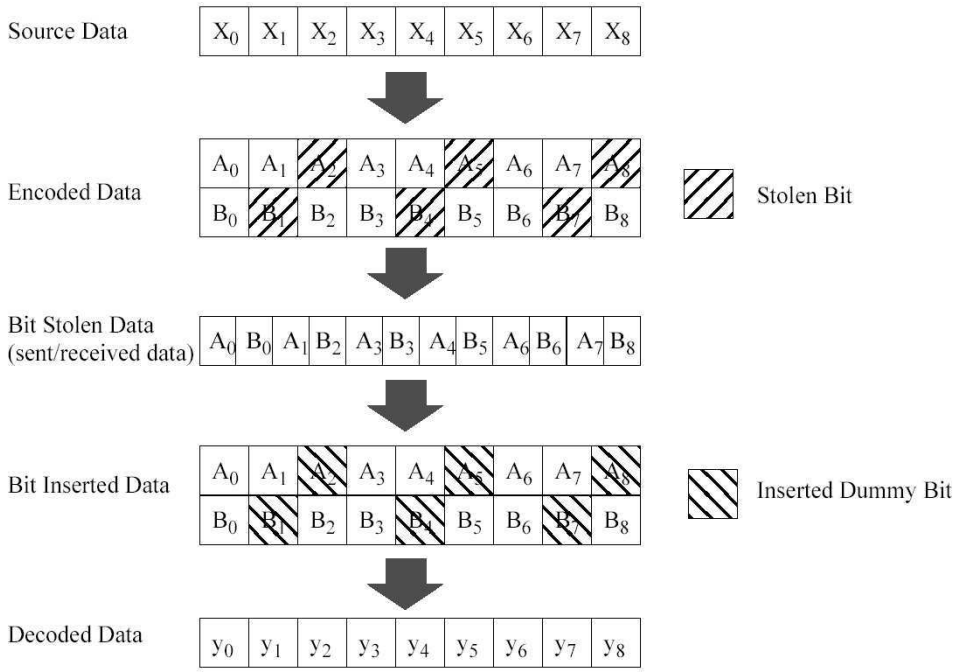

Figure 3.8: Puncturing procedure for rate R = 3/4, ©IEEE 1999.

with some redundant bits obtained after encoding that enable the decoder to correct a given number of altered bits, depending on the error-correcting code used. If a burst error occurs, resulting in a number of altered bits that is greater than the correction capability of the code, then the codeword can not be correctly decoded.

In [3], the interleaver is defined by two permutations, and all the encoded data bits provided by the convolutional encoder are interleaved by a block interleaver with a block size corresponding to the number of coded bits in a single OFDM symbol, N_{CBPS}. The first permutation of the interleaver guarantees that adjacent coded bits are mapped onto nonadjacent sub-carriers. The second ensures that adjacent coded bits are mapped alternately onto less and more significant bits of the constellation and, thereby, long runs of low reliability bits are avoided.

Let k be the index of the coded bit before the first permutation, i the index after the first and before the second permutation and j the index after the second permutation, just prior to modulation mapping. The first permutation is defined by the rule:

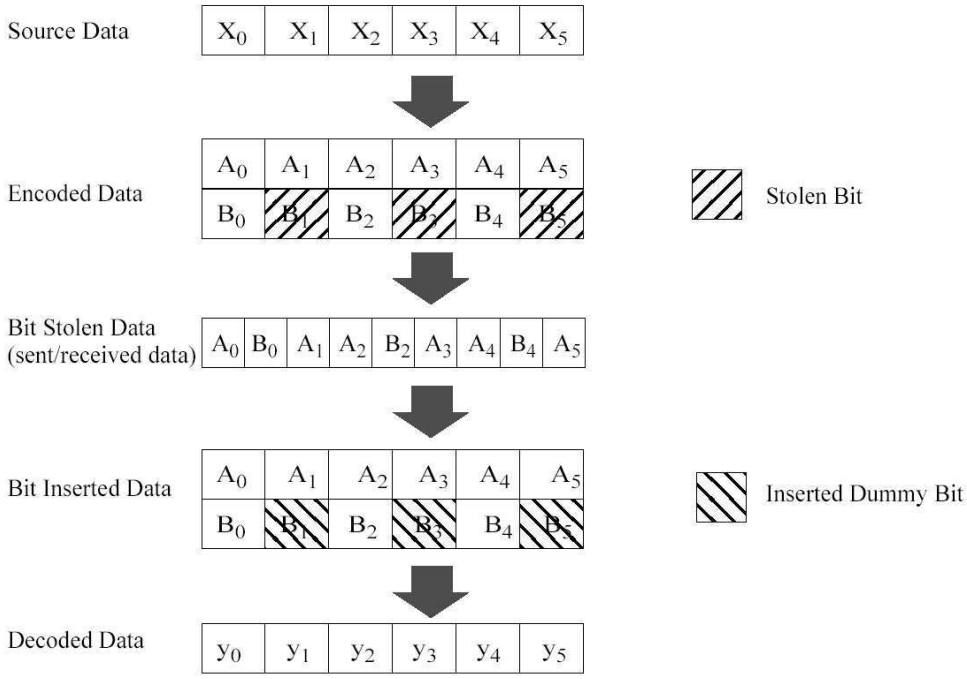

Figure 3.9: Puncturing procedure for rate R = 2/3, ©IEEE 1999.

$$i = \frac{N_{CBPS}}{16}(k \mod 16) + \left\lfloor \frac{k}{16} \right\rfloor, \quad k = 0, 1, \ldots, N_{CBPS} - 1 \tag{3.5}$$

and the second is defined by

$$j = s \cdot \left\lfloor \frac{i}{s} \right\rfloor + \left(i + N_{CBPS} - \left\lfloor 16 \frac{i}{N_{CBPS}} \right\rfloor \right) \mod s, \quad i = 0, 1, \ldots, N_{CBPS} - 1 \tag{3.6}$$

where N_{BPSC} is the number of coded bits per sub-carrier and s is given by $s = max(N_{BPSC}/2, 1)$.

The deinterleaver performs the inverse operation, also composed of two steps. Here, let j be the index of the received bit before the first permutation, i the index between the permutations, and k the index after the second permutation, before the coded bits are passed to the convolutional decoder. The first permutation is:

$$i = s \cdot \left\lfloor \frac{j}{s} \right\rfloor + \left(j + \left\lfloor 16 \frac{j}{N_{CBPS}} \right\rfloor \right) \mod s, \quad j = 0, 1, \ldots, N_{CBPS} - 1 \tag{3.7}$$

where s is given by $s = max(N_{BPSC}/2, 1)$ and the second permutation is:

Modulation	K_{MOD}
BPSK	1
QPSK	$1/\sqrt{2}$
16-QAM	$1/\sqrt{10}$
64-QAM	$1/\sqrt{42}$

Table 3.5: Modulation dependent normalization factor

$$k = 16 \cdot i - (N_{CBPS} - 1) \left\lfloor 16 \frac{i}{N_{CBPS}} \right\rfloor \qquad i = 0, 1, \ldots, N_{CBPS} - 1 \tag{3.8}$$

Subcarrier modulation mapping The encoded and interleaved bits are divided into groups of N_{BPSC} bits (equal to 1, 2, 4, or 6 as shown in Table 3.1) and converted into complex symbols representing BPSK, QPSK, 16-QAM, or 64-QAM constellation points. The modulation type is chosen depending on the requested transmission rate. The conversion into the constellation symbols is performed according to Gray-coded mapping as illustrated in figure 3.10. In order to obtain an equal average power for all mappings, the complex constellation points (I+jQ) are multiplied by a normalization factor K_{MOD}. The output values, B, are given by

$$B = (I + jQ) \times K_{MOD} \tag{3.9}$$

where K_{MOD} depends on the modulation and can assume the values reported in table 3.5.

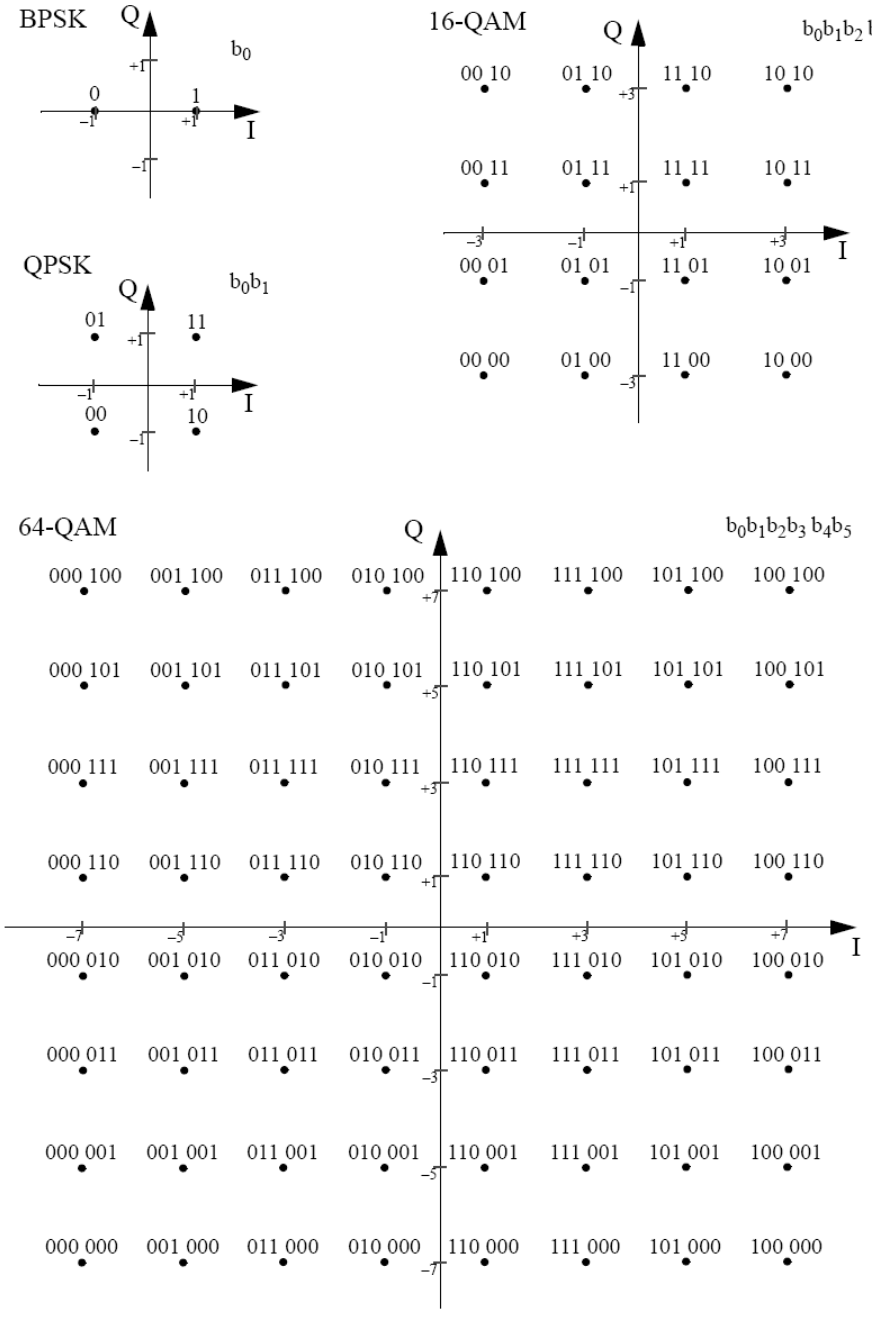

Figure 3.10: PSK, QPSK, 16-QAM, and 64-QAM constellation bit encoding, ©IEEE 1999.

Parameter	supported values
Bandwidth B	$10, 20$ MHz
Data rates	$3, \ldots, 27$ Mbps (for $B = 10$ MHz) $6, \ldots, 54$ Mbps (for $B = 20$ MHz)
Channel model	ETSI A, B, C, D, E with Jakes Doppler
CIR length	ideal knowledge or estimated
Channel estimation	ideal, TD-LS, TD-LS RR, modified-RR
DDCE	ideal, no tracking, iterative FEC aided, non-iterative FEC aided

Table 3.6: Simulator supported options

3.2.5 Implemented MATLAB model of IEEE 802.11p

The analysis and simulations presented in the following chapters have been obtained with a MATLAB chain that implements the last draft version of the IEEE 802.11p standard [3].

The simulator implements:

- the equivalent baseband transmitter compliant with [3] as described in the previous section; in particular the whole set of data rates available in IEEE 802.11p is supported;
- the discrete-time wireless channel simulator, in particular the ETSI models with Doppler effect presented in section 1.2.2 for the equivalent baseband discrete time-varying frequency selective wireless channel have been implemented;
- the equivalent baseband receiver as shown in the block diagram of figure 3.5 with perfect and real timing and frequency synchronizations. Moreover ideal and several real CE options have been modeled; these estimation algorithms are described in more details in section 4.1;
- the addition of the decision directed CE algorithms described in chapter 5.

The supported simulator options are summarized in table 3.6. Other important simulation parameters that can be specified by the user are: packet length, relative speed, SNR at the receiver, frequency offset.

Chapter 4

Channel estimation algorithms for OFDM systems

4.1 Channel estimation algorithms

The previous chapters reported a description of the wireless channel theory and the OFDM systems and the related equalization techniques, described assuming CIR (or equivalently CFR) known at the receiver. The CIR must be estimated in real systems.

This chapter describes a summary of the main channel estimation (CE) algorithms for OFDM systems.

The CE algorithms for OFDM systems can be divided into two main classes:

- *Blind techniques*, that are based only on the received data and statistically estimate the channel behavior without any further knowledge;
- *non-blind techniques*, which perform the CE task using the knowledge of previous channel estimations or some portion of transmitted data.

Blind algorithms The blind estimation techniques typically perform the CE by considering the second order statistics of the received data without any a priori knowledge of pilot symbols or previous channel estimates. Their main advantage is their high spectral efficiency, because there is no need to transmit extra data symbols for training purpose. The main drawback is the estimation long convergence time because of the long time required to achieve reliable estimated second order statistics of the received data [9], [10].

Non-blind algorithms The non-blind CE techniques exploit the knowledge at the receiver of ad-hoc transmitted data such as pilot symbols or training sequences. The a-priori knowledge of given transmitted data sequences makes the estimation task easier and faster than the blind approach. The main drawback is the consequent reduction of the spectral efficiency.

In literature *semi-blind* algorithms are also present; they make simultaneously use of both blind and non-blind approaches: in [11] a periodic sequence of pilot symbols and the first-order statistic of the time-domain received symbols are used to estimate the frequency-selective channel in OFDM systems.

Popular wireless OFDM applications foresee the transmission of a "preamble" composed of proper training sequences for CE purpose. This is also the case of IEEE 802.11p [3], that specifies the presence of the initial STS and LTS inside the PLCP preamble and of the pilot symbols inside the SIGNAL and DATA symbols, as described in section 3.2.3. For this reason the following sections are devoted to the main non-blind CE algorithms for OFDM systems.

4.1.1 Least Square channel estimation

The first basic non-blind CE technique investigated is the Least Square (LS) method. Assuming perfect time and frequency synchronization, the corresponding $M \times 1$ received symbol $\mathbf{Y}$ is:

$$\mathbf{Y} = \mathbf{AH} + \mathbf{W} = \mathbf{AF}_M\mathbf{h} + \mathbf{W} \tag{4.1}$$

where $\mathbf{A}$ is the diagonal $M \times M$ matrix of the training symbol, $\mathbf{h}$ is the $M \times 1$ CIR, $\mathbf{H}$ is the $M \times 1$ CFR, $\mathbf{F}_M$ is the $M \times M$ square DFT matrix defined in 1.2.1 and $\mathbf{W}$ is the $M \times 1$ AWGN vector with variance N_0. The time instant subscript has been omitted for notation simplicity uas we refer to the training sequence symbol only.

Considering a negligible noise contribution, the LS estimate of $\mathbf{H}$ is $\widehat{\mathbf{H}}_{LS}$ such that:

$$\widehat{\mathbf{H}}_{LS} = \min_{\widehat{\mathbf{H}}} \|\mathbf{Y} - \mathbf{A}\widehat{\mathbf{H}}_{LS}\|^2 \tag{4.2}$$

The solution of 4.2 is the $M \times 1$ vector given by:

$$\widehat{\mathbf{H}}_{LS} = \mathbf{A}^{-1}\mathbf{Y} = \mathbf{H} + \mathbf{A}^{-1}\mathbf{W} \tag{4.3}$$

It should be noted that $\mathbf{A}$ includes only the M non-zero data symbols and as such the matrix inversion $\mathbf{A}^{-1}$ is possible. It results that the LS frequency-domain estimate of $\mathbf{H}$ is performed only on the M data sub-carriers.

The related time-domain LS (TD-LS) estimation can be performed through the IDFT of $\widehat{\mathbf{H}}_{LS}$:

$$\widehat{\mathbf{h}}_{LS} = \mathbf{F}_M^{-1}\widehat{\mathbf{H}}_{LS} \tag{4.4}$$

with $\widehat{\mathbf{h}}_{LS} \in \mathbb{C}^{M\times 1}$.

The estimation error for the $m-$th sub-carrier is zero-mean with statistical power:

$$\sigma^2_{H_{LS},m} = \mathrm{E}\left[\left|\widehat{H}_{LS,m} - H_m\right|^2\right] = \mathrm{E}\left[\left|A_m^{-1}W_m\right|^2\right] = \frac{N_0}{|A_{m,m}|^2} \tag{4.5}$$

where the data $\mathbf{A}$ are known a priori and are independent of noise $\mathbf{W}$. The variance of the estimation error (4.5) of the $m-$th sub-channel results the inverse of the signal-to-noise ratio (SNR) of the $m-$th sub-channel.

The comprehensive mean square error (MSE) is given by the sum of the MSE for every sub-carrier. It results equal to the inverse of the SNR seen at the receiver, having the white noise and the constant energy of the training sequence $\mathbf{A}$ for every sub-channel, i.e.:

$$MSE_{LS} = \sum_{m=1}^{M} \sigma^2_{H_{LS},m} = \frac{1}{SNR}. \tag{4.6}$$

4.1.2 TD-LS reduced rank channel estimation

An improvement to the basic TD-LS estimator is based on the fact that channel impulse response (CIR) length $r = L_{ch}$ is typically much shorter than M and within the cyclic prefix duration L_{cp}. Under the assumption of knowing r the TD-LS reduced-rank (RR) channel estimator [15] is $\widehat{\mathbf{h}}_{r,RR}$ such as:

$$\widehat{\mathbf{h}}_{r,RR} = \min_{\widehat{\mathbf{h}}_r} \|\mathbf{Y} - \mathbf{A}\mathbf{F}_r\widehat{\mathbf{h}}_r\|^2 \tag{4.7}$$

where $\mathbf{F}_r \in \mathbb{C}^{M\times r}$ is the *Reduced-Rank* $M \times r$ Fourier Matrix obtained from the $M \times M$ DFT matrix where the last $M - r$ columns have been discarded. It must be noticed that the M rows of the reduced-rank DFT matrix $\mathbf{F}_r$ are the rows corresponding to the used sub-channels as reported in table 3.4. It results that for [3] the indexes corresponding to the virtual sub-carriers are not included in the matrix $\mathbf{F}_r$. The solution to (4.7) is the $r \times 1$ vector [15]:

$$\widehat{\mathbf{h}}_{r,RR} = (\mathbf{A}\mathbf{F}_r)^+ \mathbf{Y} = \left(\mathbf{F}_r^H \mathbf{A}^H \mathbf{A}\mathbf{F}_r\right)^{-1} \mathbf{F}_r^H \left(\mathbf{A}^H \mathbf{Y}\right). \tag{4.8}$$

In (4.8) $(\cdot)^+$ denotes the Moose-Penrose pseudo-inverse operator: $\mathbf{F}_r^+ = (\mathbf{F}_r\mathbf{F}_r^H)^{-1}\mathbf{F}_r$. From (4.8) it results that the estimated frequency response $\widehat{\mathbf{H}}_{r,RR} \in \mathbb{C}^{M\times 1}$ is:

$$\widehat{\mathbf{H}}_{r,RR} = \mathbf{F}_r \left(\mathbf{F}_r^H \mathbf{A}^H \mathbf{A}\mathbf{F}_r\right)^{-1} \mathbf{F}_r^H \left(\mathbf{A}^H \mathbf{Y}\right). \tag{4.9}$$

The estimation error of $\widehat{\mathbf{h}}_{r,RR}$ will be derived below, as it is useful for the Doppler estimation algorithms described in chapter 6. Being r the channel length, the CIR $\mathbf{h}$ is a $r \times 1$ vector. For the following derivation the matrix $\mathbf{Q} \in \mathbb{C}^{r\times r}$ has been defined as $\mathbf{Q} = (\mathbf{F}_r^H \mathbf{A}^H \mathbf{A}\mathbf{F}_r)$. The $r \times r$ autocorrelation matrix of the estimation error $\mathbf{R}_{RR} = \mathrm{E}[(\widehat{\mathbf{h}}_{\mathbf{r,RR}} - \mathbf{h})(\widehat{\mathbf{h}}_{\mathbf{r,RR}} - \mathbf{h})^H]$ results:

$$\begin{aligned}
\mathbf{R}_{e_{RR}} &= \mathrm{E}[(\widehat{\mathbf{h}}_{\mathbf{r,RR}} - \mathbf{h})(\widehat{\mathbf{h}}_{\mathbf{r,RR}} - \mathbf{h})^H] \\
&= \mathrm{E}[(\mathbf{Q}^{-\mathbf{1}}\mathbf{F}_r^H \mathbf{A}^H \mathbf{Y} - \mathbf{h})(\mathbf{Q}^{-\mathbf{1}}\mathbf{F}_r^H \mathbf{A}^H \mathbf{Y} - \mathbf{h})^H] \\
&= \mathrm{E}[(\mathbf{Q}^{-\mathbf{1}}\mathbf{F}_r^H \mathbf{A}^H (\mathbf{A}\mathbf{H} + \mathbf{W}) - \mathbf{h})(\mathbf{Q}^{-\mathbf{1}}\mathbf{F}_r^H \mathbf{A}^H (\mathbf{A}\mathbf{H} + \mathbf{W}) - \mathbf{h})^H].
\end{aligned} \tag{4.10}$$

The first factor of the argument of expectation can be simplified as:

$$\begin{aligned}
\mathbf{Q}^{-\mathbf{1}}\mathbf{F}_r^H \mathbf{A}^H (\mathbf{A}\mathbf{H} + \mathbf{W}) - \mathbf{h} &= (\mathbf{F}_r^H \mathbf{A}^H \mathbf{A}\mathbf{F}_r)^{-1}\mathbf{F}_r^H \mathbf{A}^H \mathbf{A}\mathbf{H} - \mathbf{h} + \mathbf{Q}^{-1}\mathbf{F}_r^H \mathbf{A}^H \mathbf{W} \\
&= \mathbf{Q}^{-1}\mathbf{F}_r^H \mathbf{A}^H \mathbf{A}(\mathbf{F}_r\mathbf{h}) - \mathbf{h} + \mathbf{Q}^{-1}\mathbf{F}_r^H \mathbf{A}^H \mathbf{W} \\
&= \mathbf{Q}^{-1}\mathbf{Q}\mathbf{h} - \mathbf{h} + \mathbf{Q}^{-1}\mathbf{F}_r^H \mathbf{A}^H \mathbf{W} \\
&= \mathbf{h} - \mathbf{h} + \mathbf{Q}^{-1}\mathbf{F}_r^H \mathbf{A}^H \mathbf{W} \\
&= \mathbf{Q}^{-1}\mathbf{F}_r^H \mathbf{A}^H \mathbf{W}
\end{aligned} \tag{4.11}$$

Inserting (4.11) into (4.10) the autocorrelation matrix estimation error becomes:

$$\begin{aligned}
\mathbf{R}_{e_{RR}} &= \mathrm{E}[(\mathbf{Q}^{-1}\mathbf{F}_r^H \mathbf{A}^H \mathbf{W})(\mathbf{Q}^{-1}\mathbf{F}_r^H \mathbf{A}^H \mathbf{W})^H] \\
&= \mathrm{E}[\mathbf{Q}^{-1}\mathbf{F}_r^H \mathbf{A}^H \mathbf{W}\mathbf{W}^H \mathbf{A}\mathbf{F}_r(\mathbf{Q}^{-1})^H] \\
&= \mathbf{Q}^{-1}\mathbf{F}_r^H \mathbf{A}^H \,\mathrm{E}[\mathbf{W}\mathbf{W}^H]\mathbf{A}\mathbf{F}_r(\mathbf{Q}^{-1})^H \\
&= \mathbf{Q}^{-1}\mathbf{F}_r^H \mathbf{A}^H (N_0\mathbf{I})\mathbf{A}\mathbf{F}_r(\mathbf{Q}^{-1})^H \\
&= N_0\mathbf{Q}^{-1}(\mathbf{F}_r^H \mathbf{A}^H \mathbf{A}\mathbf{F}_r)(\mathbf{Q}^{-1})^H \\
&= N_0\mathbf{Q}^{-1}\mathbf{Q}(\mathbf{Q}^{-1})^H \\
&= N_0(\mathbf{Q}^{-1})^H
\end{aligned} \tag{4.12}$$

where $\mathbf{I}_M$ is the $M \times M$ identity matrix. It should be noted that $\mathbf{A}$, being the known diagonal matrix of the training sequence, has been brought out of the expectation as $\mathbf{F}_r$.

The MSE of the $l-$th tap is given by the $l-$th diagonal element of $R_{e_{RR}}$, i.e.:

$$\sigma^2_{h_{RR,l}} = N_0 \, (Q^{-1})^H\big|_{l,l} \tag{4.13}$$

where $(Q^{-1})^H\big|_{l,l}$ is the $(l,l)-$th element of the Hermitian of the matrix $\mathbf{Q}^{-1}$.

The overall MSE of the time-domain reduced-rank estimator is:

$$MSE_{RR} = \sum_{l=0}^{L_{ch}-1} \sigma^2_{h_{RR,l}} = N_0 \sum_{l=0}^{L_{ch}-1} (Q^{-1})^H\big|_{l,l} = N_0 \, \mathrm{trace}(\mathbf{Q}^{-1}). \tag{4.14}$$

4.1.3 Modified reduced rank LS channel estimation

In [15] a simplified version of the TD-LS RR channel estimator is also described. The estimator (4.8) requires a matrix inversion for every different OFDM symbol $\mathbf{A}$.

The proposed simplified method finds $\widehat{\mathbf{h}}_{LS2}$ such that:

$$\widehat{\mathbf{h}}_{LS2} = \min_{\widehat{\mathbf{h}}} \|\widehat{\mathbf{H}}_{\mathbf{LS}} - \mathbf{F}_r \widehat{\mathbf{h}}\|^2 \tag{4.15}$$

where $\widehat{\mathbf{H}}_{\mathbf{LS}}$ is given by (4.3). The estimated channel impulse response $\widehat{\mathbf{h}}_{LS2} \in \mathbb{C}^{r \times 1}$ is:

$$\widehat{\mathbf{h}}_{LS2} = \mathbf{F}_r^+ \widehat{\mathbf{H}}_{LS} = \mathbf{F}_r^+ (\mathbf{A}^{-1}\mathbf{Y}) \tag{4.16}$$

and the related frequency response is:

$$\widehat{\mathbf{H}}_{LS2} = \mathbf{F}_r \mathbf{F}_r^+ \widehat{\mathbf{H}}_{LS} = \mathbf{F}_r^+ (\mathbf{A}^{-1}\mathbf{Y}) \tag{4.17}$$

Also in this case the CE error has been evaluated as useful for the Doppler estimation algorithms reported in chapter 6. The derivation of the autocorrelation

matrix $\mathbf{R}_{e_{LS2}}$ is given by:

$$\begin{aligned}
\mathbf{R}_{e_{LS2}} &= \mathrm{E}[(\widehat{\mathbf{h}}_{\mathbf{LS2}} - \mathbf{h})(\widehat{\mathbf{h}}_{\mathbf{LS2}} - \mathbf{h})^H] \\
&= \mathrm{E}[(\mathbf{F}_r^+(\mathbf{A}^{-1}\mathbf{Y}) - \mathbf{h})(\mathbf{F}_r^+(\mathbf{A}^{-1}\mathbf{Y}) - \mathbf{h})^H] \\
&= \mathrm{E}[(\mathbf{F}_r^+\mathbf{A}^{-1}(\mathbf{A}\mathbf{H} + \mathbf{W}) - \mathbf{h})(\mathbf{F}_r^+\mathbf{A}^{-1}(\mathbf{A}\mathbf{H} + \mathbf{W}) - \mathbf{h})^H] \\
&= \mathrm{E}[(\mathbf{F}_r^+\mathbf{H} - \mathbf{h} + \mathbf{F}_r^+\mathbf{A}^{-1}\mathbf{W})(\mathbf{F}_r^+\mathbf{H} - \mathbf{h} + \mathbf{F}_r^+\mathbf{A}^{-1}\mathbf{W})^H] \\
&= \mathrm{E}[(\mathbf{F}_r^+\mathbf{A}^{-1}\mathbf{W})(\mathbf{F}_r^+\mathbf{A}^{-1}\mathbf{W})^H] \\
&= \mathrm{E}[\mathbf{F}_r^+\mathbf{A}^{-1}\mathbf{W}\mathbf{W}^H(\mathbf{A}^{-1})^H(\mathbf{F}_r^+)^H] \\
&= \mathbf{F}_r^+\mathbf{A}^{-1}\,\mathrm{E}[\mathbf{W}\mathbf{W}^H](\mathbf{A}^{-1})^H(\mathbf{F}_r^+)^H \\
&= \mathbf{F}_r^+\mathbf{A}^{-1}(N_0\mathbf{I}_M)(\mathbf{A}^{-1})^H(\mathbf{F}_r^+)^H \\
&= N_0\left(\mathbf{F}_r^+\mathbf{A}^{-1}(\mathbf{A}^-)^H(\mathbf{F}_r^+)^H\right).
\end{aligned} \tag{4.18}$$

As for the derivation of the estimation error of the TD-LS RR estimator, $\mathbf{A}$ is the known diagonal matrix of the training sequence and has been brought out of the expectation, as $\mathbf{F}_r$. Moreover $(\mathbf{F}_r^+)^H$ denotes the Hermitian of the Pseudo-inverse of the reduced-rank $M \times r$ DFT matrix F.

The MSE of the $l-$th tap is given by the $l-$th diagonal element of $R_{e_{LS2}}$, i.e.:

$$\sigma^2_{h_{LS2,l}} = N_0\left(\mathbf{F}_r^+\mathbf{A}^{-1}(\mathbf{A}^{-1})^H(\mathbf{F}_r^+)^H\right)\Big|_{(l,l)}. \tag{4.19}$$

The overall MSE for the Modified TD-LS RR channel estimator is given by

$$MSE_{LS2} = \sum_{l=0}^{L_{ch}-1}\sigma^2_{h_{LS2,l}} = N_0\sum_{l=0}^{L_{ch}-1}\left(\mathbf{F}_r^+\mathbf{A}^{-1}(\mathbf{A}^{-1})^H(\mathbf{F}_r^+)^H\right)\Big|_{(l,l)} \tag{4.20}$$

4.1.4 MMSE channel estimation

The Minimum Mean Square Error (MMSE) channel estimator is based on the further knowledge of the second-order statistical description of the channel, in addition to the training sequence $\mathbf{A}$. This means that the receiver perfectly knows the PDP of the channel, i.e. the variance of every channel tap $\sigma^2_{h_l}$, $l = 0, \ldots, L_{ch} - 1$, and the noise variance N_0. The MMSE estimation $\widehat{\mathbf{h}}_{MMSE}$ of the channel impulse response is given by [1]:

$$\widehat{\mathbf{h}}_{MMSE} = \mathbf{R}_{\mathbf{hY}}{}^T\mathbf{R}_{\mathbf{YY}}{}^{-1}\mathbf{Y} \tag{4.21}$$

where $\mathbf{R}_{\mathbf{hY}}$ and $\mathbf{R}_{\mathbf{YY}}$ are the cross-covariance matrix between $\mathbf{h}$ and $\mathbf{Y}$ and the auto-covariance matrix of $\mathbf{Y}$, respectively. They are defined as:

$$\mathbf{R_{hY}} = \mathrm{E}\left[\mathbf{h}\mathbf{Y}^H\right] = \mathbf{R_h}\mathbf{F}_r^H\mathbf{A}^H \tag{4.22}$$

and

$$\mathbf{R_{YY}} = \mathrm{E}\left[\mathbf{Y}\mathbf{Y}^H\right] = \mathbf{A}\mathbf{F}_r\mathbf{R_h}\mathbf{F}_r^H\mathbf{A}^H + N_0\mathbf{I}_M \tag{4.23}$$

where $\mathbf{R_h} = \mathrm{E}[\mathbf{h}\mathbf{h}^H]$ is the auto-covariance matrix of $\mathbf{h}$ and, according to the WSS-US model assumption, results diagonal with the samples of the power delay profile as entries:

$$\mathbf{R_h} = \mathrm{E}[\mathbf{h}\mathbf{h}^H] = \mathrm{diag}\{\sigma^2_{h_0}, \ldots, \sigma^2_{h_{L_{ch}-1}}\} \tag{4.24}$$

Using from (4.22) to (4.24) in (4.21) the channel impulse response is given by:

$$\widehat{\mathbf{h}}_{MMSE} = \mathbf{Q}_{MMSE}\mathbf{F}_r^H\mathbf{A}^H\mathbf{Y} \tag{4.25}$$

where we defined:

$$\mathbf{Q}_{MMSE} = \mathbf{R_h}\left(\left(\mathbf{F}_r^H\mathbf{A}^H\mathbf{A}\mathbf{F}_r\right)^{-1}N_0 + \mathbf{R_h}\right)^{-1}\left(\mathbf{F}_r^H\mathbf{A}^H\mathbf{A}\mathbf{F}_r\right)^{-1} \tag{4.26}$$

The channel frequency response $\widehat{\mathbf{H}}_{MMSE}$ is finally given by:

$$\widehat{\mathbf{H}}_{MMSE} = \mathbf{F}_r\widehat{\mathbf{h}}_{MMSE} \tag{4.27}$$

The overall MSE of the MMSE estimator has been evaluated numerically for various SNRs and is shown in figures 4.1(a) and 4.1(b) for two different channel lengths. The MSE of LS and TD-LS RR given by (4.6) and (4.14) respectively are also plotted as reference. The signal input is assumed modeled as BPSK or QPSK, such as for typical training sequences, i.e. the matrix $\mathbf{A}^H\mathbf{A}$ is equal to the $M \times M$ identity matrix.

Moreover it must be noticed that for BSPK and QPSK modulated symbols the RR and the modified RR channel estimators are identical.

The MSE analysis shows the noticeable gain achieved by the TD-LS RR estimator with respect to the basic LS estimator; as expected the gain increases as the channel length L_{ch} decreases. Moreover the gain introduced by the MMSE estimator with respect to the TD-LS RR estimator is noticeable only at low SNRs and for long CIR; for $SNR > 15$ dB the two estimators have almost the same performance. Finally it should be noted that the MMSE estimator requires two matrix inversions per estimate and the knowledge of the PDP and the noise variance (4.26) where the TD-LS RR estimator requires only one matrix inversion (4.8).

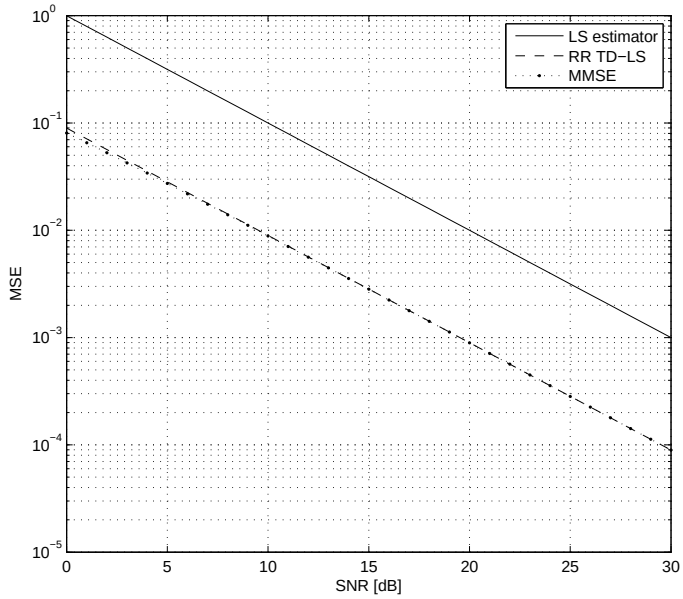

(a) $L_{ch} = 4$ taps

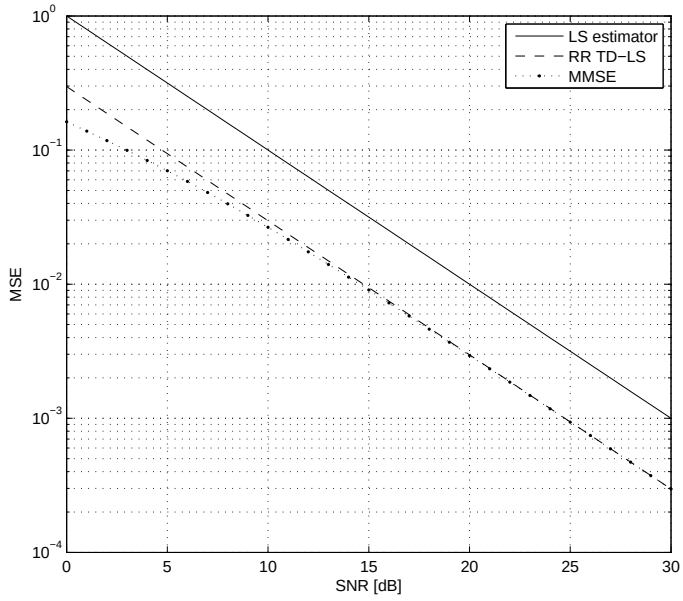

(b) $L_{ch} = 8$ taps

Figure 4.1: MSE of channel estimators

4.2 Channel length estimation

The TD-LS RR channel estimator, the modified TD-LS channel estimator and the MMSE channel estimator described in section 4.1 assumed the knowledge of the CIR length L_{ch}. The CIR length must be estimated in real systems; in the following a channel length estimation algorithm is described.

In [12] it is proposed a joint estimation of the symbol timing, channel length and channel impulse response for OFDM-based systems. In particular, an estimation algorithm based on a reduced-rank approach and on a generalized Akaike information criterion is presented. Under the assumption of correct symbol timing synchronization, the algorithm proposed in [12] can efficiently be used to achieve a joint estimation of L_{ch} and of its CIR. Let $\mathbf{P}$ be the $M \times 1$ vector containing the known data samples of the LTS, as previously described in (3.2), and let $\mathbf{Y}_P = [y_{P,0}; \ldots; y_{P,M-1}]^T$ be the corresponding received signal.

Therefore, the proposed algorithm decreases the supposed length of the channel impulse response from $L_{test} = L_{cp}$ until the following generalized Akaike information criterion (GAIC) is minimized:

$$L_{ch} = \min_{L_{test}} \left(\| \ln \mathbf{F}_{L_{test}} \mathbf{Y}_P - \mathrm{diag}(\mathbf{P}) \mathbf{F}_{L_{test}} \mathbf{h}(L_{test}) \|^2 + \gamma L_{test} \right) \tag{4.28}$$

where γ is a fixed constant [12], $\mathbf{F}_{L_{test}}$ is the $M \times L_{test}$ RR DFT matrix described in (4.1), and $\mathbf{h}(L_{test})$ is the reduced-rank LS estimation of the channel given the supposed channel length L_{test}, i.e., $\mathbf{h}(L_{test}) = \mathbf{F}^{+}_{L_{test}} \mathbf{Y}_P$, where $\mathbf{h}(L_{test})$ has dimensions $L_{test} \times 1$.

In particular, from numerical simulations we found that a convenient value for γ in (4.28) is $\gamma = 0.03$. The algorithm implements the following successive steps.

1. Fix $L_{test} = 16$.
2. Compute the reduced-rank LS estimation of the channel given the supposed channel length L_{test}.
3. Compute (4.28).
4. Decrease L_{test} and repeat points 2 ,3, 4, until (4.28) is minimized.
5. The value of $L_{test} = L_{ch}$ that minimizes (4.28) gives the estimated channel impulse response length, while the corresponding $\mathbf{h}(L_{ch})$ represents the estimation of the channel impulse response that is used to initialize the channel tracking algorithm.

If the channel is assumed to be static over the whole LTS (which is a reasonable assumption in the case under investigation) then the algorithm can use both symbols in the LTS. Consequently, it can be modified as follows:

1. Fix $L_{test} = 16$.
2. Compute the rr-LS estimation of the channel given the supposed channel length L_{test} over the first and second symbols of the LTS, obtaining $\mathbf{h}_1(L_{test})$ and $\mathbf{h}_2(L_{test})$, respectively.
3. Set $\mathbf{h}(L_{test}) = (\mathbf{h}_1(L_{test}) + \mathbf{h}_2(L_{test}))/2$.
4. Compute (4.28).
5. Decrease L_{test} and repeat point 2,3,4, until (4.28) is minimized.
6. The value of $L_{test} = L_{ch}$ that minimizes (4.28) represents the channel impulse response length, and the corresponding $\mathbf{h}(L_{ch})$ the estimated channel impulse response.

Chapter 5

Decision directed channel estimation for mobile OFDM systems

5.1 Introduction

The wireless channel in vehicular environment is time variant, as also described in detail in chapter 1. In section 5.1.1 the invariance time of the wireless channel will be evaluated for a maximum relative speed of $v = 260$ km/h that is $T_{inv} = T_{coh}/10 = 1/(f_D 10) = 70.175\ \mu s$. This implies that within a single OFDM symbol the channel can be considered static in simulations while from packet to the packet transmission it has a time-varying behavior.[1] In other words it is necessary to update the channel estimate in order to correctly perform the equalization task.

The channel tracking task can be performed in various ways widely investigated in literature; these techniques can be grouped into two categories:

- Pilot Assisted Channel Tracking (PACT) algorithms;
- Decision Directed Channel Estimation (DD-CE) algorithms.

[1] As an example a 2000 bytes PSDU 16-QAM modulated with code rate 1/2 generates a packet of 167 OFDM symbols, corresponding to a transmission time of 1336 μs.

5.1.1 Vehicular channel time invariance assessments

This section describes the time-varying effects introduced by the motion of the transmitter and the receiver in vehicular environment, which motivate the necessity to update the channel estimate in order to correctly perform the equalization task.

A maximum relative speed v in the order of 260 km/h is considered for V2V communications to perform a preliminary assessment. The maximum Doppler shift is:

$$f_D = \frac{v f_{c,max}}{c} = 1425 \text{ Hz} \tag{5.1}$$

where the maximum carrier frequency allowed in [3] is $f_{c,max} = 5.92$ GHz (sec. 3.2).

According to the definition of the coherence time of the channel [1], the transmission link can be considered almost time invariant for $T_{inv} = T_{coh}/10 = 1/10 f_D = 70.175\ \mu s$. In IEEE 802.11p specifications the OFDM symbol time T is $T = 8\ \mu s$ (see table 3.3) so the channel can be considered invariant within a single OFDM symbol.

The temporal distribution of the rays that determine the multipath nature of the wireless channel can be usually considered constant for N_S symbols if

$$\Delta\tau_l = (v/c) N_S T \tag{5.2}$$

that is the variation of the delays τ_l (1.15) for $N_S T$ seconds, is negligible compared to the temporal resolution $T_c = 1/B$ of the system. It results that, considering a radial movement between a transmitter and a receiver with relative velocity v, the condition $\Delta\tau_l \ll T_c$ implies that

$$N_S \ll \frac{c}{v} \frac{1}{M + L_{cp}} \tag{5.3}$$

where M is the total number of sub-carriers of the system, and L_{cp} is the length of the cyclic prefix. By replacing in (5.3) the system parameters summarized in (cap. 3, table 3.3) and $v = 260$ Km/h, it results that $N_S \ll 51900$ so the time delays can be considered constant for about $N_S \cong 500$ consecutive OFDM symbols. Such value is larger than the typical number of OFDM symbols per packet.

A possible undesired consequence of the Doppler spread introduced by the time-varying nature of the wireless channel is that the orthogonality between sub-carriers may not be guaranteed thus arising ICI. For an OFDM signal in presence of Doppler Spread, several bounds on the ICI degradation effect exist in literature; in particular

a significant bound applied to the WSS-US channel model has been introduced in [8]. Such an upper bound is:

$$\frac{\sigma_{ICI}^2}{\sigma_{sTX}^2} \leq \frac{1}{12}(2\pi f_D T_s)^2, \tag{5.4}$$

where σ_{ICI}^2 indicates the variance of the Inter carrier Interference modeled as additive Gaussian noise; σ_{sTX}^2 represents the variance of the useful part of the received signal; $T_s = MT_c$ is the duration of an OFDM symbol after the cyclic prefix removal. In this case for $B = 10$ MHz the length of an OFDM symbol after the cyclic prefix removal is $T_s = 6.4\ \mu s$, and considering that for $v = 260$ Km/h it results $f_D = 1425$ Hz, the upper bound (5.4) for the ICI power expressed in dB is

$$\left(\frac{\sigma_{ICI}^2}{\sigma_{sTX}^2}\right)_{dB} = 10\log_{10}\left(\frac{1}{12}(2\pi f_D T)^2\right) \cong -33.69dB. \tag{5.5}$$

The ICI effect introduced by the Doppler spread values under consideration can practically be neglected.

5.1.2 Channel tracking algorithms

Pilot Assisted Channel Tracking PACT techniques make use of the pilot symbols inserted in the OFDM symbols together with data. The algorithm proposed in [14] performs the task in two steps: first the CFR is evaluated on pilot subcarriers in the MMSE sense. Then the CFR is evaluated on the whole transmission bandwidth by linear interpolation. The system considered is an OFDM system with 1024 sub-carriers and 128 pilot tones.

The main advantage of PACT techniques is the low complexity required by the estimator with reference to the DD-CE algorithms. The drawback is that in particular conditions the pilot tones are insufficient to perform the CE accurately.

Decision Directed Channel Estimation Decision directed (DD), also known as Data-Aided, CE algorithms make use of the received data to update the channel estimation available at the receiver. DD techniques are used in two scenarios: first of all if the considered system does not contain periodic sequences of pilot tones PACT techniques are not suitable to perform the task. Moreover in [13] it has been shown that in order to estimate the CIR (or equivalently the CFR) the number of pilots N_p must be equal to or higher than the CIR length L_{ch}. The number of pilot tones per OFDM symbol specified in [3] is $N_p = 4$, that in many practical situations is smaller

than the channel length; a higher number of known symbols becomes necessary to accurately perform the CE task.

The main idea behind DD-CE is the reconstruction of the transmitted OFDM symbol in order to consider the received data as a training sequence and perform CE exploiting the new available information. The main steps of a generic DD-CE algorithm, given a received OFDM symbol $\mathbf{Y}_k$ at time instant k, is the following:

1. equalization of the $i-$th sub-carrier of the received symbol $Y_k[i]$ with the available CFR $H_{k-1}[i]$ as $X_k[i] = Y_k[i]/H_{k-1}[i]$;

2. hard or soft detection of the estimated symbol $\mathbf{A}_k$ to achieve the symbol sequence $\tilde{\mathbf{A}}_k$. The hard detection implies hard demapping of the received symbol by associating the closest QAM symbol $A_k[i]$ (from the point of view of the Euclidean distance from the received symbol) to the received equalized symbol $X_k[i]$. Soft detection implies the decoding of the estimated symbol (eventually preceded by an appropriate deinterleaving operation) and the re-encoding, interleaving and QAM mapping of the decoded bit sequence in order to reconstruct the transmitted OFDM symbol after the error correction achieved by the decoder.

3. estimation of $\mathbf{H}_k$ performed using as input the received symbol $\mathbf{Y}_k$ and the reconstructed $\tilde{\mathbf{A}}_k$;

4. store the new channel estimate $\mathbf{H}_k$ for the following received symbol and use it to perform the final equalization and decoding of the current $k-$th OFDM symbol.

The two different approaches to DD-CE are shown in figures 5.1 and 5.2.

5.2 Decision directed channel estimation

In literature DD-CE has been widely explored because of the high performance achievable. Under the assumption of perfect symbol duplication, the DD-CE becomes equivalent to CE performed with a known training sequence according to a specific algorithm as reviewed in 4.1.

The main drawback of DD-CE is the presence of incorrect detected symbols in the duplication loop that cause error propagation in the CE. The main focus in

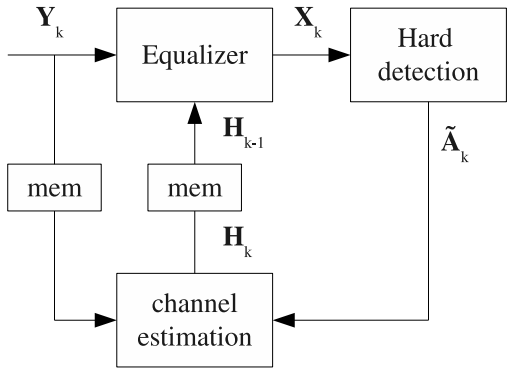

Figure 5.1: Block diagram of the decision-directed CE with hard detection

several proposed DD-CE algorithms is to reduce symbol error propagation effects by estimating detection errors or by providing high reliable symbols at the channel estimator. The estimate of the detection errors has been evaluated in different ways, as seen in the following for the two algorithms proposed respectively in [16] and [17].

In [16] an iterative DD-CE algorithm that detects and downweights incorrect symbols has been proposed; the main steps of this iterative algorithm are: CE of $\mathbf{H}_k$ performed with all the hard detected data symbols $\tilde{\mathbf{A}}_k$; evaluation of the residual error of re-projecting symbols detected with the estimated channel on the received symbols (i.e. $\mathbf{e}_k = \mathbf{Y}_k - \tilde{\mathbf{A}}_k\mathbf{H}_k$); downweighting of the symbols with higher error through a cost function for the CE performed on the following iteration. This procedure is computed for a fixed number of iterations.

In [17] a DD-CE algorithm with hard detection of the transmitted symbols and a strategy selection of the reliable symbols is presented. The proposed method is based on the concept that the instantaneous SNR of the received symbol for an OFDM sub-carrier depends on the square magnitude of the CFR evaluated for that carrier. From this consideration a threshold on the magnitude of the estimated CFR determines whether the associated symbol can be considered reliable or not. Only the subset of reliable symbols are then used to perform the CE.

Another class of DD-CE algorithms employs the error correction capability of the decoder. Most wireless communications standards employ error correction codes (ECC) to increase the link robustness. In [3] the information bit stream is encoded with a 64-state convolutional code as described in section 3.2.4. At the receiver side the presence of the ECC decoder can be exploited in the CE task to achieve reliable bit stream used to perform DD-CE.

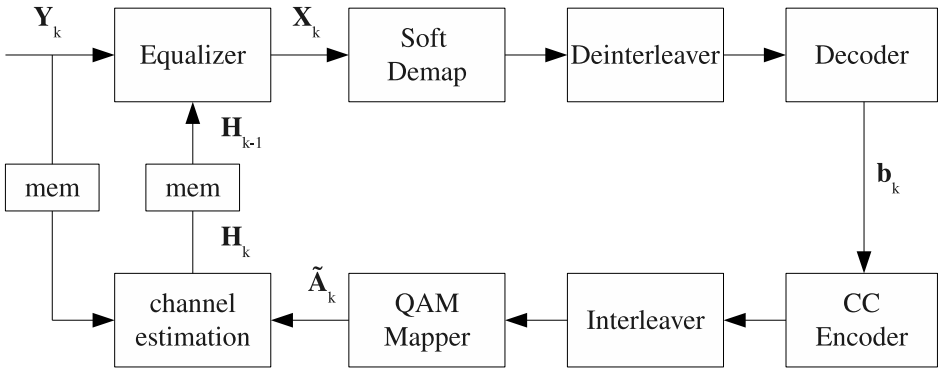

Figure 5.2: Block diagram of the data decoding-aided CE

With respect to the scheme represented in figure 5.1 that uses hard detected symbols, the introduction of the decoder in the CE task (figure 5.2) requires the hardware implementation of dedicated components such as the encoder and the interleaver and higher computational requirements due to the more complex symbol duplication loop.

According to this DD-CE scheme, Abdulhamid et al. in [18] introduce a forgetting factor in order to provide the equalizer with a CIR weighted with the past estimates CIRs (in the LS sense) and achieve a reduction in the estimation error. A similar approach has been proposed in [19] where a forgetting factor weighs the present and past channel estimates (in the MMSE sense) summed together to achieve the CIR provided at the equalizer. Furthermore in [19] authors introduce a threshold on the variation between CFR on adjacent sub-carriers in order to detect the temporarily distorted sub-carriers: in other words the sub-channels that differ more than a specific threshold with the adjacent carriers are considered momentarily distorted and the value of the CFR estimated in that carrier is replaced with the value estimated in the previous CE for the same carrier.

In [20] a DD-CE algorithm with Viterbi decoder and symbol duplication is proposed that takes into account the intrinsic delay introduced by the Viterbi decoder to provide reliable decoded bits. In more details in the proposed algorithm a delay of M OFDM symbols has been introduced before obtaining the decoded bit stream as output of the Viterbi decoder to guarantee the convergence of the decoded stream. This delay introduced in the decoding block leads to a delay in the symbol duplication loop and consequently in the estimated OFDM symbol, i.e. $X_k[i] = Y_k[i]/H_{k-M}[i]$.

In the following sections the convergence time and the reliability of the decoded

bit sequence will be investigated. These considerations will justify the unnecessity of the delay $M > 1$ OFDM symbol introduced in [20]; moreover a simplified DD-CE scheme with FEC (with respect to the DD-CE schemes presented in [18] and [19]) will be presented, together with simulation results of PER vs. SNR.

5.3 Data decoding aided channel estimation

5.3.1 First scheme: iterative data decoding aided CE

The first DD-CE scheme studied and proposed in figure 5.3 is an iterative FEC scheme that makes use of two Viterbi decoders. The first decodes the received symbol $\mathbf{Y}_k$ equalized with the CFR $\mathbf{H}_{k-1}$ estimated with the previous received symbol. The second decodes the received symbol $\mathbf{Y}_k$ equalized with the updated channel estimate $\mathbf{H}_k$. After the channel estimator a second Viterbi decoder is used to decode the received symbol equalized with the new channel estimated to obtain the final decoded bit stream. The main steps are the following:

1. the received OFDM symbol $\mathbf{Y}_k$ is first equalized with the channel estimate $\mathbf{H}_{k-1}$ determined at the $(k-1)-$th time instant;
2. the estimated OFDM symbol $\mathbf{X}_k$ is the input of the block sequence composed of soft demapper, deinterleaver and Viterbi decoder;
3. the decoded bit stream $\mathbf{b}_k$ is re-encoded, interleaved and mapped to obtain the duplicated transmitted OFDM symbol $\tilde{\mathbf{A}}_k$;
4. the channel estimate update $\mathbf{H}_k$ is computed from the received symbol $\mathbf{Y}_k$ and the duplicated symbol $\tilde{\mathbf{A}}_k$ and stored in memory;
5. the received OFDM symbol $\mathbf{Y}_k$ is equalized with the updated channel estimate $\mathbf{H}_k$ to obtain the updated OFDM symbol estimate $\mathbf{X}'_k$;
6. the updated OFDM symbol estimate is demapped, deinterleaved and decoded to achieve the final decoded bit sequence $\mathbf{b}'_k$ of the $k-$th OFDM symbol;
7. the received OFDM symbol $\mathbf{Y}_{k+1}$ is equalized and a further loop iteration begins.

Some observations on the described scheme are worth noticing :

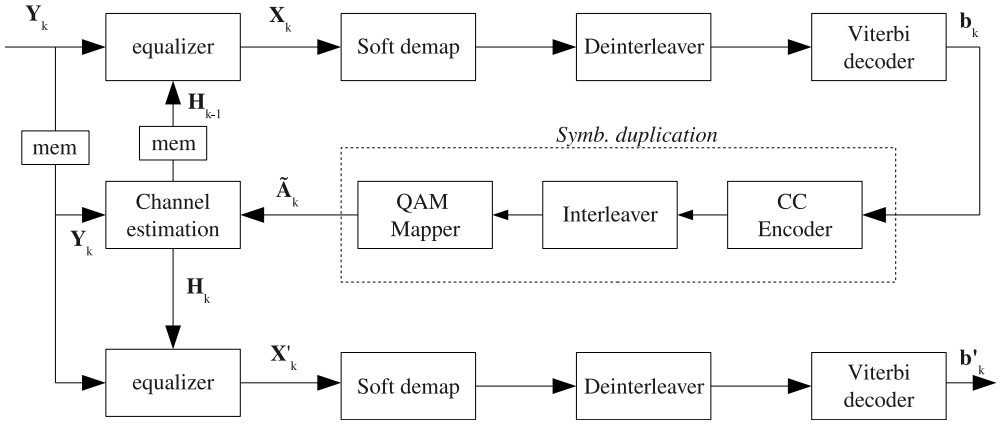

Figure 5.3: Iterative data decoding-aided CE block diagram - scheme 1

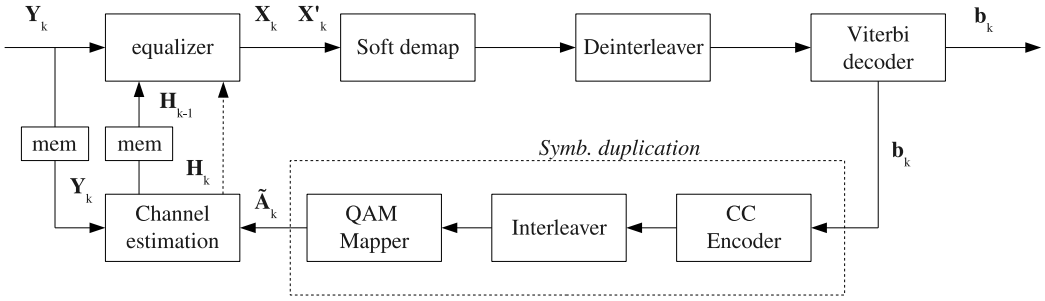

Figure 5.4: Iterative data decoding-aided CE block diagram - scheme 2

- the presented scheme has an *OFDM symbol* approach: every block works iteratively with a period corresponding to the OFDM symbol time. This is possible because the interleaver [3] operates on blocks of encoded bits with length corresponding to the number of encoded bit per OFDM symbol for the specific modulation rate (N_{CPSC}, table 3.3), i.e. it introduces one OFDM symbol latency.

- The constraint length of the 64-state convolutional encoder [3] is $c = 6$. It is a common assumption to evaluate the convergence time of the bit sequence out of the Viterbi decoder as $t_{conv} \sim 4c = 24$. In IEEE 802.11p transmission schemes the convergence time of 24 decoded bits is always lower than one OFDM symbol length: the worst case is the BPSK 1/2 modulation scheme that implies the presence of 24 information bits per OFDM symbols.

- The proposed iterative scheme has high computational and latency requirements with respect to a DD-CE with no FEC scheme because of the additional encoder and interleaver blocks, as well as the Viterbi decoder and deinterleaver.

The scheme illustrated in Figure 5.3 duplicates the sequence of soft demapper, deinterleaver and Viterbi decoder blocks; in principle, they could operate in parallel on two consecutive input OFDM symbols in order to minimize the time latency. In this case the impact on chip area compared to a commercial off-the shelf (COTS) 802.11a/g receiver is significant as many important blocks are duplicated. In alternative, and this justifies the "iterative" character of the scheme, the same performance can be obtained by iterating the data flow over a single Viterbi FEC instantiation, which in such case should be clocked at double frequency in order to employ the same processing time. An example is illustrated in figure 5.4.

5.3.2 Second scheme: non-iterative data decoding aided CE

A simplified non-iterative scheme has also been investigated. The main idea behind the non-iterative data-decoding aided CE scheme is to make use of a single Viterbi decoder and use the output bit stream at the same time for the CE task and as final output information bit stream. The block diagram is shown in figure 5.5; the main steps are the following:

1. the received OFDM symbol $\mathbf{Y}_k$ is equalized with most recent available channel estimate $\mathbf{H}_{k-1}$;

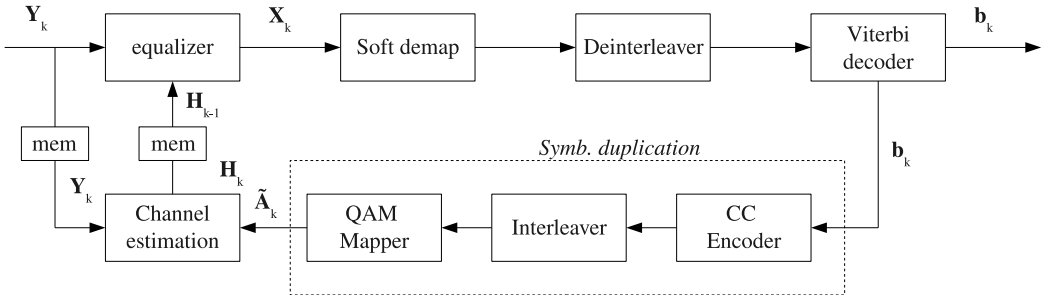

Figure 5.5: Non-iterative data decoding-aided CE scheme

2. the estimated OFDM symbol $\mathbf{X}_k$ is input to the block sequence of soft demapper, deinterleaver and Viterbi decoder;

3. the decoded bit stream $\mathbf{b}_k$ is re-encoded, interleaved and mapped to obtain the duplicated transmitted OFDM symbol $\tilde{\mathbf{A}}_k$ and at the same time is the final decoded bit stream for the $k-$th OFDM symbol;

4. the channel estimate $\mathbf{H}_k$ is obtained using the received OFDM symbol $\mathbf{Y}_k$ and the duplicated OFDM symbol $\tilde{\mathbf{A}}_k$ and is used to perform the equalization of the $(k+1)-$th OFDM symbol, as for step 1, and a new loop iteration starts.

Some observations on the non-iterative scheme are reported below:

- as for the iterative case, in the non-iterative scheme every block works iteratively with a period corresponding to the OFDM symbol time. This is possible because the interleaver [3] operates on blocks of encoded bits with length corresponding to the number of encoded bit per OFDM symbol for the specific modulation rate (N_{CPSC}, table 3.3).

- The proposed non-iterative scheme has almost the same computational requirements with respect to a DD-CE with no FEC scheme as only encoder, interleaver and mapper blocks are added, but a single Viterbi decoded - which is the most computationally intensive - is used in both cases.

NOTE: an important point to be outlined for both FEC aided DD-CE schemes concern the handling of the last bits output by the Viterbi. As well know, frame termination is present only for the last OFDM symbol in the PSDU frame [3]. This means that the last bits of every frame (i.e. OFDM symbol, as the deinterleaver size

corresponds to the length of an OFDM symbol) input to the Viterbi will produce non reliable decoder decisions unless a following OFDM symbol is appended to the current one. This is considered tolerable for CE purposes; for the output bit stream the last portion of the decoded frame has a delay of one OFDM symbol in order to guarantee the reliability convergence.

The performance results shown in sec. 5.3.3 for both schemes correspond to:

- introduce one OFDM symbol delay latency in order to generate the decoded information bits output by the Viterbi; in other words, the information bits corresponding to the k-th OFDM symbol are decoded only after the $(k+1)-$th symbol is processed too;
- however in both cases, the updated channel estimates need to be ready in time to equalize the $(k+1)-$th OFDM symbol: this is accomplished tolerating less reliable bits in the last portion of the Viterbi output frame used for symbol duplication and CE purposes.

5.3.3 Performance results

The simulation results for iterative and non-iterative schemes are presented in figures 5.6 to 5.50 in terms of packet error rate (PER) vs. SNR for ETSI B and ETSI C channels and Jakes Doppler effect with various relative speeds. The values considered of the simulation parameters are summarized in table 5.1.

Unless otherwise stated, the performance curves of PER vs. SNR presented in this thesis are obtained as follows:

- for every simulated packet an independent channel realization is taken into account;
- the Doppler effect is added to the channel realization and its temporal evolution is observed for the whole packet transmission;
- the average per packet channel energy is normalized to the unitary value.

Performance curves obtained with perfect CIR knowledge and with DD-CE employing hard detection performed with all data and with SSA [17] are also plotted as reference. With respect to the legend taken into account in the selected figures, *Perfect CIR* employs the perfect knowledge of the CIR; *TD-LS all data* employs the

TD-LS RR CE (sec. 4.1.2), *TD-LS SSA thr 0.05* employs the DD-CE algorithm presented in [17], *TD-LS iterative Vit.* employs the scheme presented in sec. 5.3.1 and *TD-LS iterative Vit.* employs the scheme presented in sec. 5.3.2.

In every DD-CE scheme considered the employed CE is the TD-LS technique exploiting the knowledge of the CIR length as described in sec. 4.1.2. Moreover ideal time and frequency synchronization at the receiver has been considered.

Parameter	Simulated values
Bandwidth	10 MHz
Data rates	6, 12, 27 Mbps
Packet length L	50, 400, 2000 bytes
Channel models	ETSI B, C
Relative speed v	60, 120, 200 km/h
CIR length	estimated
Channel estimation	TD-LS RR
Simulated frames per SNR value	3000

Table 5.1: Values of the simulated scenarios

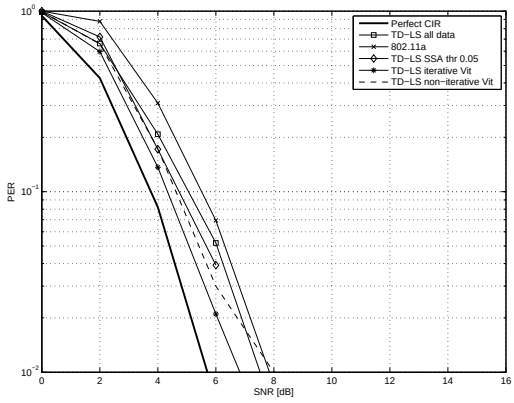

Figure 5.6: PER vs. SNR. ETSI B, v = 60 km/h, QPSK 1/2, L = 50 B

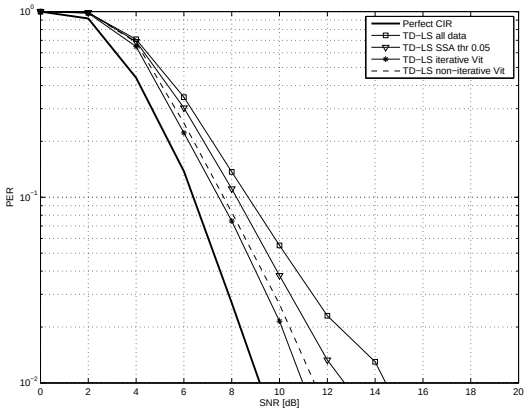

Figure 5.7: PER vs. SNR. ETSI B, v = 60 km/h, QPSK 1/2, L = 400 B

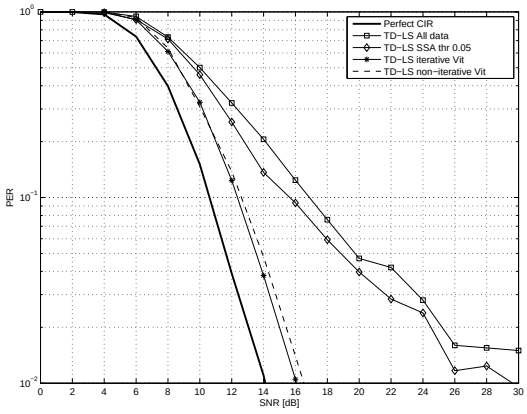

Figure 5.8: PER vs. SNR. ETSI B, v = 60 km/h, QPSK 1/2, L = 2000 B

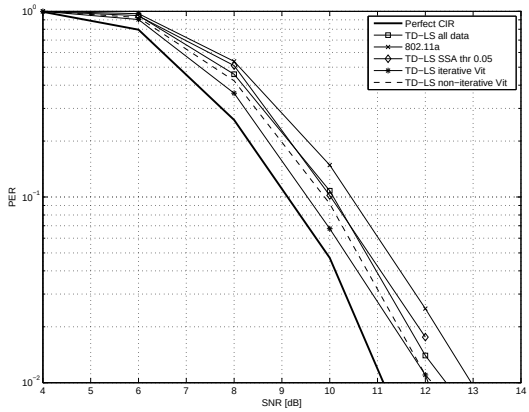

Figure 5.9: PER vs. SNR. ETSI B, v = 60 km/h, 16-QAM 1/2, L = 50 B

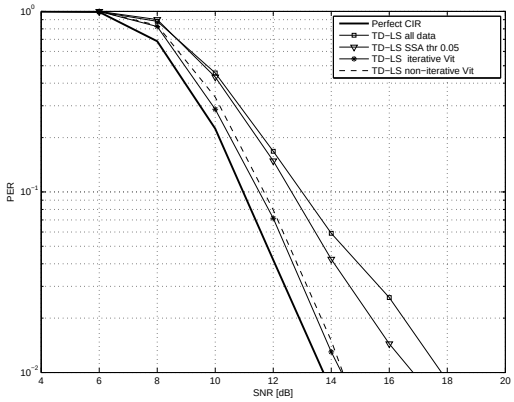

Figure 5.10: PER vs. SNR. ETSI B, v = 60 km/h, 16-QAM 1/2, L = 400 B

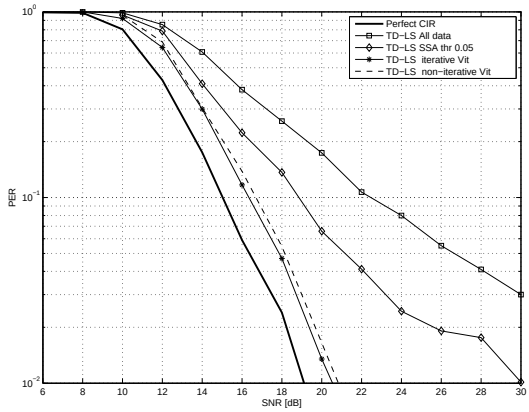

Figure 5.11: PER vs. SNR. ETSI B, v = 60 km/h, 16-QAM 1/2, L = 2000 B

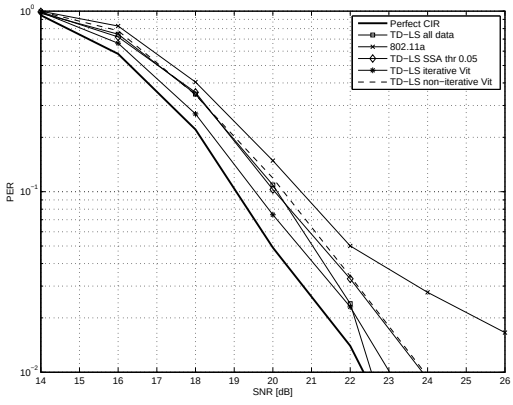

Figure 5.12: PER vs. SNR. ETSI B, v = 60 km/h, 64-QAM 3/4, L = 50 B

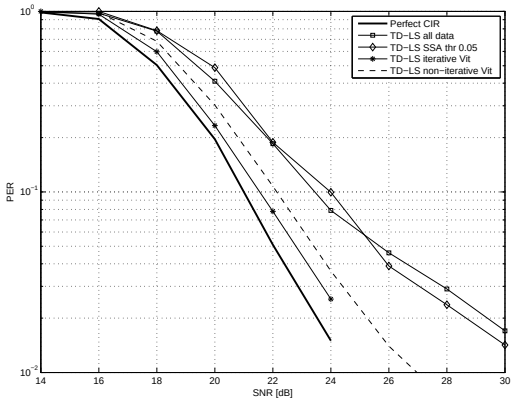

Figure 5.13: PER vs. SNR. ETSI B, v = 60 km/h, 64-QAM 3/4, L = 400 B

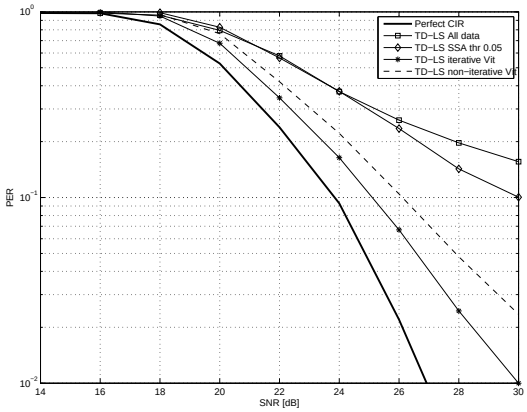

Figure 5.14: PER vs. SNR. ETSI B, v = 60 km/h, 64-QAM 3/4, L = 2000 B

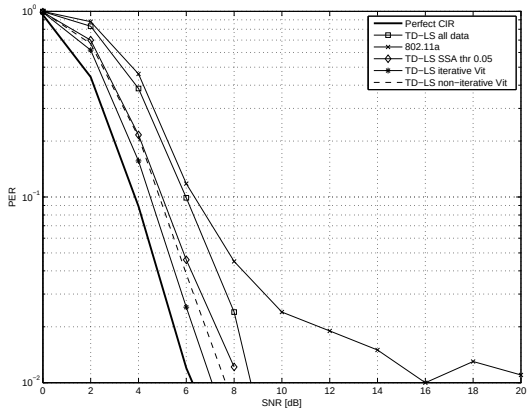

Figure 5.15: PER vs. SNR. ETSI B, v = 120 km/h, QPSK 1/2, L = 50 B

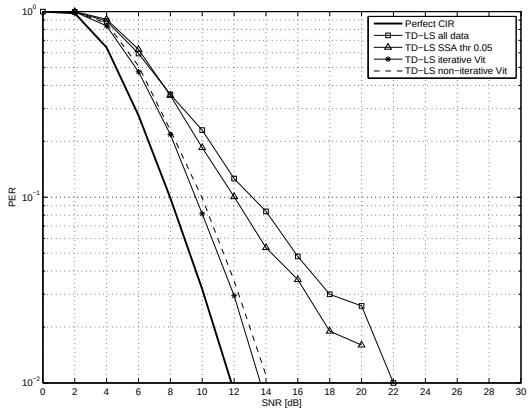

Figure 5.16: PER vs. SNR. ETSI B, v = 120 km/h, QPSK 1/2, L = 400 B

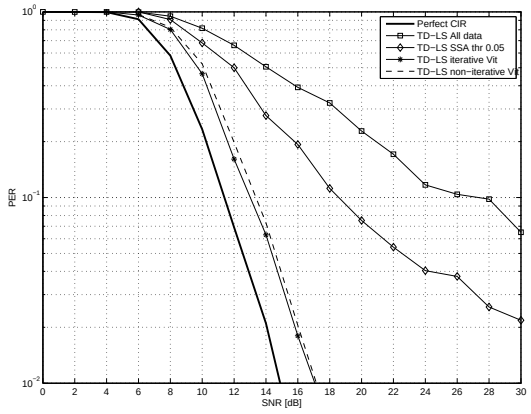

Figure 5.17: PER vs. SNR. ETSI B, v = 120 km/h, QPSK 1/2, L = 2000 B

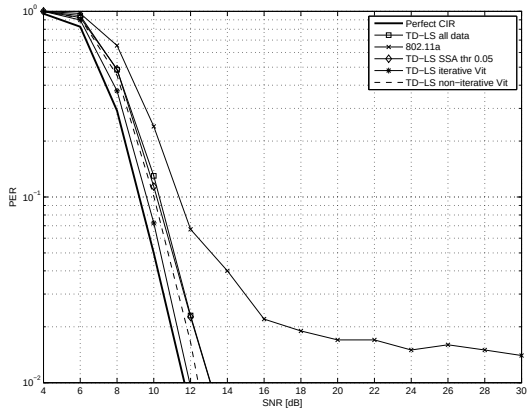

Figure 5.18: PER vs. SNR. ETSI B, v = 120 km/h, 16-QAM 1/2, L = 50 B

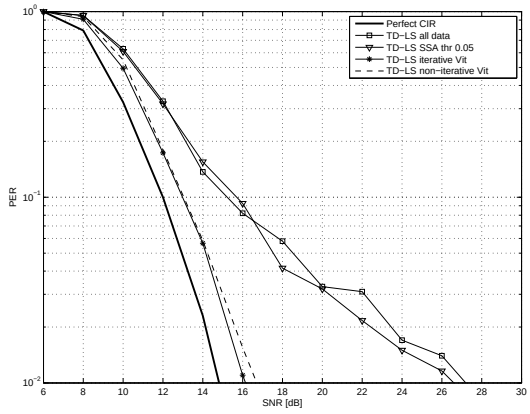

Figure 5.19: PER vs. SNR. ETSI B, v = 120 km/h, 16-QAM 1/2, L = 400 B

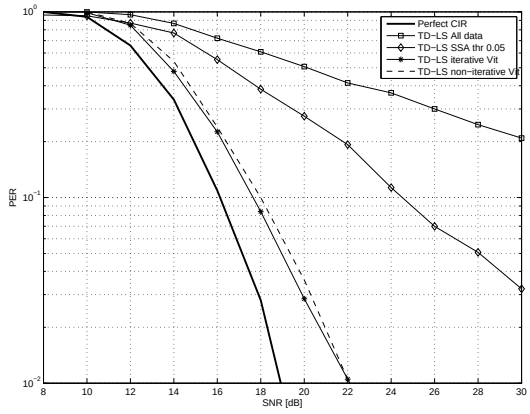

Figure 5.20: PER vs. SNR. ETSI B, v = 120 km/h, 16-QAM 1/2, L = 2000 B

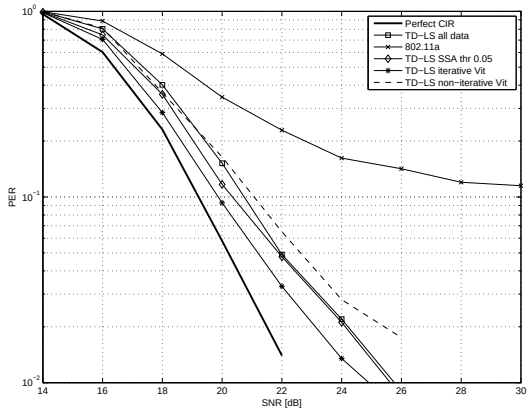

Figure 5.21: PER vs. SNR. ETSI B, v = 120 km/h, 64-QAM 3/4, L = 50 B

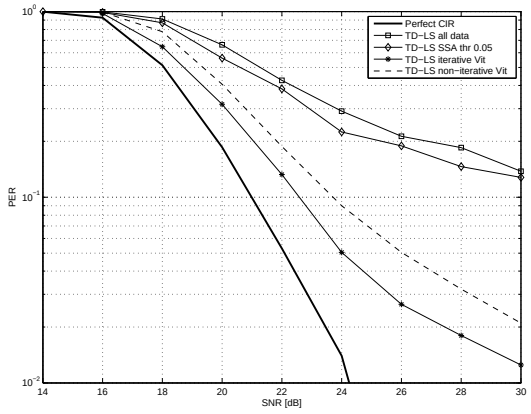

Figure 5.22: PER vs. SNR. ETSI B, v = 120 km/h, 64-QAM 3/4, L = 400 B

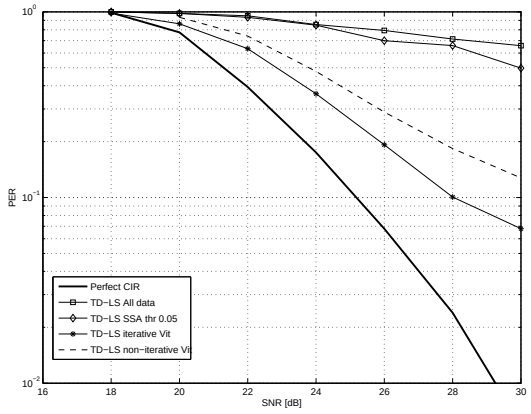

Figure 5.23: PER vs. SNR. ETSI B, v = 120 km/h, 64-QAM 3/4, L = 2000 B

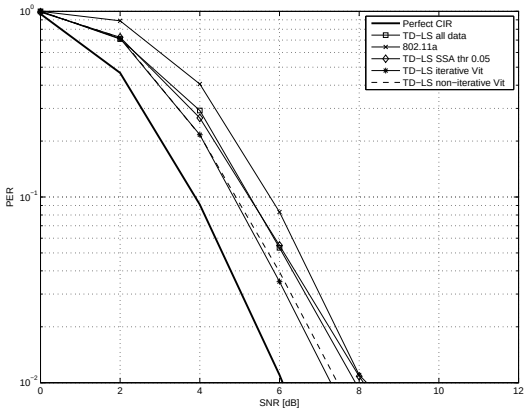

Figure 5.24: PER vs. SNR. ETSI C, v = 60 km/h, QPSK 1/2, L = 50 B

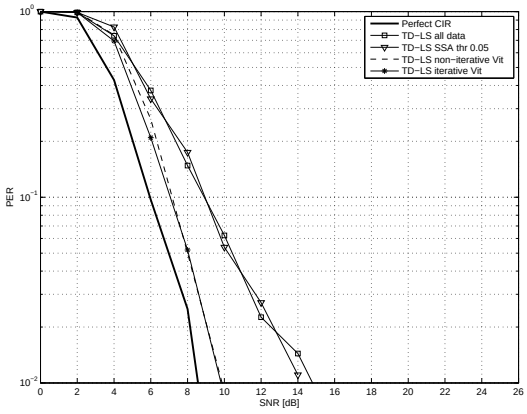

Figure 5.25: PER vs. SNR. ETSI C, v = 60 km/h, QPSK 1/2, L = 400 B

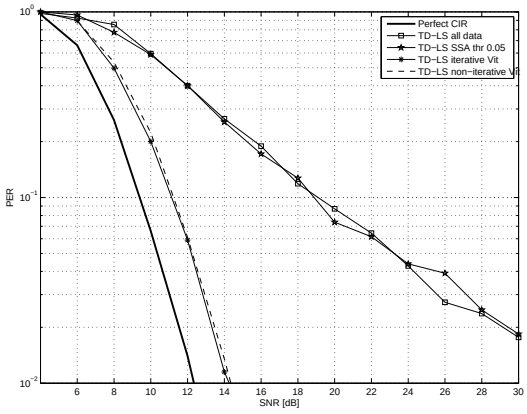

Figure 5.26: PER vs. SNR. ETSI C, v = 60 km/h, QPSK 1/2, L = 2000 B

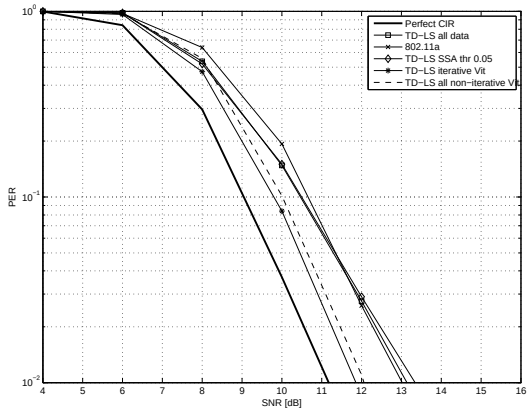

Figure 5.27: PER vs. SNR. ETSI C, v = 60 km/h, 16-QAM 1/2, L = 50 B

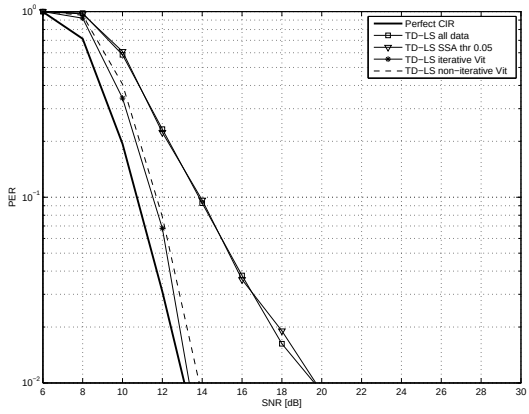

Figure 5.28: PER vs. SNR. ETSI C, v = 60 km/h, 16-QAM 1/2, L = 400 B

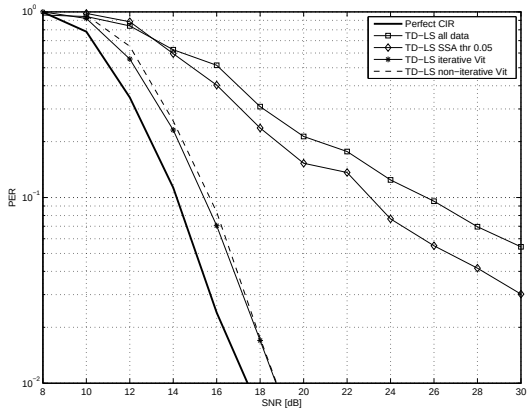

Figure 5.29: PER vs. SNR. ETSI C, v = 60 km/h, 16-QAM 1/2, L = 2000 B

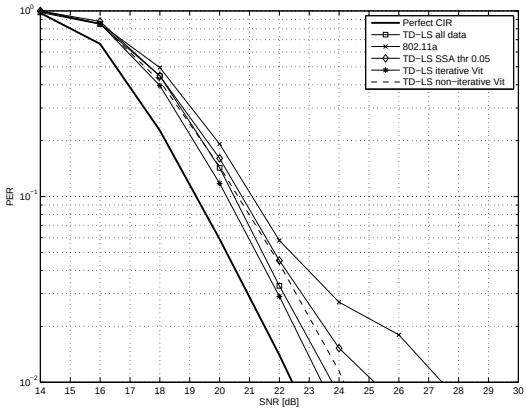

Figure 5.30: PER vs. SNR. ETSI C, v = 60 km/h, 64-QAM 3/4, L = 50 B

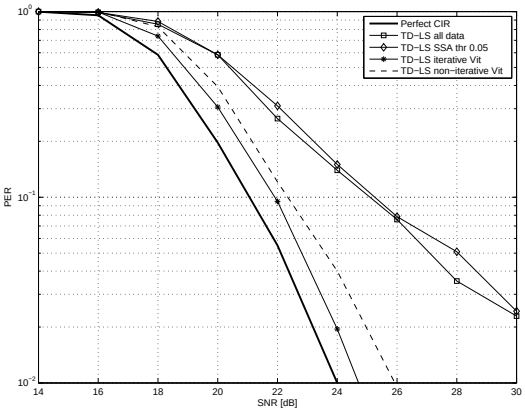

Figure 5.31: PER vs. SNR. ETSI C, v = 60 km/h, 64-QAM 3/4, L = 400 B

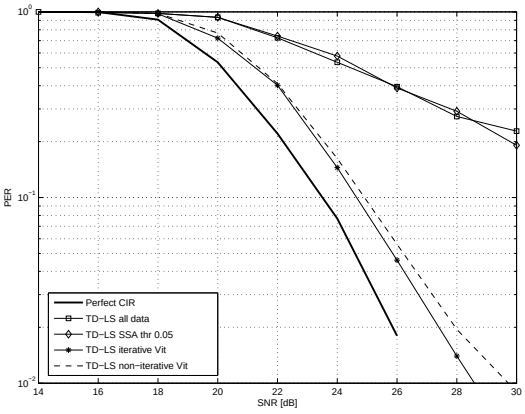

Figure 5.32: PER vs. SNR. ETSI C, v = 60 km/h, 64-QAM 3/4, L = 2000 B

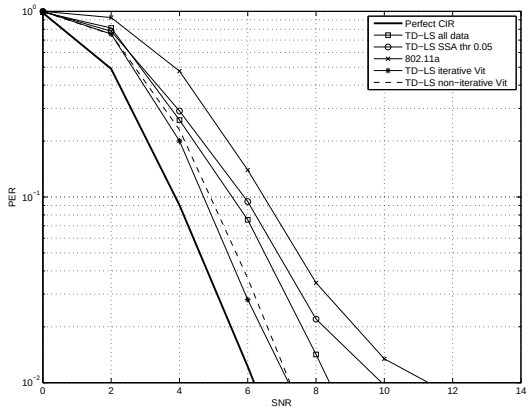

Figure 5.33: PER vs. SNR. ETSI C, v = 120 km/h, QPSK 1/2, L = 50 B

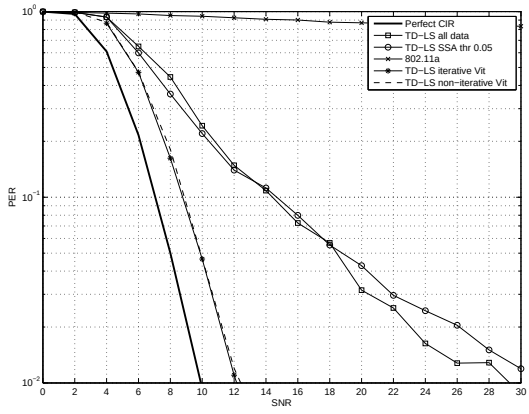

Figure 5.34: PER vs. SNR. ETSI C, v = 120 km/h, QPSK 1/2, L = 400 B

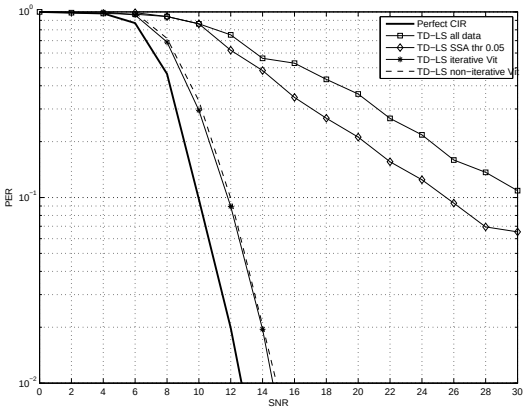

Figure 5.35: PER vs. SNR. ETSI C, v = 120 km/h, QPSK 1/2, L = 2000 B

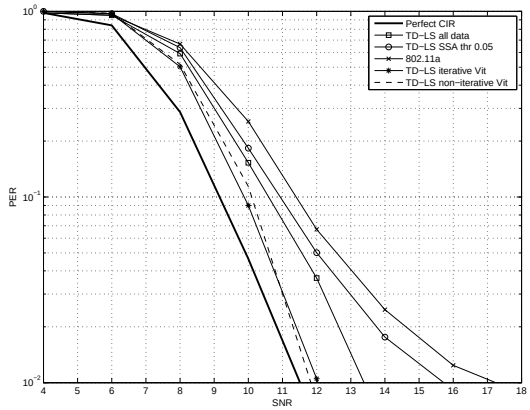

Figure 5.36: PER vs. SNR. ETSI C, v = 120 km/h, 16-QAM 1/2, L = 50 B

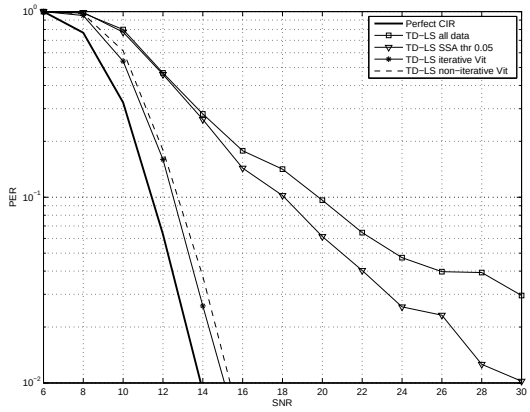

Figure 5.37: PER vs. SNR. ETSI C, v = 120 km/h, 16-QAM 1/2, L = 400 B

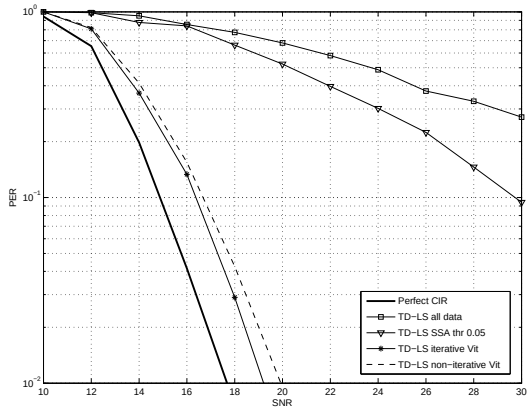

Figure 5.38: PER vs. SNR. ETSI C, v = 120 km/h, 16-QAM 1/2, L = 2000 B

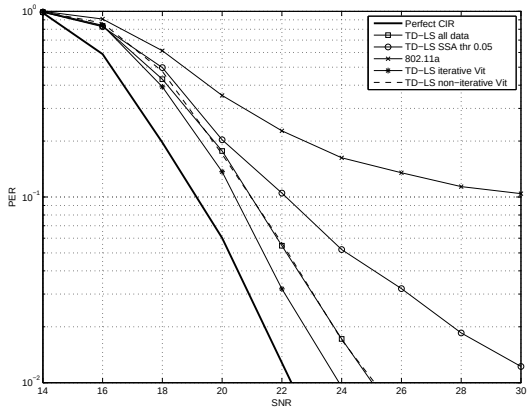

Figure 5.39: PER vs. SNR. ETSI C, v = 120 km/h, 64-QAM 3/4, L = 50 B

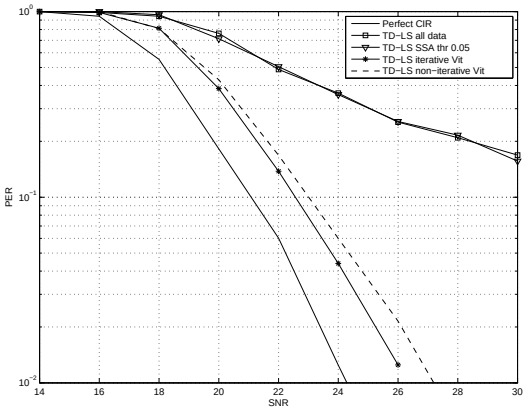

Figure 5.40: PER vs. SNR. ETSI C, v = 120 km/h, 64-QAM 3/4, L = 400 B

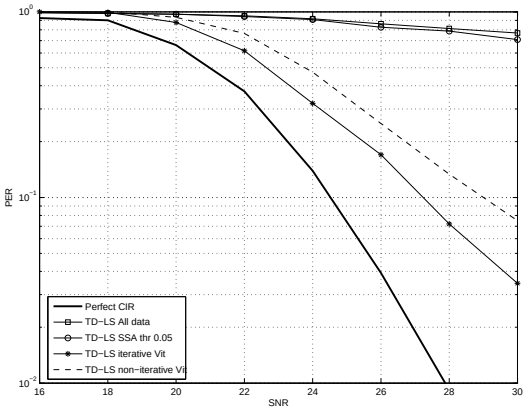

Figure 5.41: PER vs. SNR. ETSI C, v = 120 km/h, 64-QAM 3/4, L = 2000 B

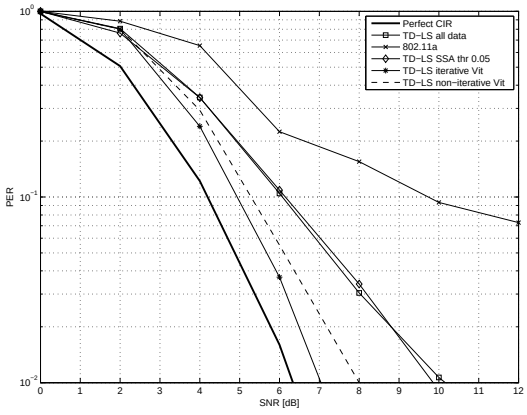

Figure 5.42: PER vs. SNR. ETSI C, v = 200 km/h, QPSK 1/2, L = 50 B

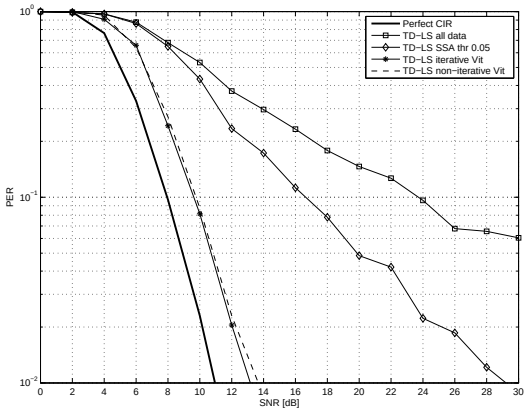

Figure 5.43: PER vs. SNR. ETSI C, v = 200 km/h, QPSK 1/2, L = 400 B

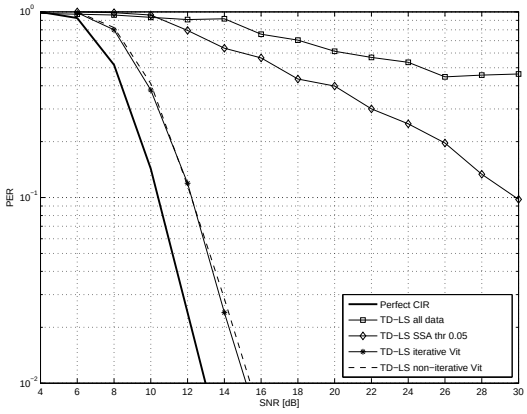

Figure 5.44: PER vs. SNR. ETSI C, v = 200 km/h, QPSK 1/2, L = 2000 B

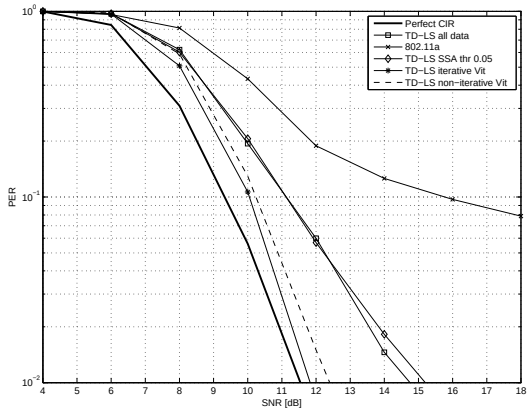

Figure 5.45: PER vs. SNR. ETSI C, v = 200 km/h, 16-QAM 1/2, L = 50 B

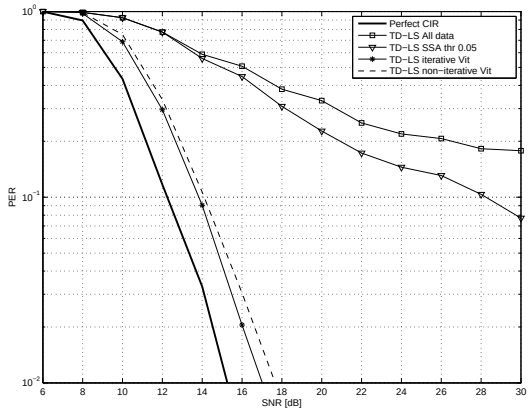

Figure 5.46: PER vs. SNR. ETSI C, v = 200 km/h, 16-QAM 1/2, L = 400 B

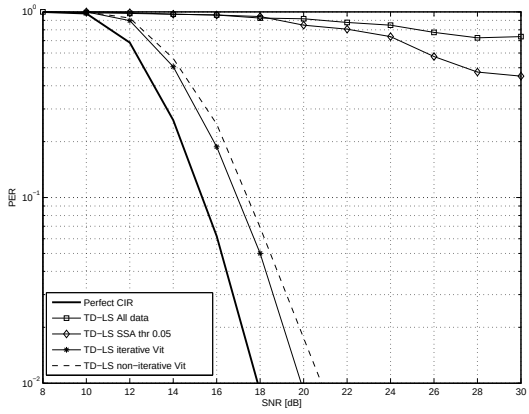

Figure 5.47: PER vs. SNR. ETSI C, v = 200 km/h, 16-QAM 1/2, L = 2000 B

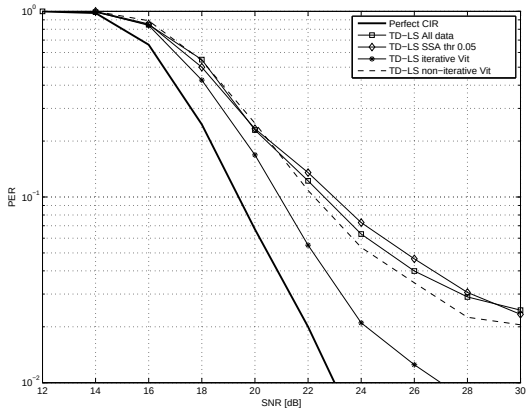

Figure 5.48: PER vs. SNR. ETSI C, v = 200 km/h, 64-QAM 3/4, L = 50 B

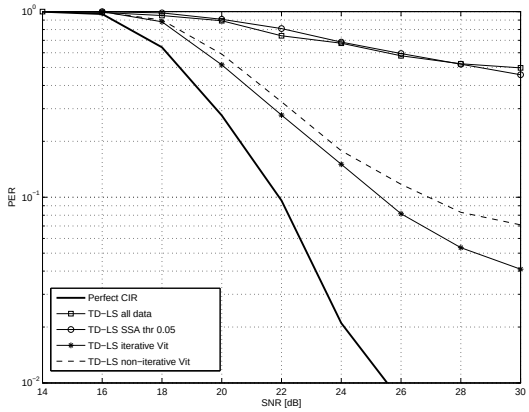

Figure 5.49: PER vs. SNR. ETSI C, v = 200 km/h, 64-QAM 3/4, L = 400 B

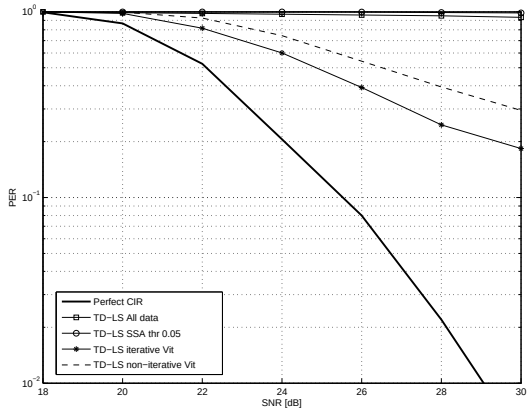

Figure 5.50: PER vs. SNR. ETSI C, v = 200 km/h, 64-QAM 3/4, L = 2000 B

Rate [mbit/s]	Modulation scheme	Coding rate	Decoded bit per OFDM symbol
12	16-QAM	1/2	96
18	16-QAM	3/4	144
27	64-QAM	3/4	216

Table 5.2: Transmission parameters for Rates = 12, 18, 27 mbit/s

The simulation results show that forward error correction mitigates almost completely the error propagation effect. For both short (ETSI B) and long (ETSI C) channels, data decoding aided DD-CE performs well even for high speed and high modulation rates. A significant degradation of performance with reference to the ideal case (i.e. perfect knowledge of CIR at the equalizer) is noticeable only in few scenarios:

- Scenario 2: ETSI B 120 km/h - 64-QAM 3/4 L = 2000B;
- Scenario 5: ETSI C 200 km/h - 64-QAM 3/4 L = 400B;
- Scenario 5: ETSI C 200 km/h - 64-QAM 3/4 L = 2000B.

The two presented schemes of figures 5.3 and 5.5 have almost the same performance in most scenarios, a degradation higher than 1 dB at PER = 0.1 can be seen only in 64-QAM 3/4 modulated packets.

To evaluate the impact on performance of the reliability of the decoded bits with trellis truncation, the bit error probability (BER) as a function of the decoded bit index within the frame is considered for rates 12, 18 and 27 Mbit/s under different scenarios. The performance curves have been obtained simulating a total number of 200000 decoded OFDM symbols for every considered data rate.

These selected data rates permit to evaluate the BER in different modulation schemes for the same coding rate (18 vs. 24 Mbit/s) or the BER in the same modulation scheme for different coding rates (12 vs. 18 Mbit/s). In table 5.2 the transmission parameters are summarized for the simulated rates.

Figures 5.51(a), 5.51(b) and 5.51(c) show the bit error probability (BER) out of the Viterbi decoder for various relative speeds. As expected the last decoded bits of the OFDM symbol result less reliable, in particular the assumed convergence time t_{conv} of 24 information bit for the 1/2 coding rate is confirmed by the performed

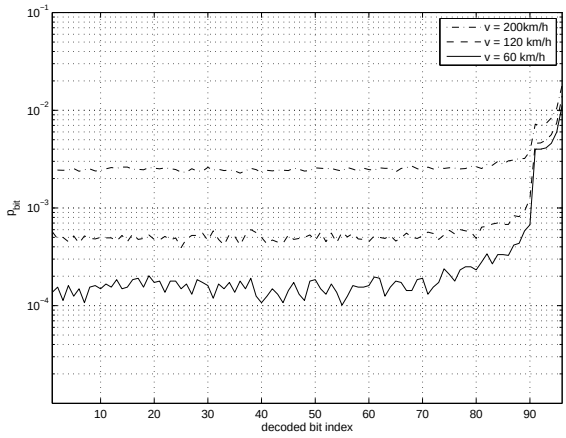

(a) 16-QAM 1/2, SNR = 18dB

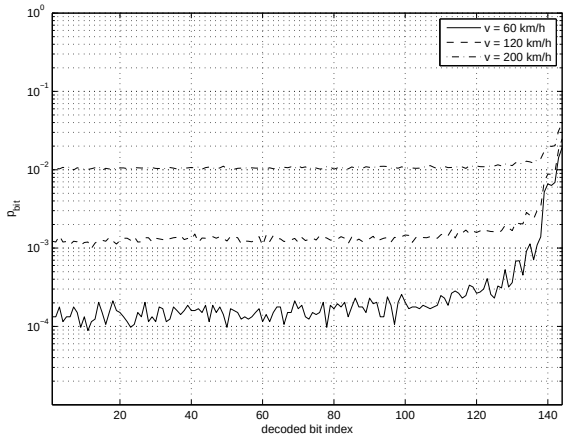

(b) 16-QAM 3/4, SNR = 24dB

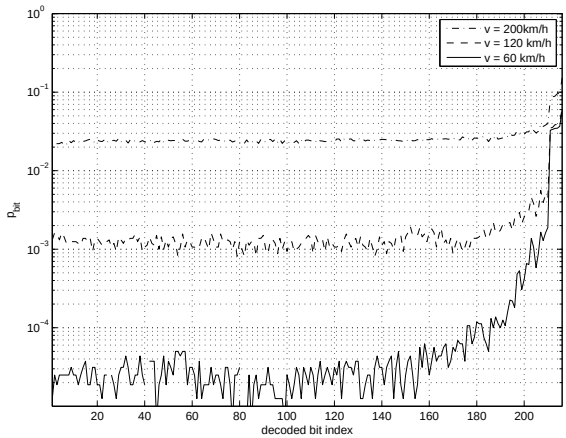

(c) 64-QAM 3/4, SNR = 27dB

Figure 5.51: BER of the decoded bit sequence as a function of the bit position within the frame

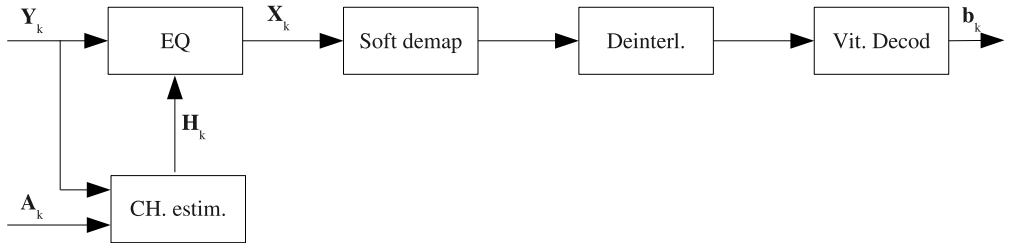

Figure 5.52: Iterative DD-CE scheme with perfect decoding and symbol duplication

simulations. For punctured codes a heuristic rule determined in [25] defines the convergence time, expressed in number of trellis steps (i.e. in number of decoded bits), as

$$t_{conv} = 2.5c/(1 - R) \tag{5.6}$$

where c is the constraint length of the code and R is the code rate. It results that for $R = 2/3$ and $c = 6$ is $t_{conv} = 45$ and for $R = 3/4$ and $c = 6$ is $t_{conv} = 60$. In general it states that the convergence time increases as the coding rate increases.

In the selected scenarios the convergence time is kept lower than the OFDM symbol length: this guarantees the convergence of the decoded bit within one OFDM symbol delay. In figures 5.51(a) and 5.51(b) the effect of reducing the code rate from 1/2 to 3/4 can be seen: the overall BER increases while there is almost no variation in the reliability of the last bits.

Ideal decoding To evaluate the effect of the residue decoding error in the CE loop, the scenario with perfect decoded data passed to channel estimator is simulated. Considering the iterative and non-iterative DD-CE schemes of figures 5.3 and 5.5, the scenario with no decoding errors and thus with $\tilde{\mathbf{A}}_k = \mathbf{A}_k$, has been considered. The resulting schemes are represented respectively in figures 5.52 and 5.53 where the input $\mathbf{A}_k$ represents the *ideal* unknown OFDM data symbol.

It should be noticed that such a scenario is not realistic but acts as a bound to evaluate the effect of the residue decoding error of the Viterbi decoder on the performance.

Simulation results have been considered in terms of PER vs. SNR for the previously selected subset of worst cases, i.e. 64-QAM 3/4 modulated packets and $v = 120, 200$ km/h relative speeds.

In figures 5.54, 5.55, 5.56 and 5.57 the effect of perfect data decoding can be seen with respect to the real decoded DD-CE schemes.

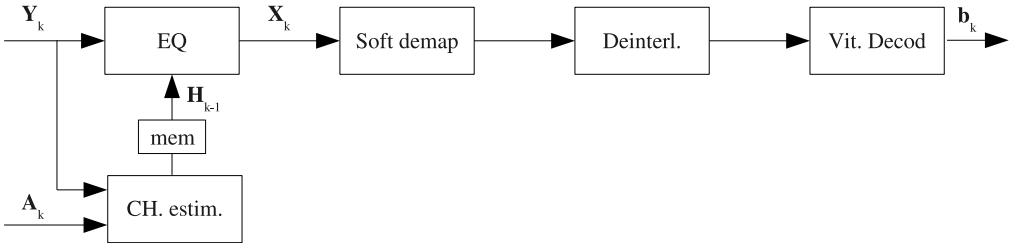

Figure 5.53: Non-iterative DD-CE scheme with perfect decoding and symbol duplication

In particular it should be noted that:

- in the iterative scheme with two Viterbi decoders the CE is performed having as input the perfectly reconstructed transmitted symbol $\mathbf{A}_k$ and the received symbol $\mathbf{Y}_k$; it results that at the second Viterbi decoder the channel estimate $\mathbf{H}_k$ has no delay with respect to the received symbol and the estimation error is not affected by residual decoding errors.

- In the non-iterative DD-CE scheme the CE is performed having as input the perfectly reconstructed transmitted symbol $\mathbf{A}_k$ and the received symbol $\mathbf{Y}_k$; the input coded bit stream at the Viterbi decoder is equalized with the estimated CFR $\mathbf{H}_{k-1}$ that has a delay of one received OFDM symbol.

Considering the simulation results of the two DD-CE schemes with ideal decoding illustrated in figures 5.54 to 5.57, the gain achieved by the scheme shown in figure 5.52 with respect to the scheme of figure 5.53 represents the effect of the degradation of the channel estimate due to the Doppler effect, that increases with the increase of the relative speed.

Moreover, as shown in figures 5.54 to 5.57, it should be noticed that, with reference to the non-iterative scheme, the ideal decoding has almost no increase in performance with respect to the real decoded data. In other words in high mobility scenarios the effect of the residual decoding error of the non-iterative DD-CE scheme can be considered negligible with respect to the degradation introduced by the Doppler effect.

From the results achieved some kind of compensation to the delay introduced by the symbol duplication loop should be considered, as reviewed is section 5.4.

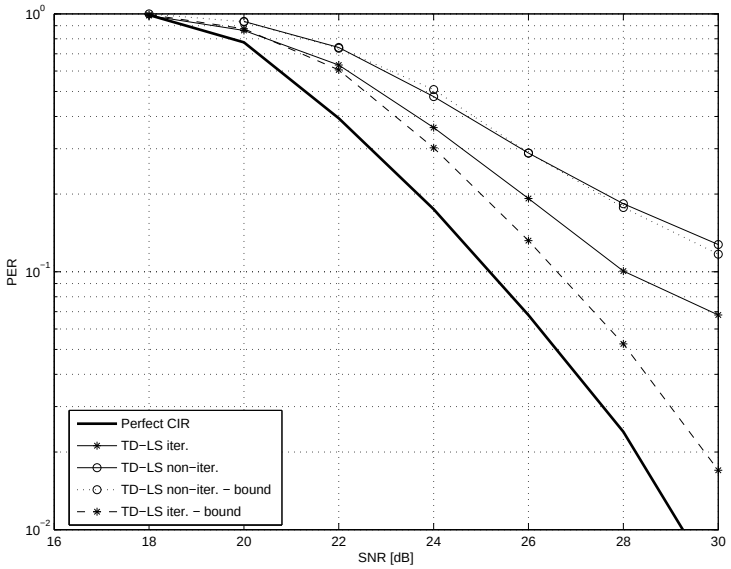

Figure 5.54: Ideal decoding - PER vs. SNR, v = 120 km/h, 64QAM 3/4, L = 2000 B

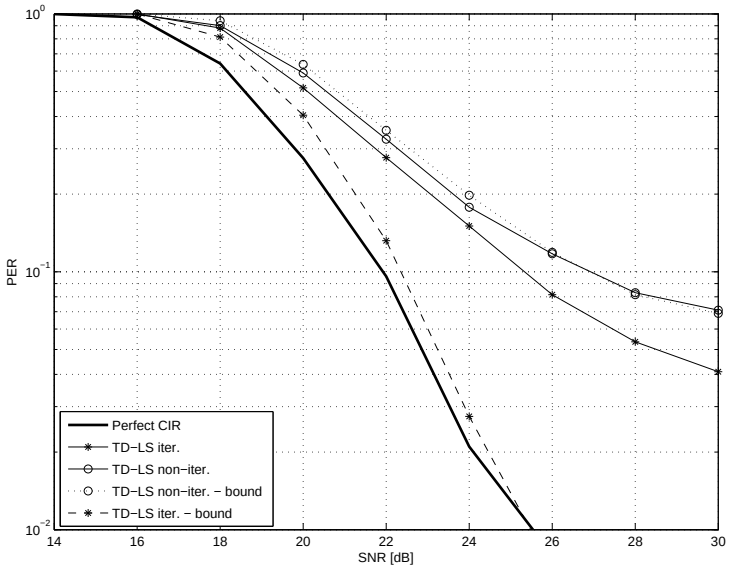

Figure 5.55: Ideal decoding - PER vs. SNR, v = 200 km/h, 64QAM 3/4, L = 400 B

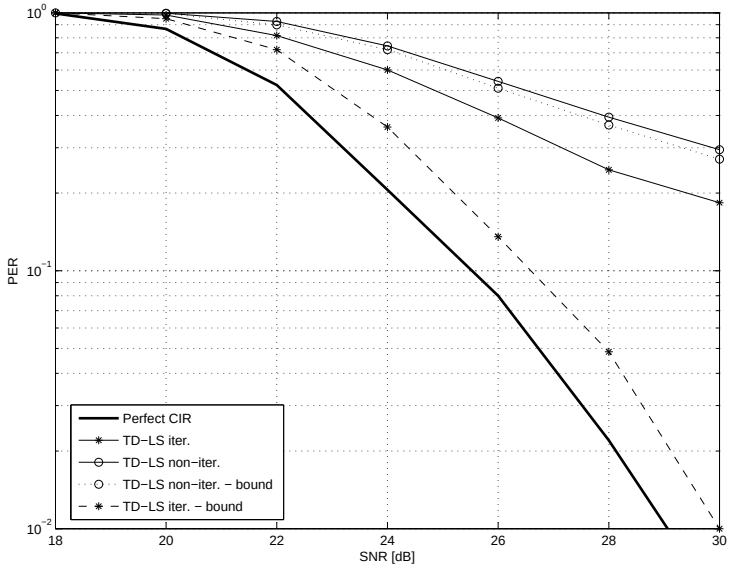

Figure 5.56: Ideal decoding - PER vs. SNR, v = 200 km/h, 64QAM 3/4, L = 2000 B

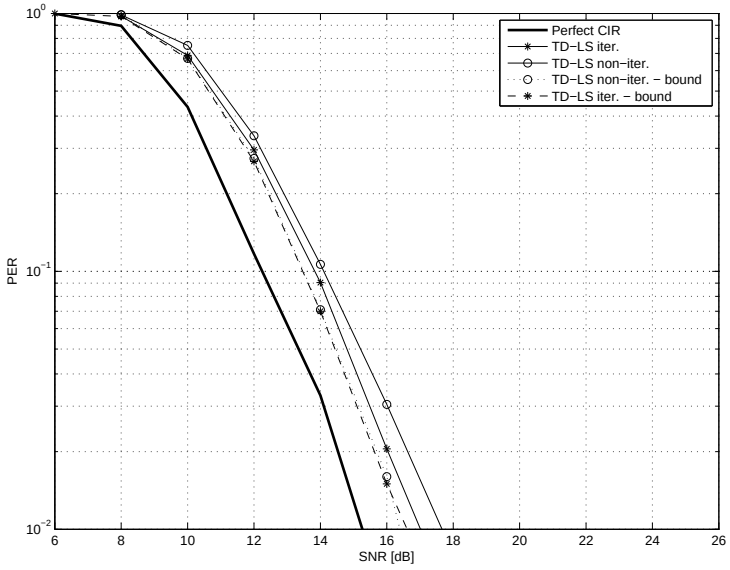

Figure 5.57: Ideal decoding - PER vs. SNR, v = 200 km/h, 16QAM 1/2, L = 400 B

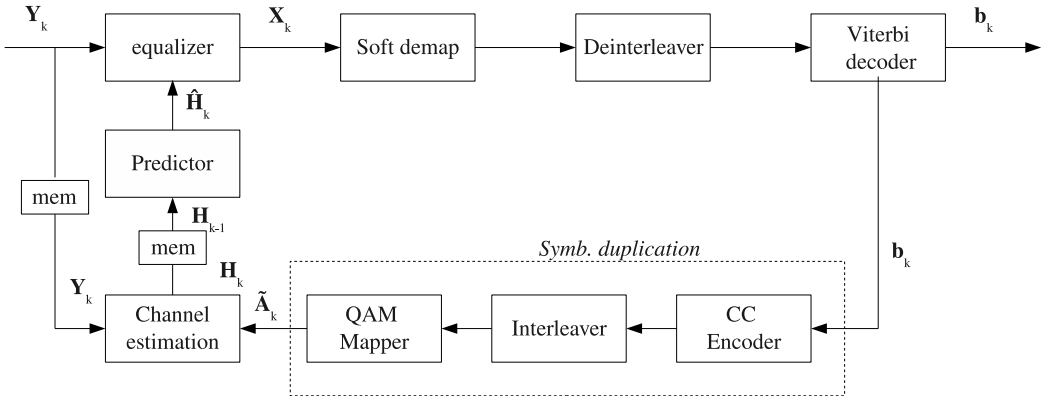

Figure 5.58: Non-iterative Data decoding-aided DD-CE scheme with prediction element

5.4 Linear prediction

In the previous section the residual decoding error and the effect of perfect data decoding have been analyzed. Under the hypothesis of perfect data decoding, the degradation of the performance introduced by the delay in the CE loop is noticeable and increases with the increase of the relative speed. In section 6.1 this degradation as a function of the relative speed will be further investigated.

To reduce the effect of the delay in the CE loop, the linear prediction theory has been considered. The general principle is to use the knowledge of the current and previous time instant channel estimates $(\mathbf{h}_k, \mathbf{h}_{k-1}, \ldots, \mathbf{h}_{k-N})$ in order to derive a *prediction* of the channel at the $(k+1)$-th time instant and compensate the degradation of the CIR due to the Doppler evolution. In other words in the reminder several CE algorithms that take into account not only the current but also the previous channel estimates in order to predict the evolution of the time-varying channel are described.

The general block diagram is shown in figure 5.58. It is understood that DD-CE algorithms with channel predictors should be seen as possible improvements of the non-iterative Viterbi DD-CE scheme (sec. 5.3.2) which is therefore the underlying reference for comparisons.

5.4.1 Linear MMSE prediction

The prediction theory [1] states that from a sequence of N past observations of a stationary random process $\mathbf{x}^T(k-1) = [x(k-1), x(k-2), \ldots, x(k-N)]$ with

autocorrelation vector $\mathbf{r}_N^T = [r_x(1), \ldots, r_x(N)]$, where the $j-$th entry is defined as $r_x(j) = \mathrm{E}[x(k)x^*(k-j)]$, the MMSE future estimation of $x(k)$ is

$$\hat{x}\left(k|\mathbf{x}(k-1)\right) = \sum_{i=1}^{N} c_i x(k-i) \tag{5.7}$$

that minimizes the prediction error:

$$f_N(k) = x(k) - \hat{x}\left(k|\mathbf{x}(k-1)\right) = x(k) - \sum_{i=1}^{N} c_i x(k-i). \tag{5.8}$$

The MSE of the predictor is $J = \mathrm{E}[|f_N(k)|^2]$. The derivation of the optimum coefficients $\mathbf{c}_{opt}^T = [c_{opt,1}, \ldots, c_{opt,N}]$ comes with the Wiener optimization theory [1]. It results that the optimum coefficient vector satisfies the equation:

$$\mathbf{R}_N \mathbf{c}_{opt} = \mathbf{r}_N \tag{5.9}$$

where $\mathbf{R}_N$ is the $[N \times N]$ autocorrelation matrix of the process defined as $\mathbf{R}_N = \mathrm{E}[\mathbf{x}(k)\mathbf{x}^H(k)]$. The minimum value of the cost function is

$$J_{min} = J_N = r_x(0) - \mathbf{r}_N^H \mathbf{c}_{opt} \tag{5.10}$$

From equations (5.9) and (5.10) the following equation can be derived:

$$\begin{bmatrix} r_x(0) & \mathbf{r}_N^H \\ \mathbf{r}_N & \mathbf{R}_N \end{bmatrix} \begin{bmatrix} 1 \\ -\mathbf{c}_{opt} \end{bmatrix} = \begin{bmatrix} J_N \\ \mathbf{0}_N \end{bmatrix} \tag{5.11}$$

that can also be written as:

$$\mathbf{R}_{N+1} \mathbf{a}_N^T = \begin{bmatrix} J_N \\ \mathbf{0}_N \end{bmatrix} \tag{5.12}$$

where $\mathbf{0}_N$ in the column vector of N zeros, $\mathbf{R}_{N+1}$ is the is the $[N \times N]$ autocorrelation matrix of the process with the $(i,j)-$th element defined as $R_{(i,j)} = \mathrm{E}[x(k-j)x^*(k-i)]$, with $i, j = 0, 1, \ldots, N$ and

$$\mathbf{a}_N^T = [1, -c_{opt,1}, \ldots, -c_{opt,N}]. \tag{5.13}$$

The optimum coefficient vector $\mathbf{c}_{opt}$ is obtained by solving the (5.12). The solution of (5.12) can be efficiently computed with Levinson-Durbin algorithm [1].

As an example the vector $\mathbf{a}_N^T = [1, -c_{opt,1}, -c_{opt,2}]$ have been derived for the case $N = 2$ past observations. It results that the optimum coefficients $\mathbf{c}_{opt}$ are:

$$c_{opt,1} = \frac{r_x(1)r_x(0) - r_x^*(1)r_x(2)}{r_x^2(0) - |r_x(1)|^2} \tag{5.14}$$

and

$$c_{opt,2} = \frac{r_x(0)r_x(2) - r_x^2(1)}{r_x^2(0) - |r_x(1)|^2} \tag{5.15}$$

It must be noted that the formulation (5.9) recalls the Yule-Walker equation defined as:

$$\mathbf{Ra} = -\mathbf{r} \tag{5.16}$$

that gives the $N \times 1$ coefficient vector $\mathbf{a}$ of the $N-$th order autoregressive (AR) process with $N \times N$ autocorrelation matrix $\mathbf{R}$ and $N \times 1$ autocorrelation vector $\mathbf{r}$. The AR model of a random process $x(k)$ of order N with coefficient vector $\mathbf{a} = [a_1, a_2, \ldots, a_N]$ is defined as:

$$x(k) = -\sum_{n=1}^{N} a_n x(k-n) + w(k) \tag{5.17}$$

where $w(k)$ is AWGN with variance σ_w^2.

In particular it results that the coefficients $\mathbf{a}_N^T = [1, -c_{opt,1}, \ldots, -c_{opt,N}]$, solution of (5.12), are the coefficients of the AR(N) model that approximate in the MMSE sense the fading channel with autocorrelation matrix $\mathbf{R}_{N+1}$. In other words the coefficients $\mathbf{a}_N^T = [1, -c_{opt,1}, \ldots, -c_{opt,N}]$ model both the MMSE predictor of a random process $x(k)$ given N past observations and the AR(N) model of the N-th order autoregressive process that better approximates (in the MMSE sense) the process $x(k)$. These considerations will be taken into account in section 5.4.2.

The MMSE predictor can be applied to the CE algorithms. As shown in section 1.2.1, the wireless channel can be modeled as a WSS-US process with T_c spaced taps defined as:

$$h(kT, nT_c) = \sum_{l=0}^{L_{ch}-1} h_l(kT)\delta(nT_c - lT_c) \tag{5.18}$$

with L_{ch} denoting the number of taps. It should be noted that the above equation takes into account the US property of the $h_l(kT)$ taps, $l = 0, 1, \ldots, L_{ch} - 1$ and that, in vehicular environment, the channel tap can be considered invariant within one OFDM symbol period T for the typical relative speeds under consideration.

The related autocorrelation function is given by:

$$r_h(\Delta t, \Delta\tau) = \mathrm{E}\left[h(kT, \tau)h^*(kT - \Delta t, \tau - \Delta\tau)\right] = \sum_{i=0}^{L_{ch}-1} r_{h_i}(\Delta t)\delta(\Delta\tau - iT_c) \tag{5.19}$$

and

$$r_{h_l}(\Delta t) = \mathrm{E}\left[h_l(kT)h_l^*(kT-\Delta t)\right]. \tag{5.20}$$

As said in section 5.1.1, a suitable Doppler spectrum for vehicular environment is the classical Jakes model defined in (1.11) and applied independently to every channel tap, for which (5.20) becomes:

$$r_{h_l}(\Delta t) = \sigma_{h_l}^2 J_0(2\pi f_D \Delta t) \tag{5.21}$$

being f_D the Doppler spread and $J_0(z)$ the first order Bessel function of first kind, defined as:

$$J_0(z) = \sum_{k=0}^{\infty}(-1)^k \frac{\left(\frac{z}{2}\right)^{2k}}{(k!)^2}. \tag{5.22}$$

The (i,j)-th element of the $N \times N$ autocorrelation matrix $\mathbf{R}_{h_l}$ of the $l-$th tap of the fading channel with Jakes Doppler spectrum is $R_{h_l,(i,j)} = \sigma_{h_l}^2 J_0(2\pi f_D(j-i)T)$. It results that the autocorrelation matrix $\mathbf{R}_{h_l}$ and the autocorrelation vector $\mathbf{r}_{h_l}$ of the $l-$th tap of the channel are the same for every tap, except for the multiplicative factor $\sigma_{h_l}^2$. It results that the vector $\mathbf{c_{opt}}$, solution of (5.9), is constant for every channel tap.

As a first DD-CE scheme with predictor, MMSE linear prediction has been applied to the current and past estimated CIRs in order to provide a delay-free CIR to the equalizer compared to the received OFDM symbol.

The $l-$th predicted channel tap $\hat{h}_l(k+1)$ at time instant $(k+1)$ is:

$$\hat{h}_l(k+1) = \sum_{i=1}^{k} c_{opt,i} h_l(k-i). \tag{5.23}$$

In vector notation the $L_{ch} \times 1$ predicted CIR $\hat{\mathbf{h}}_{k+1}$ at time instant $(k+1)$ can be written as:

$$\hat{\mathbf{h}}_{k+1} = \mathbf{h}_{k,1}\mathbf{c}_{opt} \tag{5.24}$$

where the $L_{ch} \times k$ matrix $\mathbf{h}_{k,1} = [\mathbf{h}_k \ldots, \mathbf{h}_1]^T$ has been defined as the matrix of the k past estimated CIRs.

The coefficients $\mathbf{c}_{opt}$ applied independenlty to every tap are calculated from the knowledge of the autocorrelation matrix $\mathbf{R}_{h_l}$ and the autocorrelation vector $\mathbf{r}_{h_l}$ of the $l-$th channel tap of the fading channel with Jakes spectrum. In particular, as previously stated, the coefficients $\mathbf{c}_{opt}$ are independent from the factor $\sigma_{h_l}^2$ that can

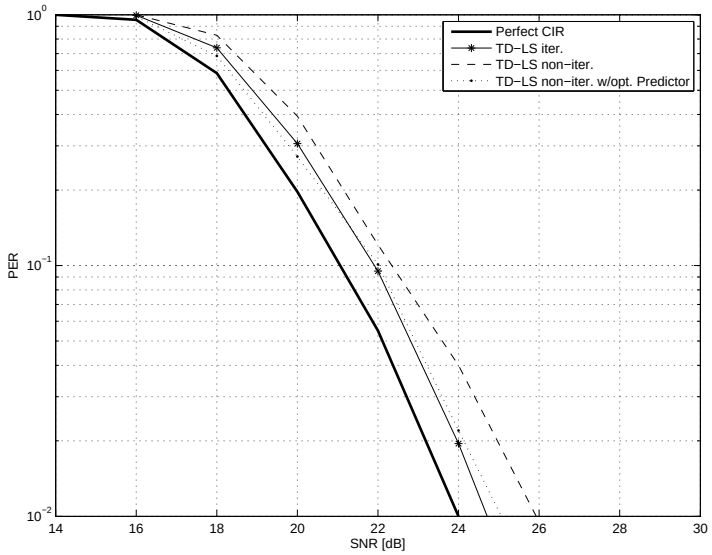

Figure 5.59: PER vs. SNR, ETSI C, v = 60 km/h - 64-QAM 3/4, L = 400B

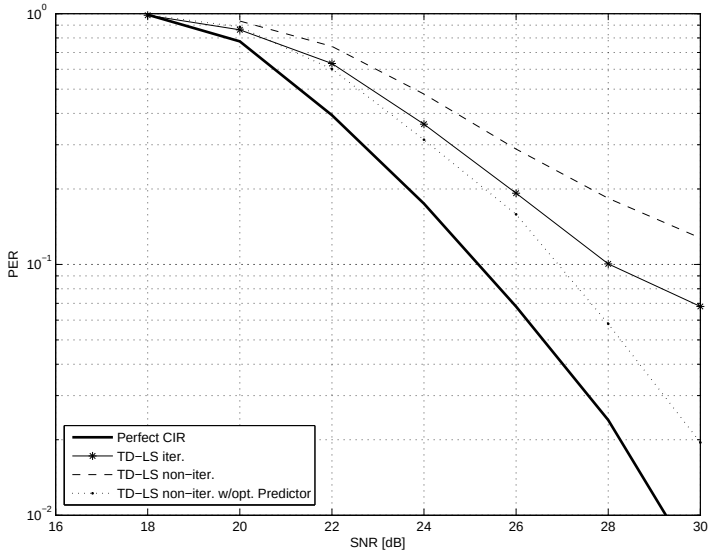

Figure 5.60: PER vs. SNR, ETSI B, v = 120 km/h - 64-QAM 3/4, L = 2000B

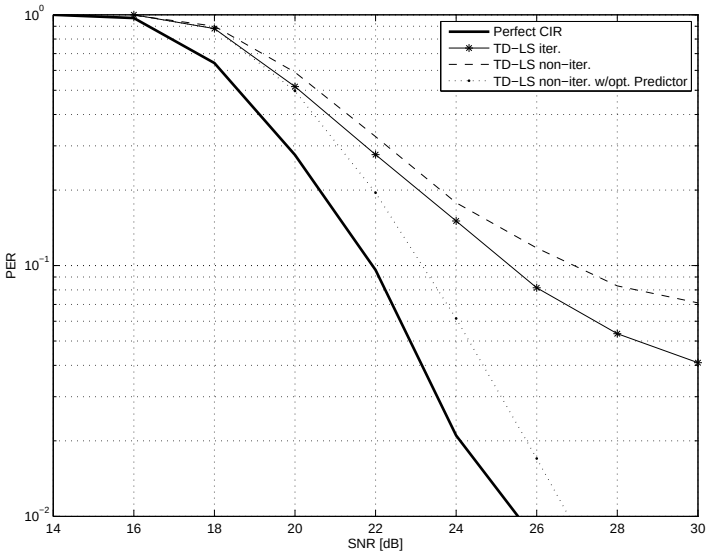

Figure 5.61: PER vs. SNR, ETSI C, v = 200 km/h - 64-QAM 3/4, L = 400B

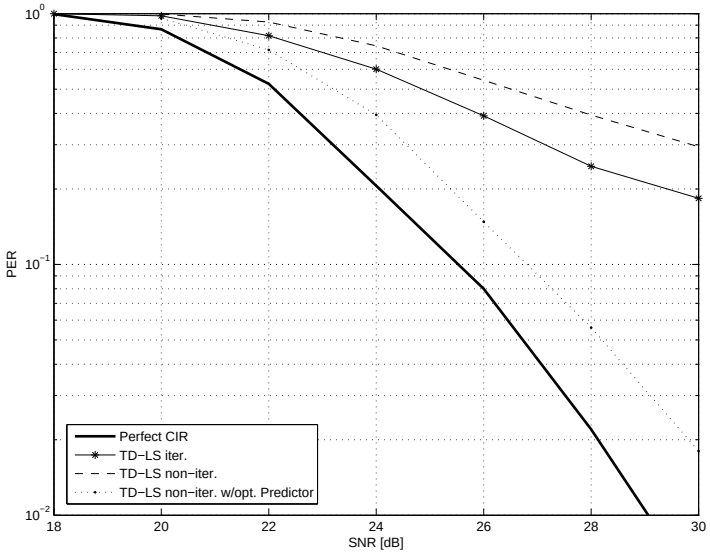

Figure 5.62: PER vs. SNR, ETSI C, v = 200 km/h - 64-QAM 3/4, L = 2000B

be considered unitary; in other words the knowledge of the PDP $\{\sigma^2_{h_1}, \ldots, \sigma^2_{h_{L_{ch}-1}}\}$ of the channel is not necessary to derive $\mathbf{c}_{opt}$.

Simulations of PER vs. SNR obtained using the scheme shown in figure 5.58 are reported in figures 5.59, 5.60, 5.61 and 5.62 where the gain achieved by the MMSE predictor can be observed. Further significant comments on the results are:

- in low-mobility scenarios the prediction element acts as an average of the CIRs at various time instants; it results in a reduction of the CE error. In particular in the case of no mobility, i.e. $v = 0$ km/h, the optimum coefficient vector $\mathbf{c}^T_{opt} = [c_{opt,1}, \ldots, c_{opt,N}]$ is constant with elements $c_{opt,i} = 1/N$, $i = 1, \ldots, N$;

- in high mobility scenarios the prediction element compensates the degradation introduced by the delay in the CE loop. In particular the highest improvement can be seen for high data rate and high mobility.

Moreover it can be seen that MMSE prediction outperforms the iterative Viterbi DD-CE scheme (sec. 5.3.1) without predictor where the final equalizer has no delay between the channel estimate and the received OFDM symbol.

A possible motivation for this result is that, in the iterative scheme without predictor, the degradation of the CIR due to the delay in the CE loop causes error propagation that the Viterbi decoder is not able to recover.

The main drawbacks of this MMSE predictor are the high computational and memory requirements (the actual memory size being related to the total number of OFDM symbols per packet):

- all the past estimated CIRs for all the OFDM symbols in the packet must be stored;

- the solution of the equation (5.12) must be updated for every received OFDM symbol because of the always increasing number of input past CIRs and it requires a number of operations proportional to k^2, where k is the number of past received OFDM symbols, when performed efficiently with the Levinson-Durbin algorithm.

The computation of the optimum MMSE predictor is practically unfeasible in real systems, but is is useful for simulations as an upper bound on performance gain achievable by a prediction element.

5.4.2 AR(N) model

The first simplification of the optimum MMSE predictor taken into account considers a fixed number of N past estimated CIRs (corresponding to as many past received OFDM symbols); it results that the optimum coefficient vector $\mathbf{c}_{opt}^T = [c_{opt,1}, \ldots, c_{opt,N}]$ must be calculated only once (assuming the wireless chanel modeled as a stationary process, otherwise the autocorrelation function is time-varying).

The method is computationally simpler because a fixed number of past input CIRs translates into a limited predictor filter length and $\mathbf{R}_N$ autocorrelation matrix size. Such number can be chosen ad-hoc based on the desired trade-off between performance and complexity.

The band-limited nature of the Doppler spectrum considered has consequently an infinite-length autocorrelation function of the channel process. In [26] details on the AR modeling for fading channels can be found; the authors derive the $N \times 1$ coefficient vector $\mathbf{a}$ of the AR(N) process that better approximates the fading channel with Jakes Doppler spectrum. As also previously reviewed in section 5.4.1 the coefficient vector $\mathbf{a}$ of the AR(N) process is related to the relative optimum predictive coefficient vector with the $\mathbf{a}_N^T = [1, -c_{opt,1}, \ldots, -c_{opt,N}]$.

Moreover from the analysis presented in [26] the MSE $\sigma_N^2 = J_N$, defined in (5.4.1) applied to the fading channel with Jakes Doppler spectrum, of the one-step AR(N) predictor can be evaluated for a fixed filter length N as

$$\sigma_N^2 \sim k[\sin(\pi f_D T)]^{2N} \tag{5.25}$$

where k is a constant and T is the prediction time that equals to the OFDM symbol time.

It should be noted that the normalized Doppler spread for a maximum relative speed $v = 260$km/h is $f_D T = 1425T = 0.0114$. In figure 5.63 the prediction error σ_N^2 of the AR(N) predictor as a function of the model order N is shown.

For the normalized maximum Doppler spread considered in vehicular scenarios and for the frame structure of the IEEE 802.11p packet, the AR(2) approximation of the fading channel with Jakes Doppler Spectrum has been chosen as trade-off: as shown in section 3.2.3, in a IEEE 802.11p packet the OFDM data symbols are preceded by a training sequence and the SIGNAL OFDM symbol modulated with the most robust modulation (BPSK, code rate = 1/2).

Let "0" be the time instant of the first received data OFDM symbol, "-1" the time instant of the received SIGNAL OFDM symbol and "-2" the time instant of

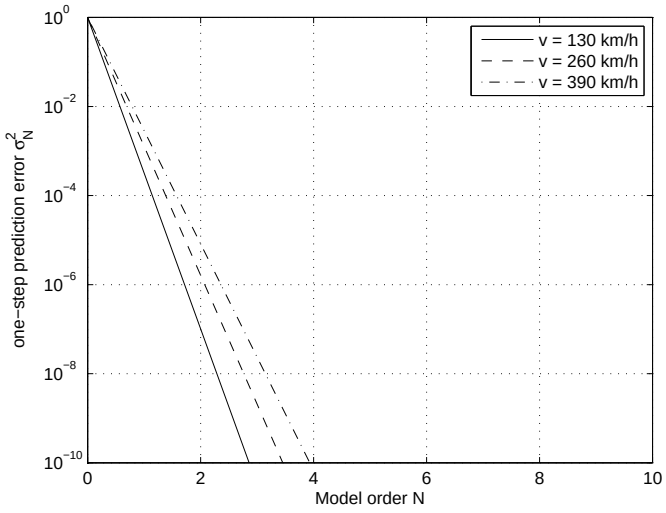

Figure 5.63: One-step prediction error of the AR(N) model.

the last LTS OFDM symbol received. It results that at time "0" two previous channel estimates have been computed and can be used from the prediction element to evaluate the channel estimate used to equalize the first received OFDM data symbol. It results that the AR(2) predictor can be exploited from the first OFDM data symbol.

The AR(2) predictor applied to the two stored estimated CIRs results:

$$\hat{\mathbf{h}}_{k+1} = \mathbf{h}_{k,k-1}\mathbf{c}_{opt} \tag{5.26}$$

where the $L_{ch} \times 2$ matrix $\mathbf{h}_{k,k-1} = [\mathbf{h}_k, \mathbf{h}_{k-1}]^T$ has been defined as the matrix of the 2 past estimated CIRs at time instant k. The coefficient vector $\mathbf{c}_{opt}$ has elements defined in (5.14) and (5.15).

Simulations of PER vs. SNR of figures 5.64, 5.65 and 5.66 show the performance achieved with the AR(2) predictor filter.

The low chosen order of the predictive filter, that corresponds to the approximation of the fading channel through an AR(2) process, leads to a substantial decrease in performance with respect to the optimum MMSE predictor shown previously:

- improvements can be seen in the three selected scenarios with respect to the non-iterative DD-CE scheme without predictor, in particular, as expected, for the highest speed considered $v = 200km/h$. This confirms the predictive nature of the AR(2) filter;

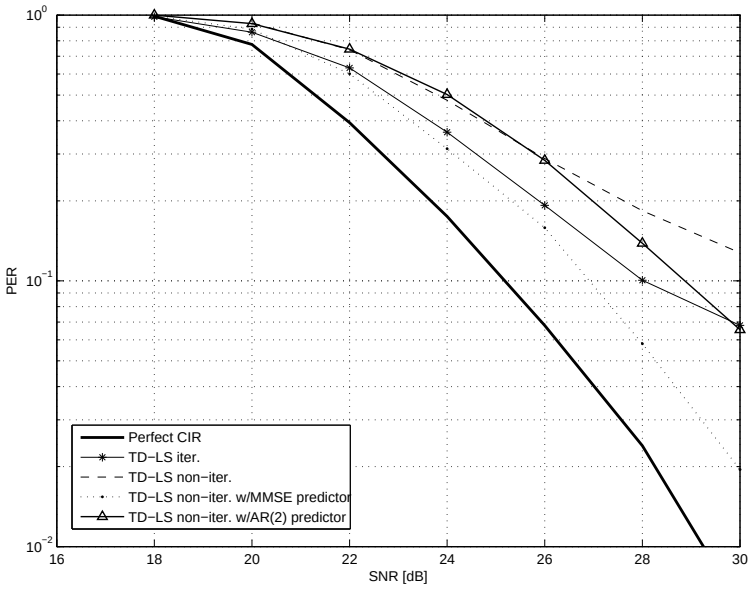

Figure 5.64: PER vs. SNR, DD-CE with AR(2) predictor - ETSI B, v = 120 km/h - 64-QAM 3/4, L = 2000 B

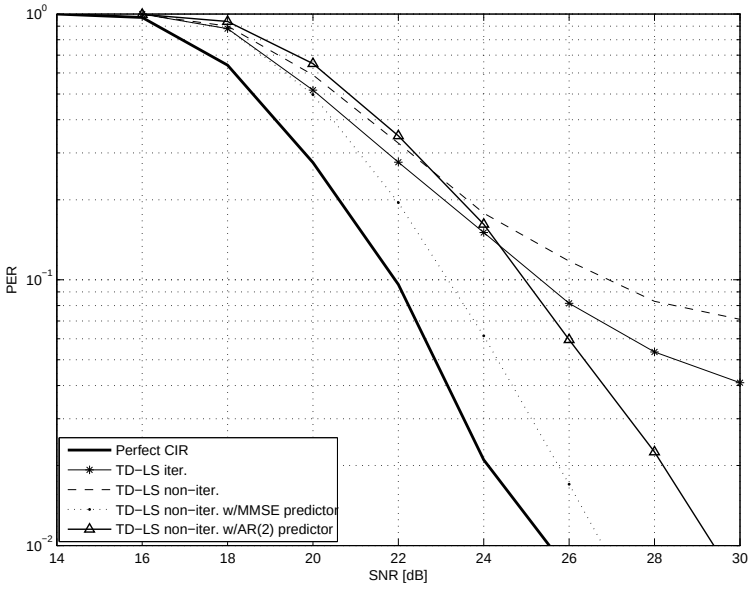

Figure 5.65: PER vs. SNR, DD-CE with AR(2) predictor - ETSI C, v = 200 km/h - 64-QAM 3/4, L = 400 B

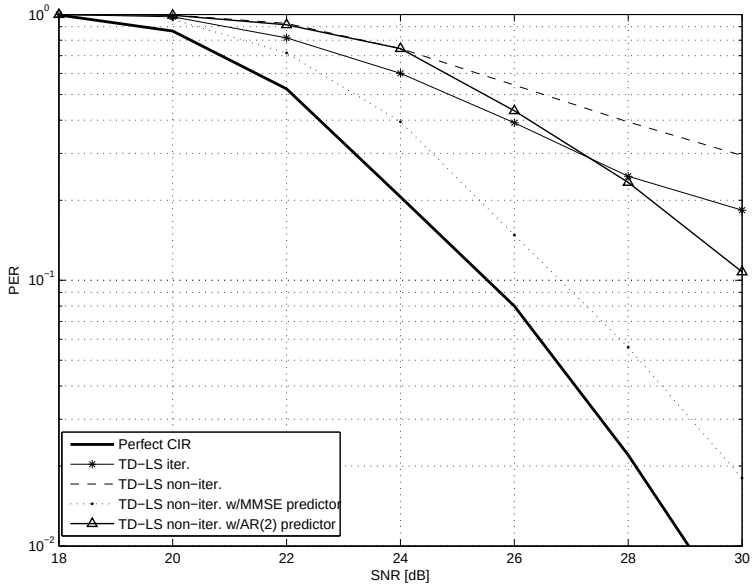

Figure 5.66: PER vs. SNR, DD-CE with AR(2) predictor - ETSI C, v = 200 km/h - 64-QAM 3/4, L = 2000 B

- the decrease in performance with respect to the MMSE predictor confirms the sub-optimal nature of the AR(2) prediction filter.

5.4.3 Kalman filter

As a term of comparison for the AR(2) predictor presented in section 5.4.2, in the following the widely used Kalman filter [27] will be briefly described and applied to the non-iterative DD-CE scheme as predictor element.

Kalman filter is a recursive estimator that follows the state of a dynamic system from a series of incomplete and noisy measurements. In detail, the underlying dynamical system is modeled as a Markov chain with the state of the finite state machine given by a vector of complex numbers $\mathbf{\Theta}_m$. At each discrete time increment a linear operator $\mathbf{F}_m$ is applied to the current state $\mathbf{\Theta}_{m-1}$ to generate the new state $\mathbf{\Theta}_m$ with some noise $\mathbf{n}_m$ mixed in. Then another linear operator $\mathbf{G}_m$ applied to the new hidden state $\mathbf{\Theta}_m$ generates the visible outputs $\mathbf{\Omega}_m$ corrupted by some more noise $\mathbf{e}_m$.

A schematic representation of Kalman filter framework is given in figure 5.67.

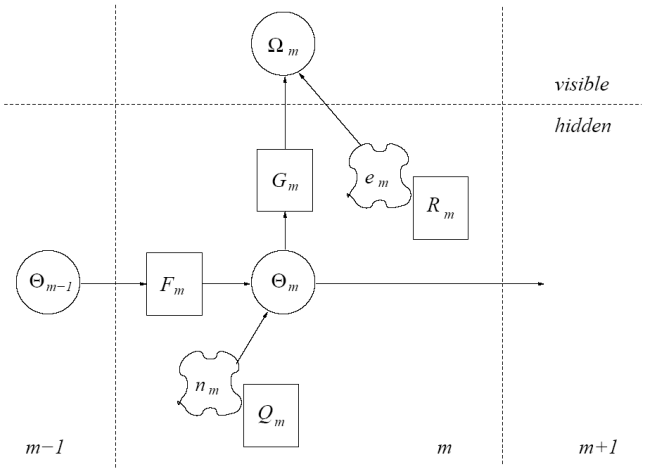

Figure 5.67: Schematic representation of Kalman filter framework

Hence the true system state $\mathbf{\Theta}_m$ at time m evolves from the state $\mathbf{\Theta}_{m-1}$ at time step $(m-1)$ according to the following:

$$\mathbf{\Theta}_m = \mathbf{F}_m \mathbf{\Theta}_{m-1} + \eta_m \tag{5.27}$$

where

- $\mathbf{\Theta}_m$ is the true hidden state at time step m,
- $\mathbf{F}_m$ is the state transition matrix applied to the previous state $\mathbf{\Theta}_{m-1}$,
- η_m is the process noise modeled as a complex-valued Gaussian vector process with zero mean and covariance $\mathbf{Q}_m$.

Moreover an observation $\mathbf{\Omega}_m$ of the true state at time step m is achieved according to:

$$\mathbf{\Omega}_m = \mathbf{G}_m \mathbf{\Theta}_m + \mathbf{e}_m \tag{5.28}$$

where

- $\mathbf{G}_m$ is the observation matrix that maps the true state space into the measured space,
- $\mathbf{e}_m$ is the zero mean Gaussian white observation noise with covariance $\mathbf{R}_m$

The initial state and the noise vectors at each step are assumed to be mutually independent. The Kalman filter is an algorithm that using both an estimate of the true system state relative to the $(m-1)-$th step, $\mathbf{\Theta}_{m-1}$ with error covariance matrix $\mathbf{P}_{m-1|m-1}$, and the observation vector $\mathbf{\Omega}_m$ gives an estimate of the $m-$th true state $\mathbf{\Theta}_m$.

This Kalman filter has two distinct phases: *predict* and *update*. The predict phase uses the estimate from the previous timestep $\mathbf{\Theta}_{m-1}$ to produce an estimate of the current state $\mathbf{\Theta}_m$.

Next in the update phase, measurements of the current timestep $\mathbf{\Omega}_m$ are used to refine the prediction and achieve a possibly better estimate $\mathbf{\Theta}_m$.

The Kalman filter has been applied to the non-iterative scheme as a predictor filter. In particular, as a term of comparison for the AR(2) predictor, the Kalman filter applied to $N = 2$ past observed CIRs has been derived.

The true hidden state is the CIR, the noisy observed state is the estimated CIR and the state transition matrix is made up of the prediction coefficient $\mathbf{c}_{opt}$ derived in (5.9). It results that the Kalman filter framework applied to the channel prediction at time instant k is defined with the following equations.

Predict phase

$$\widehat{\mathbf{h}}_k = \widehat{\mathbf{h}}_{k-1,k-2}\mathbf{c}_{opt} \tag{5.29}$$

$$\mathbf{P}_k = \mathbf{A}\mathbf{P}_{k-1}\mathbf{A}^T + \mathbf{Q} \tag{5.30}$$

Update phase

$$\mathbf{k}_k = \mathbf{P}_{k-1}(\mathbf{P}_{k-1} + \mathbf{R})^{-1} \tag{5.31}$$

$$\widehat{\mathbf{h}}_k = \widehat{\mathbf{h}}_{k-1} + \mathbf{k}_k(\mathbf{z}_k - \widehat{\mathbf{h}}_{k-1}) \tag{5.32}$$

$$\mathbf{P}_k = \mathbf{P}_{k-1} - \mathbf{k}_k\mathbf{P}_{k-1} \tag{5.33}$$

where

- $\widehat{\mathbf{h}}_k$ is the predicted CIR at time instant k;
- $\mathbf{c}_{opt}$ is the optimum coefficient vector as shown in (5.9);

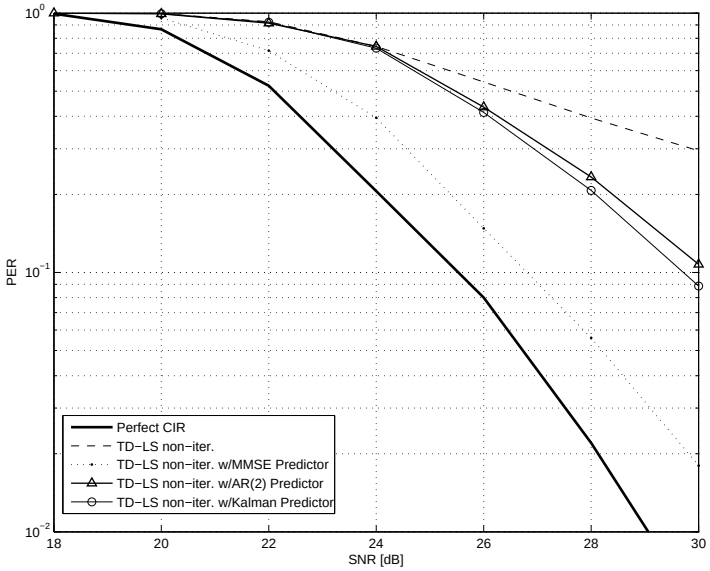

Figure 5.68: PER vs. SNR, DD-CE with Kalman filter - ETSI B, v = 120 km/h - 64-QAM 3/4, L = 2000 B

- $\widehat{\mathbf{h}}_{k-1,k-2}$ is the $L_{ch} \times 2$ matrix of the past predicted CIRs;
- $\mathbf{A}$ is the 2×2 state transition matrix of the process where each column is the vector $\mathbf{c}_{copt}$;
- $\mathbf{P}_k$ is the 2×2 estimate error covariance matrix;
- $\mathbf{Q}$ is the 2×2 process noise covariance matrix with diagonal elements equal to $\sigma^2_{h_l}$;
- $\mathbf{k}_k$ is the 2×2 Kalman gain matrix;
- $\mathbf{z}_k$ is the observed (estimated) CIR.

Simulation results of PER vs. SNR shown in figures 5.68 to 5.70 for the three worst cases selected in section 5.3.3 show the gain achieved by the Kalman filter with reference to the DD-CE scheme with no predictor. Moreover a slightly gain in performance can be seen with respect to the AR(2) predictor.

It should be noted that the Kalman filter leads to higher computational requirements with respect to the AR(2) predictor: the equations (5.29) to (5.33) are nec-

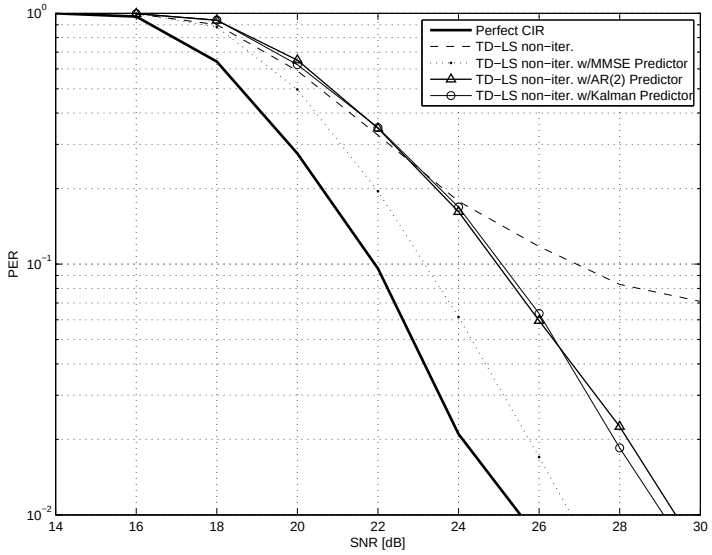

Figure 5.69: PER vs. SNR, DD-CE with Kalman filter - ETSI C, v = 200 km/h - 64-QAM 3/4, L = 400 B

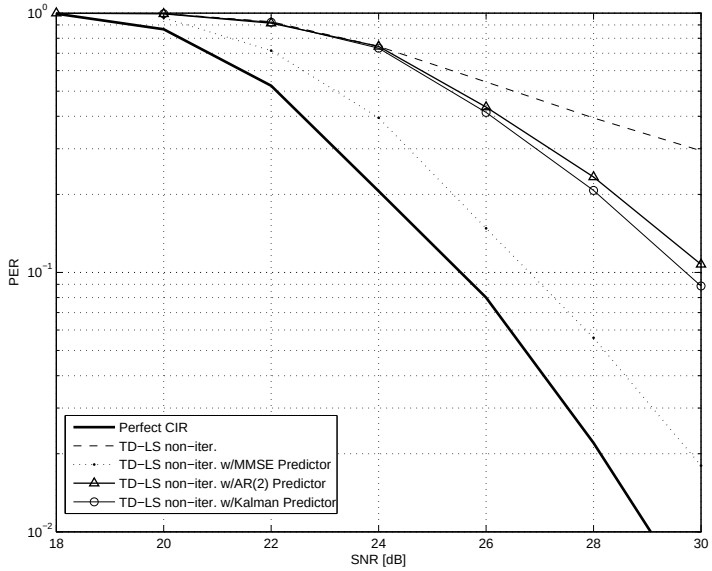

Figure 5.70: PER vs. SNR, DD-CE with Kalman filter - ETSI C, v = 200 km/h - 64-QAM 3/4, L = 2000 B

essary to implement the Kalman filter, on the contrary the AR(2) predictor makes use only of the prediction phase (5.29).

Chapter 6

Doppler estimation techniques for OFDM-based vehicular systems

Doppler effect estimation in vehicular systems can be important in order to determine a proper channel update refresh period, tailored to the relative speed between transmitter and receiver. The well-known idea of DD-CE and tracking is that, in the limit of static channel, one CE processing per packet, based on the initial preamble, is sufficient while for non negligible vehicle speed CE tracking is required after an initial CE instance.

The simulation results previously presented are related to the case of one CE tracking update per each OFDM symbol, which can serve as lower bound on the performance with respect to the CE tracking occurrence impact.

Aim of the investigations described in this section is to find out whether it is possible to adaptively decrease the CE update period compared to the rate of the input OFDM systems based on the relative speed between transmitter and receiver, without significantly degrading the performance shown in the previous chapter.

This would be advantageous for power consumption and/or processing complexity reduction of IEEE802.11p compliant receivers. A reliable relative speed estimation must be accomplished in order to apply this idea. It could be objected that most vehicular connectivity systems are envisioned to include GPS (satellite global positioning systems) apparatuses that can provide speed information reliably. However, the required speed value is relative, so the two terminals should exchange speed information. Moreover, the power consumption target would likely target portable devices for which the GPS locator, if present, probably should not be always active. In such cases baseband techniques for Doppler spread (and thus speed, intrinsically

already relative between transmitter and receiver) estimation would likely be appealing for future vehicular conncetivity systems. The above considerations motivate the assessment of the state-of-the-art Doppler spread estimation algorithms presented in this chapter, and their application to vehicular systems.

6.1 Problem definition: impact of CE occurrence on PHY performance

In this section the degradation of the channel estimate as a function of the speed and the impact of CE occurrence on PER vs. SNR performance will be derived.

As shown in section 1.2.1, the wireless channel can be modeled as a WSS-US process with T_c spaced taps defined as:

$$h(kT, nT_c) = \sum_{l=0}^{L_{ch}-1} h_l(kT)\delta(nT_c - lT_c) \tag{6.1}$$

with L_{ch} denoting the number of taps. It should be noted that the above equation takes into account the US property of the $h_l(kT)$ taps, $l = 0, 1, \ldots, L_{ch} - 1$ and that, in vehicular environment, the channel tap can be considered invariant within one OFDM symbol period T for the typical relative speeds under consideration.

It can be shown that the related autocorrelation function is given by:

$$r_h(\Delta t, \Delta\tau) = \mathrm{E}\left[h(kT, \tau)h^*(kT - \Delta t, \tau - \Delta\tau)\right] = \sum_{i=0}^{L_{ch}-1} r_{h_i}(\Delta t)\delta(\Delta\tau - iT_c) \tag{6.2}$$

and

$$r_{h_l}(\Delta t) = \mathrm{E}\left[h_l(kT)h_l^*(kT - \Delta t)\right]. \tag{6.3}$$

By expressing the channel impulse response (6.1) in compact vectorial notation as $\mathbf{h}_k = [h_0(kT), h_1(kT), \ldots, h_{L_{ch}-1}(kT)]^T$, then the variation of the CIR at the time instant kT with reference to the time $(k - n)T$ canbe written:

$$\mathbf{\Delta h}_k^n = \mathbf{h}_k - \mathbf{h}_{k-n}. \tag{6.4}$$

As shown in [24] it results that the degradation $\Delta h_{l,k}^n$ of the $l-$th channel tap $h_{l,k}$ at the time instant kT with reference to the $l-$th channel tap $h_{l,k-n}$ at time $(k-n)T$ can be estimated as:

$$\begin{aligned}\mathrm{E}\left[\Delta h_{l,k}^{n}\Delta h_{l,k}^{*,n}\right] &= \mathrm{E}\left[\left(h_{l,k}-h_{l,k-n}\right)\left(h_{l,k}-h_{l,k-n}\right)^{*}\right]\\ &= \mathrm{E}\left[h_{l,k}h_{l,k}^{*}-h_{l,k}h_{l,k-n}-h_{l,k-n}h_{l,k}^{*}+h_{l,k-n}h_{l,k-n}^{*}\right]\\ &= \mathrm{E}\left[h_{l,k}h_{l,k}^{*}\right]-\mathrm{E}\left[h_{l,k}h_{l,k-n}^{*}\right]-\mathrm{E}\left[h_{l,k-n}h_{l,k}^{*}\right]+\mathrm{E}\left[h_{l,k-n}h_{l,k-n}^{*}\right]\\ &= 2\cdot\left(r_{h_l}(0)-r_{h_l}(nT)\right)\end{aligned} \tag{6.5}$$

then the MSE of the channel estimate introduced by the degradation of the channel due to Doppler effect for a delay of n OFDM symbols is:

$$\begin{aligned}\sigma_d^2(n) &= \mathrm{E}\left[\|\mathbf{\Delta h}_k^n\|^2\right]\\ &= \mathrm{E}\left[\mathbf{\Delta h}_k^{n,*}\mathbf{\Delta h}_k^{n,*}\right]\\ &= \sum_{l=0}^{L_{ch}-1} 2\cdot\left(r_{h_l}(0)-r_{h_l}(nT)\right)\end{aligned} \tag{6.6}$$

The Doppler spread that characterizes independently the $l-$th tap is the Fourier transform of the autocorrelation function of the $l-$th channel tap:

$$D_l(f) = \int_{-\infty}^{+\infty} r_{h_l}(\Delta t)e^{-j2\pi f\Delta t}dt. \tag{6.7}$$

As said in chapter 5, a suitable Doppler spectrum for vehicular environment is the classical Jakes model defined in (1.11) and applied independently to every channel tap, for which (6.3) becomes:

$$r_{h_l}(\Delta t) = \sigma_{h_l}^2 J_0(2\pi f_D\Delta t) \tag{6.8}$$

being f_D the Doppler spread and $J_0(z)$ the first order Bessel function of first kind.

Combining 6.6 with 6.8, $\sigma_d^2(n)$ becomes:

$$\sigma_d^2(n) = \sum_{l=0}^{L_{ch}-1} 2\cdot\left(r_{h_l}(0)-r_{h_l}(nT)\right) = \sum_{l=0}^{L_{ch}-1} 2\cdot\sigma_{h_l}^2\left(1-J_0(2\pi f_D nT)\right) \tag{6.9}$$

If CE tracking is performed once every n OFDM symbols, i.e. $\mathbf{H}_{k-n}$ is used to perform equalization of $\mathbf{Y}_k$ instead of $\mathbf{H}_k$, the mean estimation error $e(n)$ experienced for varying time instants from 1 to n can be evaluated as:

$$e(n) = \frac{1}{n}\sum_{i=1}^{n}\sigma_d^2(i) = \frac{2}{n}\sum_{i=1}^{n}\sum_{l=0}^{L_{ch}-1}\sigma_{h_l}^2(1-J_0(2\pi f_D iT)) = \frac{2}{n}\sum_{i=1}^{n}\left(1-J_0(2\pi f_D iT)\right) \tag{6.10}$$

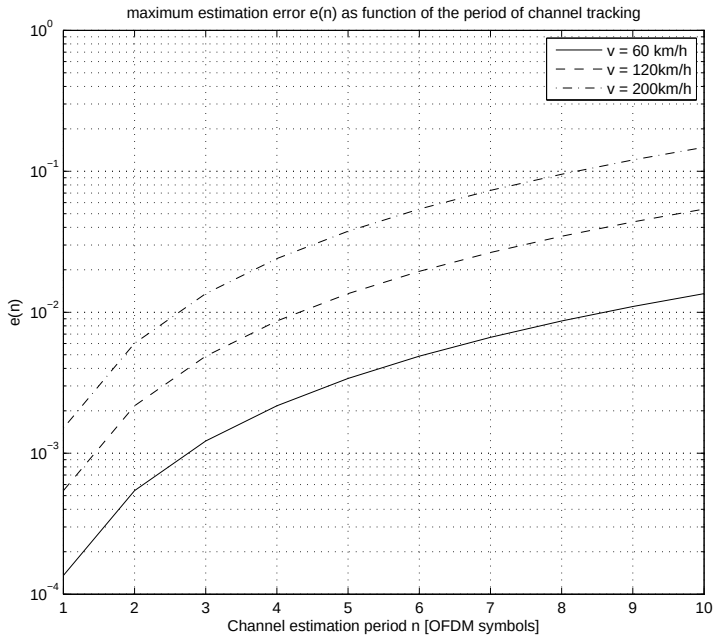

Figure 6.1: Mean square error as function of the estimation period n and different relative speeds

where the inner summation in (6.10) takes into account that the PDP of the channel is usually normalized to 1, as shown in (1.20). $e(n)$ is shown as a function of n in figure 6.1, for three different relative speeds between transmitter and receiver.

In equation 6.9 the MSE of the channel estimate introduced by the degradation of the channel for a delay of n OFDM symbols has been derived. It should be noted that in static scenario the autocorrelation of the $l-$th channel tap is $r_{h_l}(\Delta t) = \sigma^2_{h_l}$ $\forall \Delta t \in \mathbb{R}$ and no degradation occurs, i.e. $\sigma^2_d(n) = 0 \ \forall n$.

As shown in [24] the error introduced by the variation of the channel, for a delay of n OFDM symbols, can be seen as an equivalent noise contribution at the receiver, i.e. being $\sigma^2_d(n) = \mathrm{E}[\|\mathbf{\Delta h}^n(kT)\|^2]$, then the equivalent SNR of the system as a function of n is given by:

$$SNR'(n) = \frac{\mathrm{E}[|A_n|^2]}{\sigma^2_w + \sigma^2_d(n)} \tag{6.11}$$

where $\mathrm{E}[|A_n|^2]$ is the signal energy and $\sigma^2_w = N_0$ is the AWGN PSD.

In case the CE is updated once every n OFDM symbols, then (6.11) should be

evaluated for all the intermediate time instants $j = 1, \ldots, n$ and an average SNR can be taken as an effective measure of the average experienced SNR. However, a conservative measure given by (6.11) for the largest time instant only can be taken as reference in order to determine a proper CE tracking interval and limit the performance degradation. This will be better explained in the following.

Figures 6.2(a), 6.2(b) and 6.2(c) plot $SNR'(n)$ versus the ideal SNR as a function of different values for the relative speed v and for different CE tracking intervals n. Such plots are important as they indicate a bound on the achievable effective SNR for a given CE tracking interval. Based on them, a value for n can be chosen as a function of speed and theoretical SNR range, once a maximum limit on the acceptable SNR degradation is set by the designer.

A strategy to relate the value to different speeds is a threshold on the maximum degradation introduced on SNR' by $\sigma_d^2(n)$.

For example, setting 1 dB as the maximum acceptable SNR degradation, the resulting tolerable CE tracking interval n is reported in Table 6.1. The values have been determined taking into account Figure 6.2 and three speed ranges having as mid-range thresholds the speed values used for the PER vs. SNR simulations presented in this work, i.e. $v = 0, 60, 120, 200$ km/h. For a speed $v < 30$ km/h the channel is considered time-invariant and channel tracking is not performed.

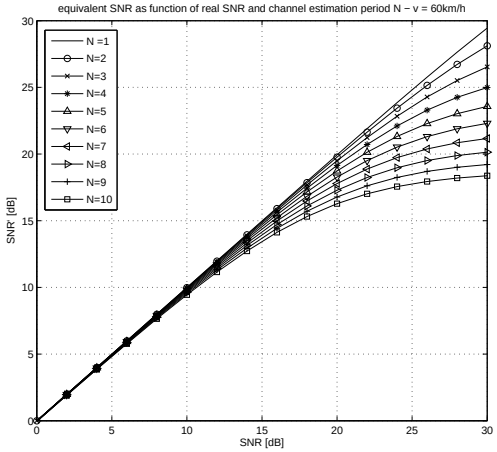

(a) v = 60 km/h

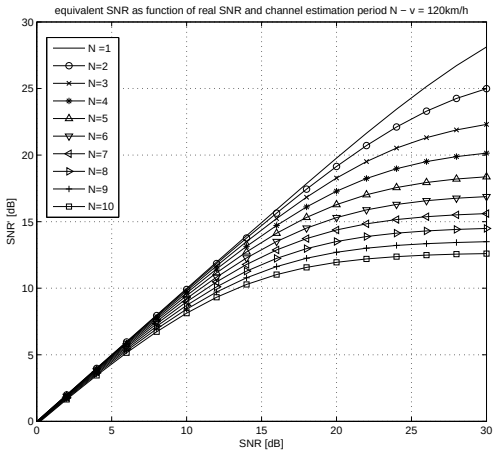

(b) v = 120 km/h

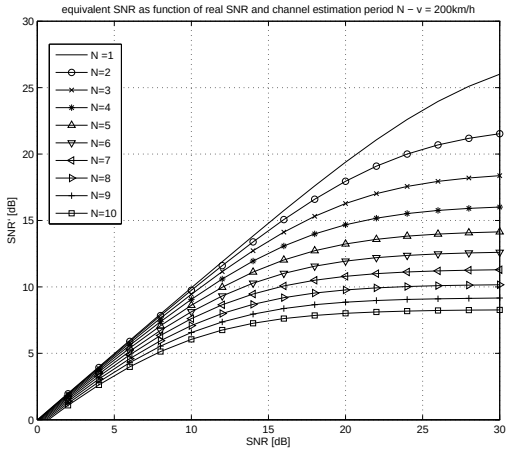

(c) v = 200 km/h

Figure 6.2: SNR' as function of SNR for different values of n and three relative speeds between transmitter and receiver

SNR	CE occurrence (n) for $30 < v < 90$ km/h	n for $90 < v < 160$ km/h	n for $v > 160$ km/h
1	10	10	10
2	10	10	10
3	10	10	9
4	10	10	8
5	10	10	7
6	10	10	6
7	10	9	5
8	10	8	5
9	10	7	4
10	10	6	4
11	10	6	3
12	10	5	3
13	9	4	2
14	8	4	2
15	7	3	2
16	6	3	2
17	6	3	1
18	5	2	1
19	4	2	1
20	4	2	1
21	3	1	1
22	3	1	1
23	3	1	1
24	2	1	1
25	2	1	1
26	2	1	1
27	1	1	1
28	1	1	1
29	1	1	1
30	1	1	1

Table 6.1: CE tracking interval for 1 dB SNR degradation as a function of the theoretical imposed SNR.

6.2 Techniques for Doppler spread estimation

In order to be able to extrapolate an effective value of the channel estimation period n, the relative speed between transmitter and receiver must be estimated.We recall that the relative speed is directly related to the Doppler spread f_D of the CIR as:

$$v = \frac{f_D c}{f_c} \tag{6.12}$$

where v is the relative speed expressed in [m/s], c is the speed of light and f_c is the carrier frequency. In literature a large number of Doppler spread estimators have been proposed; these can be divided in two classes: one is based on level-crossing rate (LCR) measurement of the considered process, the other is based on the estimation of the auto-covariance function of the process [29], [30]. In vehicular environment the main requirements for speed estimation are the robustness to noise, i.e. the ability to track Doppler Spread even at low SNR, and low convergence time, derived from the fast time-varying nature of the scenarios.

The Doppler Spread estimation method based on the zero-crossing rate (ZCR) measurement [28] has been considered, that is a particular case of the LCR estimators. The main advantage of this technique is the low complexity of its implementation, however it requires a very long convergence time. Another significant investigated method based on the estimation of the autocorrelation function of the channel is [29], which will be shown to provide good performance when applied to IEEE 802.11p systems.

The next sections report the analysis of the mentioned Doppler spread estimators, evaluation of their performance and effectiveness in vehicular environment.

6.2.1 Hybrid autocorrelation-based Doppler spread estimator

This section refers to the algorithm proposed in [29]. It is based on the evaluation of the autocorrelation of the CIR, and is named hybrid because it then uses the autocorrelation estimate according to either a curvature estimator or a first zero detection method, depending on the Doppler spread value range. The estimated autocorrelation coefficient of the $l-$th tap of the CIR evaluated for a delay of m

OFDM symbols is given by:

$$\rho_{h_l}(mT) = \frac{\frac{1}{(N-m)T}\sum_{i=1}^{N-m} h_l(iT)h_l^*(iT+mT)}{\frac{1}{N}\sum_{i=1}^{N}|h_l(iT)|^2} \tag{6.13}$$

where NT is the observation time, meaning that the estimate is performed considering N OFDM symbols. Despite in [29] the estimator is described as un-biased, for real CE estimates $\tilde{h}_l$ one has:

$$\sigma^2_{\tilde{h}_l} = \mathrm{E}[\tilde{h}_l\tilde{h}_l^*] = \mathrm{E}[(h_l+n_l)(h_l+n_l)^*] \simeq \frac{1}{NT}\sum_{i=1}^{N}|\tilde{h}_l(iT)|^2 \simeq \sigma^2_{h_l} + \sigma^2_{n_l} \tag{6.14}$$

where n_l has been defined as the CE error of the CIR at the $l-$th tap and $\sigma^2_{n_l} = \mathrm{E}[|\tilde{h}_l - h_l|^2]$ is the mean square error (MSE). Thus, (6.13) has been modified to remove the bias thus obtaining:

$$\rho_{\tilde{h}_l}(mT) = \frac{\frac{1}{N-m}\sum_{i=1}^{N-m} \tilde{h}_l(iT)\tilde{h}_l^*((i+m)T)}{\frac{1}{N}\sum_{i=1}^{N}|\tilde{h}_l(iT)|^2 - \sigma^2_{n_l}} \tag{6.15}$$

where it has been assumed that n_l at different time instants is statistically independent and thus does not affect the numerator on average.

The expression of the term $\sigma^2_{n_l}$ depends on the employed CE technique. An example is provided in chapter 4 with reference to the TD-LS and the modified TD-LS RR of [15], in sections 4.1.2 and 4.1.3, respectively.

After estimating the normalized autocorrelation coefficient for every channel tap, the method proposed in [29] improves the estimation accuracy by averaging the normalized $\rho_{h_l}(mT)$ for K taps:

$$\rho_h(mT) = \frac{1}{K}\sum_{l=1}^{K}\rho_{\tilde{h}_l}(mT) \tag{6.16}$$

An example of the behavior of $\rho_h(mT)$ estimator for a single channel realization and tap combining with $K = 1, \ldots, 4$ and $m = 1$ (we recall that $T = 8\mu s$), is reported in figures 6.3(a) and 6.3(b) as a function of the estimation time expressed in WLAN packets (16QAM 2000Byte packet length), for v = 60 km/h and v = 200 km/h respectively.

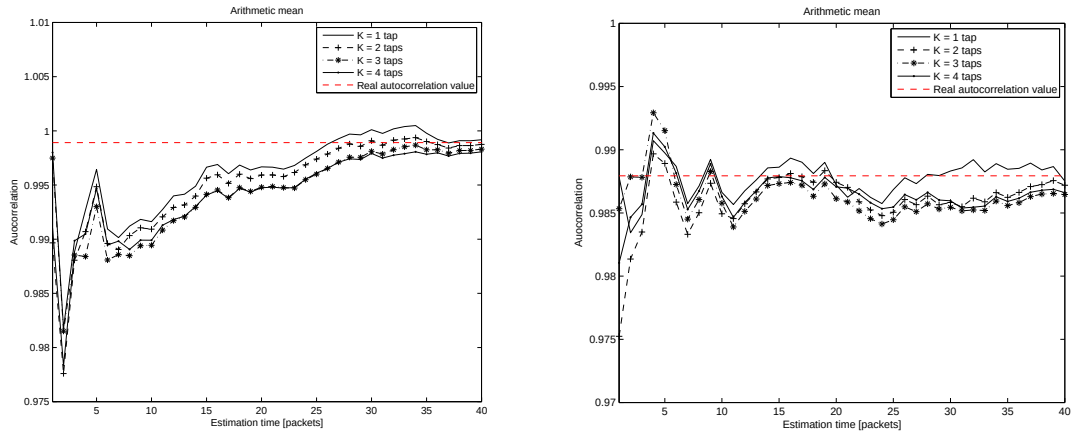

(a) v = 60 km/h

(b) v = 200 km/h

Figure 6.3: Autocorrelation estimate performed for 1,2,3,4 taps and the ideal value

To show a better picture than $\rho_h(mT)$ estimation based on a single channel realizations, the MSE estimator of $\rho_h(mT)$ for tap combining with $K = 1, \ldots, 4$ and $m = 1$ has been evaluated as a function of the estimation time expressed in WLAN packets.

For simplicity referring to a single tap, the MSE has been evaluated as:

$$MSE = \mathrm{E}\left[\left|\rho_{\tilde{h}_l}(mT) - \rho_{h_l}(mT)\right|^2\right] = \\ = \mathrm{E}\left[\left|\frac{\frac{1}{N-m}\sum_{i=1}^{N-m}\tilde{h}_l(iT)\tilde{h}_l^*((i+m)T)}{\frac{1}{N}\sum_{i=1}^{N}|\tilde{h}_l(iT)|^2 - \sigma_{n_l}^2} - J_0(2\pi f_D mT)\right|^2\right] \quad (6.17)$$

Figures 6.4 to 6.6 show the MSE evaluated respectively for $v = 60$, 120 and 200 km/h.

The Doppler spread f_D (and therefore the speed v) can be estimated from $r_h(\Delta t)$ (i.e. $\rho_{h_l}(mT)$ with $\Delta t = mT$) recalling (6.8) and (6.15) and in particular that $r_h(\Delta t) \propto J_0(2\pi f_D \Delta t)$. In particular the hybrid technique considers two options according to the Doppler range:

- f_D is determined from the first zero t_0 of $r_h(\Delta t)$, i.e.

$$f_D = \frac{\xi_0}{2\pi t_0} \simeq \frac{0.38}{t_0} \quad (6.18)$$

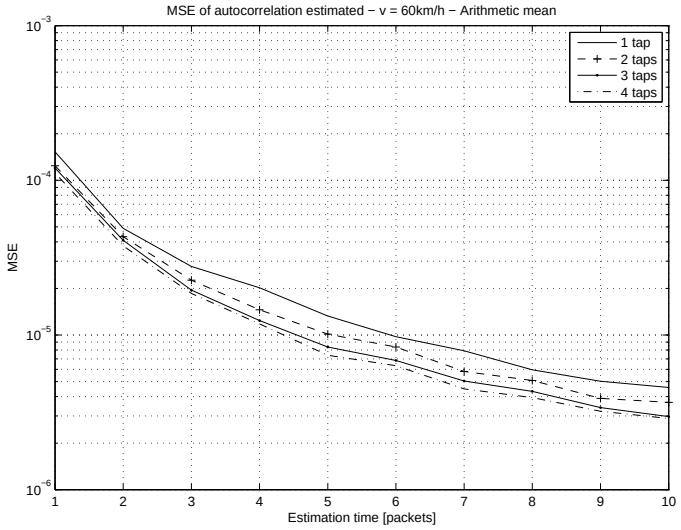

Figure 6.4: MSE of the autocorrelation values estimated, v = 60 km/h

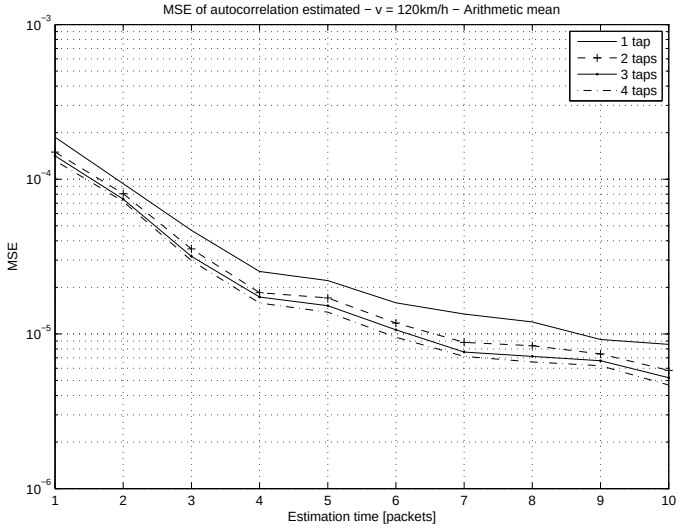

Figure 6.5: MSE of the autocorrelation values estimated, v = 120 km/h

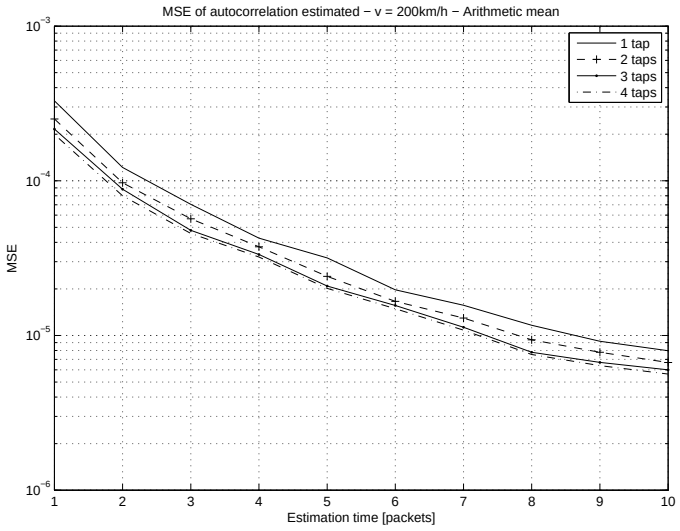

Figure 6.6: MSE of the autocorrelation values estimated, v = 200 km/h

where ξ_0 is the first zero of the Bessel function $J_0(\xi)$. This technique is suitable for Doppler spread sufficiently high so that $f_D \Delta t = f_D m T > 0.38$.

For vehicular systems at $f_c = 5.9$ GHz, $T = 8\mu s$ (i.e. $BW = 10$ MHz) and relative speed in the order of $v = 200$ km/h, the first value such that $r_h(m_0 T)$ is negative is $m_0 = 43$. As a lower estimation time is desirable, an alternative Doppler estimation technique can be employed.

- a *curvature estimator* determines f_D as

$$f_D = \frac{1}{2\pi}\sqrt{\frac{-2r_h''(0)}{r_h(0)}} \tag{6.19}$$

The term $r_h''(0)$ can be approximated through a polynomial fit. As shown in [29], the higher the degree of the polynomial fitting function, the better is the approximation for high Doppler spread values.

It should be recalled that the zero-th order Bessel function of the first kind can be well approximated by the following polynomial representation obtained through truncation of its series expression to the second or fourth degree:

$$J_0(z) = \sum_{=0}^{\infty}(-1)^i \frac{\left(\frac{z}{2}\right)^{2i}}{(i!)^2} \approx 1 - \frac{z^2}{4} + \frac{z^4}{64} \tag{6.20}$$

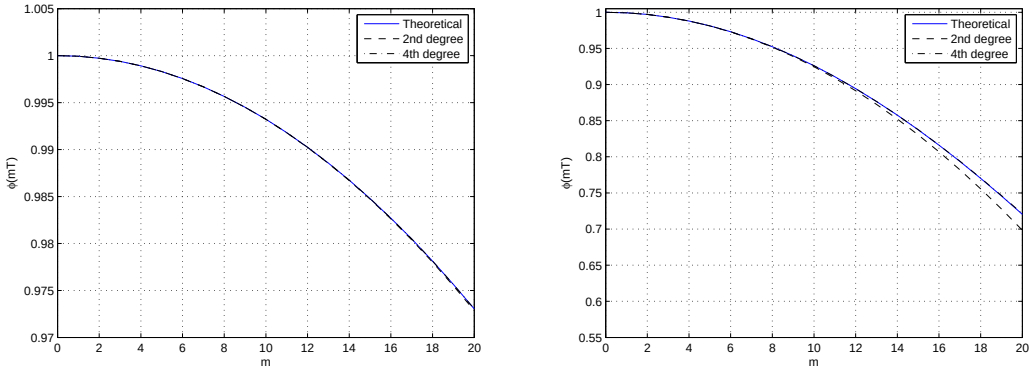

(a) v = 60 km/h (b) v = 200 km/h

Figure 6.7: Zero-th order Bessel function of first kind $J_0(2\pi f_D mT)$ and its approximation

Actually the fourth degree polynomial approximation is not required for the value range of interest to us, as shown in Figure 6.7.

From (6.20) the general expression for the fourth order polynomial fit of $r_h(\Delta t)$, based on the estimated discrete values $\hat{r}_h(iT)$, with $i = 1, \ldots, m$, is given by:

$$p(x) = a_0 + a_2 x^2 + a_4 x^4, \quad x = \frac{\Delta t}{T} \tag{6.21}$$

In vector notation we define $\mathbf{a} = (a_0, a_2, a_4)^T$, $\mathbf{r} = (\hat{r}_h(T), \ldots, \hat{r}_h(mT))$ and $\mathbf{p} = (p(1), p(2), \ldots, p(m))$. It results that $\mathbf{p} = \mathbf{H}\mathbf{a}$ is the system of equations of the problem, where the matrix $\mathbf{H}$ has been defined as:

$$\mathbf{H} = \begin{pmatrix} 1 & 1 & 1 \\ 1 & 2^2 & 2^4 \\ \vdots & \vdots & \vdots \\ 1 & m^2 & m^4 \end{pmatrix} \tag{6.22}$$

The least square fit of $\mathbf{r}$ is $\hat{\mathbf{a}}$ that minimizes $\|\mathbf{r} - \mathbf{H}\hat{\mathbf{a}}\|^2$. It results that:

$$\hat{\mathbf{a}} = (\mathbf{H}^T\mathbf{H})^{-1}\mathbf{H}^T\mathbf{r} = \mathbf{B}\mathbf{r} \tag{6.23}$$

where $\mathbf{B} = (\mathbf{H}^T\mathbf{H})^{-1}\mathbf{H}^T$.

For a $k-$th degree polynomial approximation only the first k entries of $\hat{\mathbf{a}}$ can be retained. Finally, for either $k = 2$ or $k = 4$ the Doppler spread estimate can be obtained from (6.19) as:

$$\hat{f}_D = \frac{1}{\pi T}\sqrt{\frac{-\hat{a}_2}{\hat{a}_0}} \tag{6.24}$$

An alternative simplified estimate can also be obtained as follows. A reduced vector $\mathbf{r}$ is considered, i.e. $\mathbf{r} = (\hat{r}_h(0), \hat{r}_h(mT))$, $m > 0$, and considering a 2nd order polynomial fit. It results that

$$\mathbf{H} = \begin{pmatrix} 1 & 0 \\ 1 & m^2 \end{pmatrix} \tag{6.25}$$

and

$$\mathbf{B} = \begin{pmatrix} 1 & 0 \\ -1/m^2 & 1/m^2 \end{pmatrix}. \tag{6.26}$$

From (6.23) the elements of the coefficient vector $\hat{\mathbf{a}}$ are given by:

$$\begin{aligned} \hat{a}_0 &= \hat{r}_h(0) \\ \hat{a}_2 &= (-\hat{r}_h(0) + \hat{r}_h(mT))/m^2 \end{aligned} \tag{6.27}$$

The result (6.27) can also be obtained considering the second order approximation of $r_h(mT)$:

$$r_h(mT) \approx P(mT) = a_0 + a_2 m^2. \tag{6.28}$$

and derive the unknown coefficient estimates $\hat{a}_0$ and $\hat{a}_2$ as:

$$\hat{a}_0 = \hat{r}_h(0) \tag{6.29}$$

$$\hat{a}_2 = \frac{\hat{r}_h(mT) - \hat{a}_0}{m^2} \tag{6.30}$$

Substituting (6.29) and (6.30) in (6.24) it results that the estimated Doppler spread $\hat{f}_D$ is:

$$\hat{f}_D = \frac{1}{\pi T}\sqrt{\frac{-\hat{a}_2}{\hat{a}_0}} = \frac{1}{\pi m T}\sqrt{\frac{\hat{r}_h(0) - \hat{r}_h(mT)}{\hat{r}_h(0)}} \tag{6.31}$$

Recalling that $\rho_h(mT) = \hat{r}_h(mT)/\hat{r}_h(0)$, $\hat{f}_D$ can finally be expressed as:

$$\hat{f}_D = \frac{1}{\pi m T}\sqrt{\frac{\hat{r}_h(0) - \rho_h(mT)\hat{r}_h(0)}{\hat{r}_h(0)}} = \frac{\sqrt{1 - \rho_h(mT)}}{\pi m T}. \tag{6.32}$$

As reference the relative speed v has been estimated with both Doppler estimators (6.24) and (6.32). The general fitting method was computed with $\hat{r}_h(mT)$, $m = 1, \ldots, 10$ and the simplified method with $\hat{r}_h(0)$ and $\hat{r}_h(mT)$, $m = 1$. The considered simulation scenario was 16-QAM CR 1/2, 2000 B packet length, ETSI C channel model; the estimated speeds are shown in figures 6.8(a) and 6.8(b). The CE algorithm used is the TD-LS RR described in section 4.1.2.

It can be observed that the simplified method does not yield an appreciable estimate accuracy degradation compared to the generalized fitting method and $m = 10$ observations, so the other simulations shown in the present section were obtained using the simplified method and $m = 1$.

Doppler speed estimation simulations have been performed for v = 60, 120 and 200 km/h, for 400B packets with QPSK modulation, code rate 1/2 and for 2000B packets with 16-QAM 1/2 and 64-QAM 3/4 and different SNR values: they are reported in Figures 6.9 to 6.13. The considered algorithm shows a reliable speed estimate after a few tenths of packets, the actual value depending on the considered modulation order and code rate set (MCS). The results show that the speed estimator based on the hybrid method is reliable at low and high SNR (12-30dB), thanks to the correction factor of the autocorrelation estimator related to the TD-LS CE error, as described in section 4.1.2.

Similar results have been obtained using modified rr-LS CE presented in section 4.1.3; Doppler speed estimation simulations have been performed for v = 60, 120 and 200 km/h, for 400B and 2000B 16-QAM packets with code rate 1/2 and for 400B 64-QAM 3/4 packets.; they are shown in figures 6.14 to 6.16.

As shown in simulations, a reliable speed estimate can be obtained after an estimation time of about $5 \div 10$ ms. Such a convergence time can be considered suitable for vehicular environment where a high-performance car has a maximum acceleration of 10 m/s^2, i.e. has a speed variation of 10 km/h in about 0.3 s.

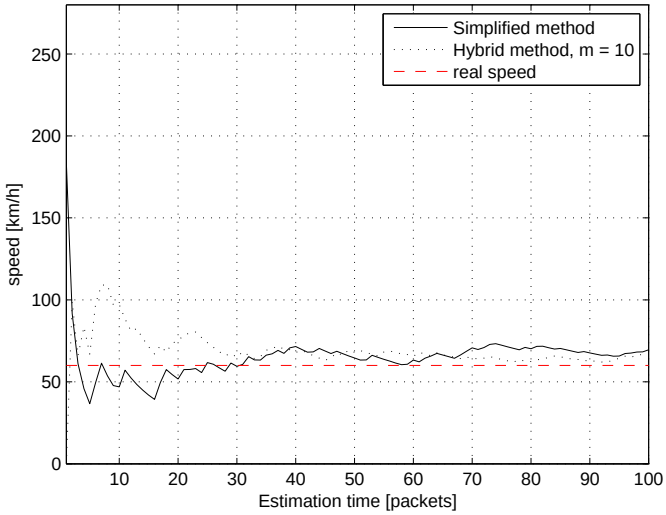

(a) v = 60 km/h

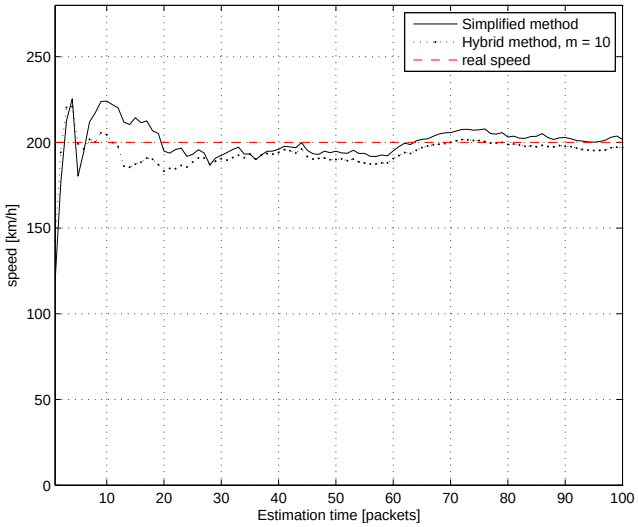

(b) v = 200 km/h

Figure 6.8: Estimated speed with Hybrid and simplified methods

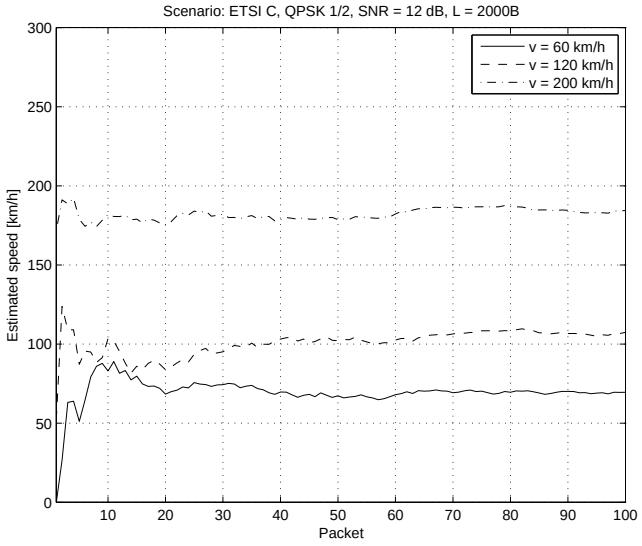

Figure 6.9: Estimated speed, QPSK, L = 2000B, SNR = 12dB

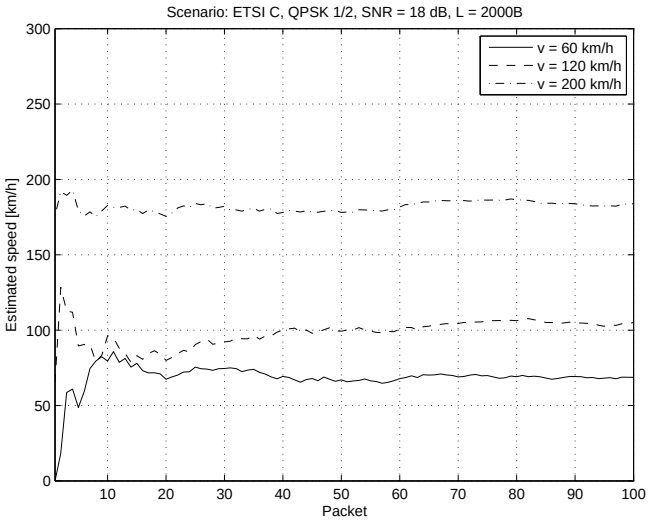

Figure 6.10: Estimated speed, QPSK, L = 2000B, SNR = 18dB

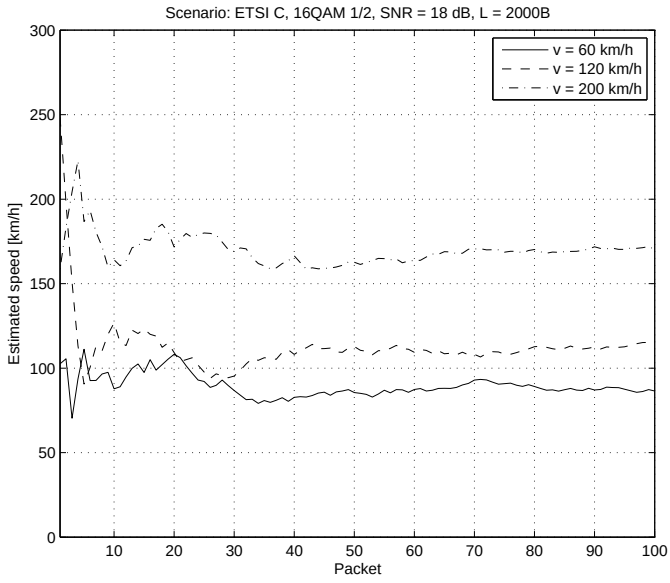

Figure 6.11: Estimated speed, 16-QAM, L = 2000B, SNR = 18dB

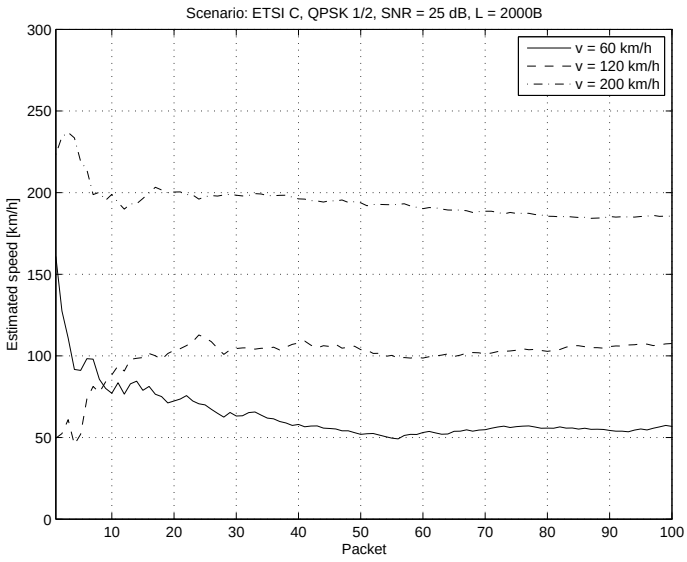

Figure 6.12: Estimated speed, ETSI C, QPSK, L = 2000B, SNR = 25dB

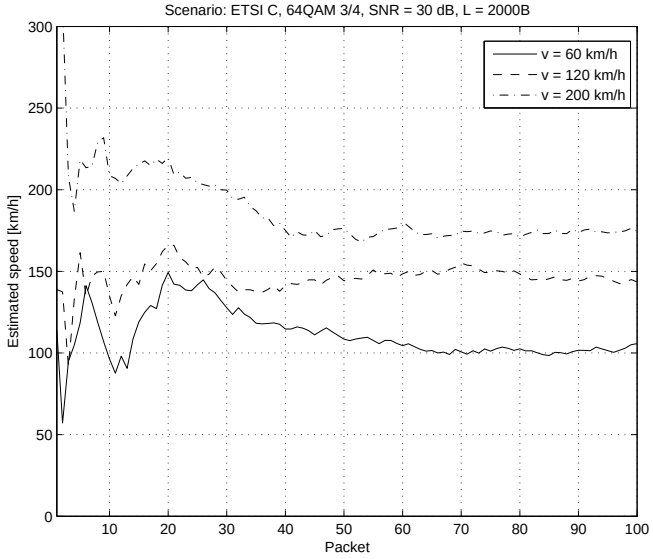

Figure 6.13: Estimated speed. ETSI C, 64-QAM, L = 2000B, SNR = 30dB

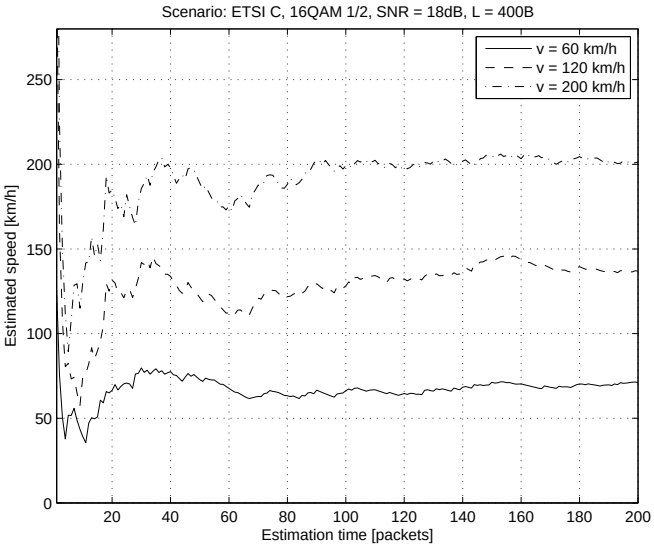

Figure 6.14: Estimated speed. ETSI C, 16-QAM 1/2, L = 400B, SNR = 18dB

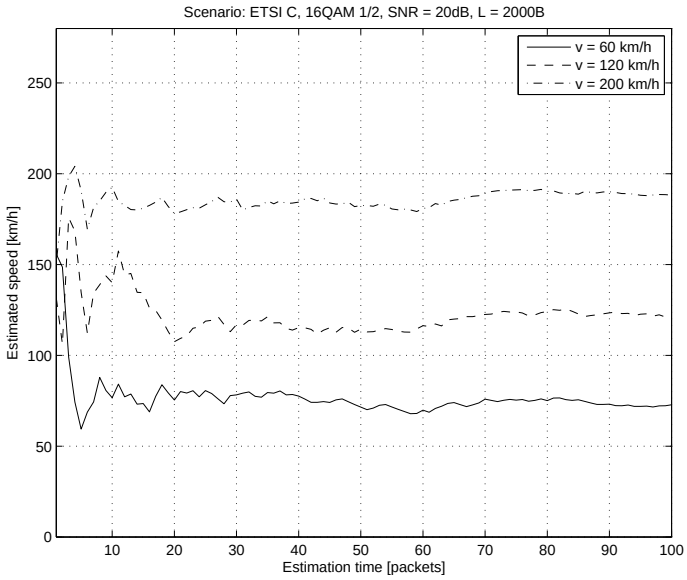

Figure 6.15: Estimated speed. ETSI C, 16-QAM 1/2, L = 2000B, SNR = 20dB

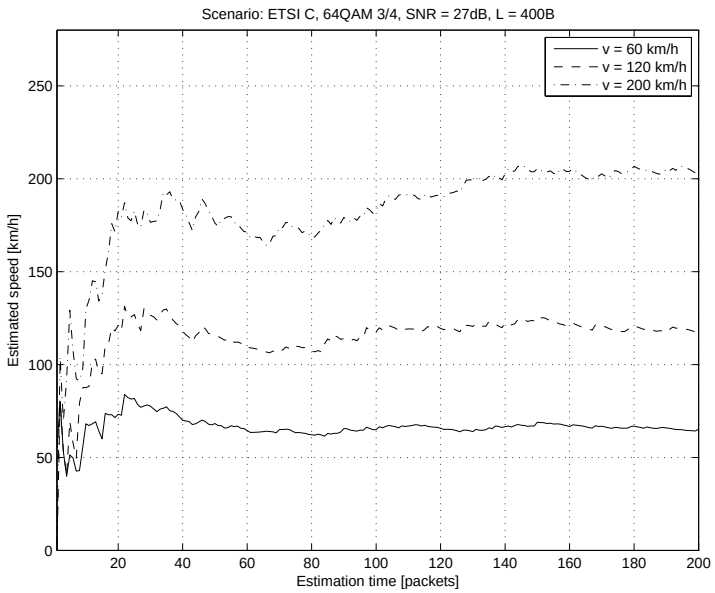

Figure 6.16: Estimated speed. ETSI C, 64-QAM 3/4, L = 400B, SNR = 27dB

6.2.2 Doppler spread estimation based on ZCR measurement

The second Doppler spread estimator evaluated is based on the estimation of the zero crossing rate (ZCR) of the channel taps [28]; the ZCR of a differentiable stationary random process is the average number of zero-crossing event in the unitary time. Being $S(f)$ the Power Spectral density of the process, the ZCR η in the unitary time results [28]:

$$\eta^2 = \frac{-r''(0)}{\pi^2 r(0)} = \frac{\int_{-\infty}^{+\infty} \omega^2 S(\omega) d\omega}{\pi^2 \int_{-\infty}^{+\infty} S(\omega) d\omega} \tag{6.33}$$

where $r(\Delta\tau)$ is the autocorrelation function of the process evaluated for a delay $\Delta\tau$. Applying the Classical Jakes spectrum model defined in (1.11) to the equation 6.33, it results:

$$\eta^2 = 2f_D^2. \tag{6.34}$$

The presence of noise in the process reflects in a bias estimate of f_D when inverting (6.34); in other words, as shown in chapter 4, the AWGN noise that introduces an estimation error in the channel estimate, causes a bias estimate of f_D. The authors in [28] introduces a correcting factor to take into account the influence of the noise in the channel estimate; the unbiased estimate results:

$$I_D^{(2)} = \eta^2\pi^2 - \frac{I_N^{(2)} - \eta^2\pi^2 I_N^{(0)}}{2\text{SNR}} \tag{6.35}$$

where SNR is the signal-to-noise ratio seen by the channel impulse response and the terms $I_N^{(0)}$ and $I_N^{(2)}$ are defined as:

$$I_N^{(n)} = \int_{-\infty}^{+\infty} \omega^n |H(\omega)|^2 d\omega, \tag{6.36}$$

being $H(\omega)$ the low-pass filter transfer function of the receiver equipment. The relation between $I_D^{(2)}$ and the estimated Doppler Spread is $\hat{f}_D$:

$$\hat{f}_D = \frac{1}{\pi}\sqrt{\frac{1}{2} I_D^{(2)}}. \tag{6.37}$$

Speed [km/h]	Doppler spread f_D [Hz]	ZCR η	ZCR in the OFDM symbol time (ηT)
60	327	231	0.0018
120	655	463	0.0037
200	1092	772	0.0061

Table 6.2: Theoretical ZCR in absence of noise

From equation (6.34) the ZCR in absence of noise can be estimated for given Doppler frequencies, as reported in table 6.2. It should be recalled that the Doppler Spread is $f_D = f_c v/c$ with carrier frequency $f_c = 5.9$ GHz and the symbol time T is $T = 8\mu s$.

From table 6.2 it can be noted the mean time expected to see a minimum amount of zero-crossing events necessary to achieve a reliable ZCR estimation. For example the mean number of OFDM symbols expected to see 20 zero-crossing events at $v = 60$ km/h is $N = 5550$, that corresponds to $\simeq$ 70 16-QAM 1/2 $L = 2000B$ packets. This example clarifies that the convergence time of the ZCR method is significantly larger than the hybrid method above described, as confirmed by the simulations results reported in 6.17 to 6.19 and obtained by measuring the actual ZCR of the estimated channel taps (given in practice by the number of times the sign changes from positive to negative) for a single channel realization with its time evolution given by the Doppler effect. It should also be noted that the estimator accuracy is highly susceptible to noise, as shown in 6.19 where the behavior is comparable to the plots obtained with the hybrid autocorrelation based method but with a high SNR such as 40 dB.

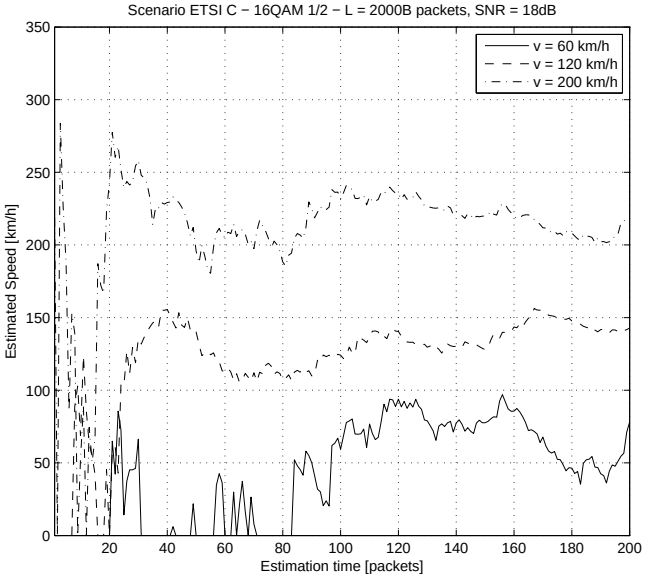

Figure 6.17: Estimated speed. ETSI C, 16-QAM 1/2, L = 2000B

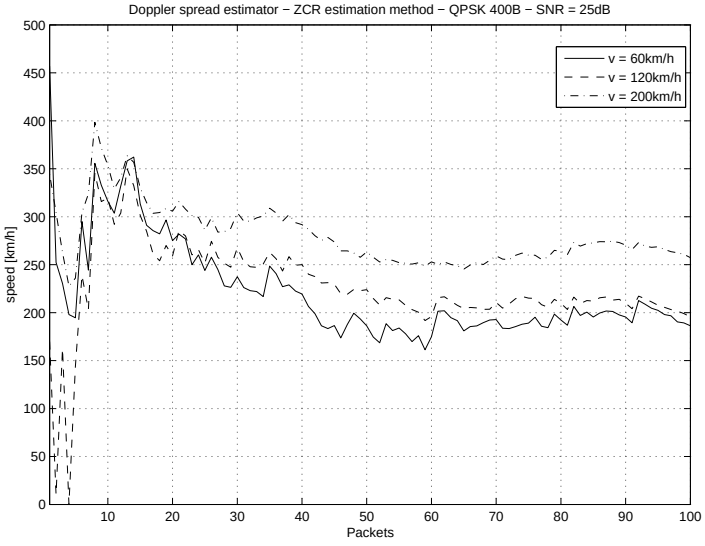

Figure 6.18: Estimated speed. ETSI C, QPSK 1/2, L = 400B

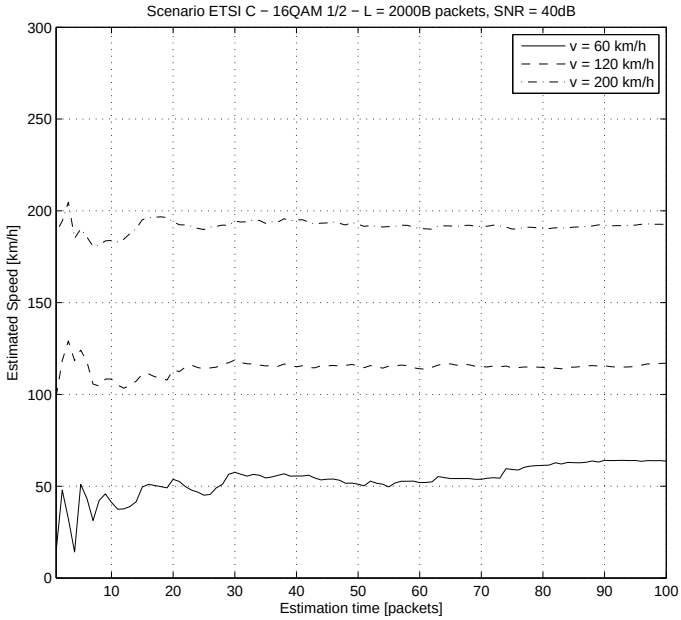

Figure 6.19: Estimated speed. ETSI C, 16-QAM 1/2, L = 2000B, SNR = 40dB

In conclusion, the ZCR based technique [28] performs worse than then the hybrid autocorrelation based estimator [29] regarding the Doppler spread estimation accuracy at low SNR and the required convergence speed, when applied to vehicular systems. The motivation is due to the characteristics of the system under focus and the related Doppler spread ranges (depending on the carrier frequency and the vehicle speed, as well known).

The only possible advantage of the ZCR estimator compared to the autocorrelation based one is represented by its lower complexity and lower amount of data to be processed, but this is not accompanied to an adequate estimation accuracy for vehicular system Doppler spread values.

6.3 Performance curves with variable CE occurrence

The procedure used to evaluate the effectiveness of the algorithm that estimates the Doppler spread for the considered system is the following:

1. Initially channel tracking is performed for every OFDM symbol with the TD-LS reduced-rank Viterbi FEC technique;

2. during a period of time equivalent to P (table 6.4) transmitted packets the Doppler estimator based on autocorrelation function performs the estimate and the Doppler spread measured at the end of this period is returned;

3. the relative speed is derived from the Doppler spread measured as $v = \frac{f_{Dc}}{f_c}$;

4. the CE period n is selected as proposed in table 6.3;

5. from packet $P + 1$ onwards, the CE is performed every n symbols.

From simulations on the estimated speed a minimum estimation period can be set to achieve a reliable estimated speed. In table 6.4 the selected number of packets P has been reported for the various scenarios in which the estimation speed is performed. The equivalent estimation time for the selected values of P is $\approx 5 \div 10$ ms. Simulations have been performed for QPSK 1/2 L = 400B, 16-QAM 1/2 L = 2000B and 64-QAM 3/4 L = 400 B packets.

length [*bytes*]	n_{symb} for QPSK 1/2	n_{symb} for 16-QAM 1/2	n_{symb} for 64-QAM 3/4
50	9	5	2
400	67	34	15
2000	334	167	75

Table 6.3: Correspondence between Packet length [bytes] and number of OFDM symbols

Modulation, code rate set	P
QPSK 1/2, L = 400 B	10
16-QAM 1/2, L = 2000 B	10
64-QAM 3/4, L = 400 B	40

Table 6.4: Estimation time P expressed in number of packets for the simulated scenarios

The PER vs. SNR results are reported in Figure 6.20 to 6.28. The results show that it is possible to limit the performance degradation within 1 dB (actually, even lower as a conservative lower bound has been considered for the design as previously described) compared to the case where CE tracking is performed once for every received OFDM symbol, by applying instead the occurrence values n reported in Table 6.1. As mentioned in the introduction, reducing CE occurrence may be useful in practical systems to reduce processing time/latency and/or receiver power consumption.

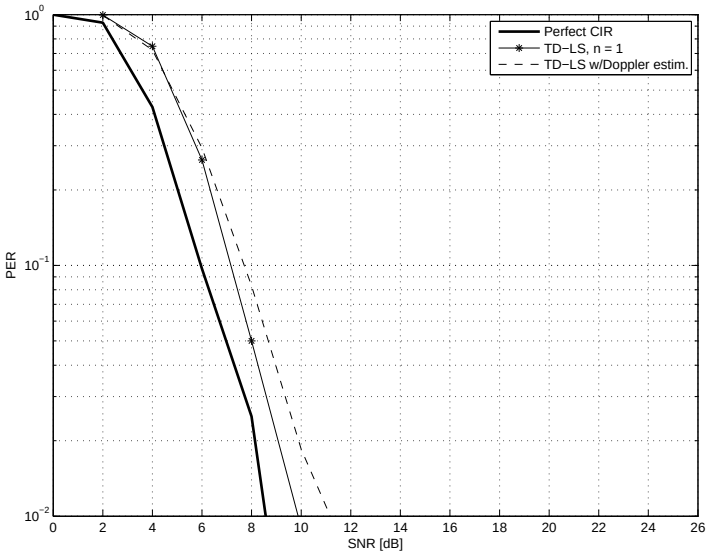

Figure 6.20: PER vs. SNR. QPSK 1/2, L=400B, v = 60 km/h, reduced CE occurrance

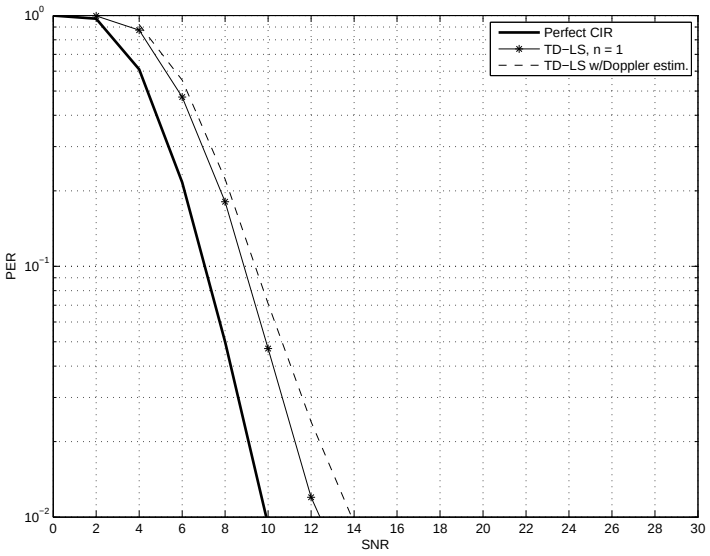

Figure 6.21: PER vs. SNR. QPSK 1/2, L=400B, v = 120 km/h, reduced CE occurrance

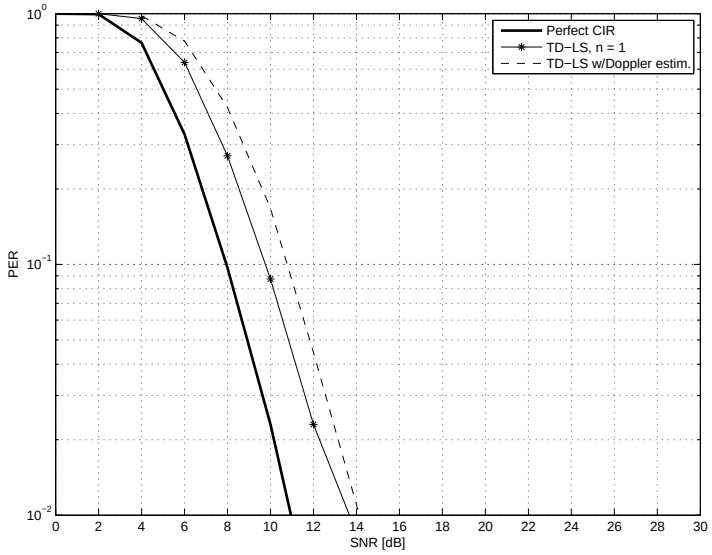

Figure 6.22: PER vs. SNR. QPSK 1/2, L=400B, v = 200 km/h, reduced CE occurrance

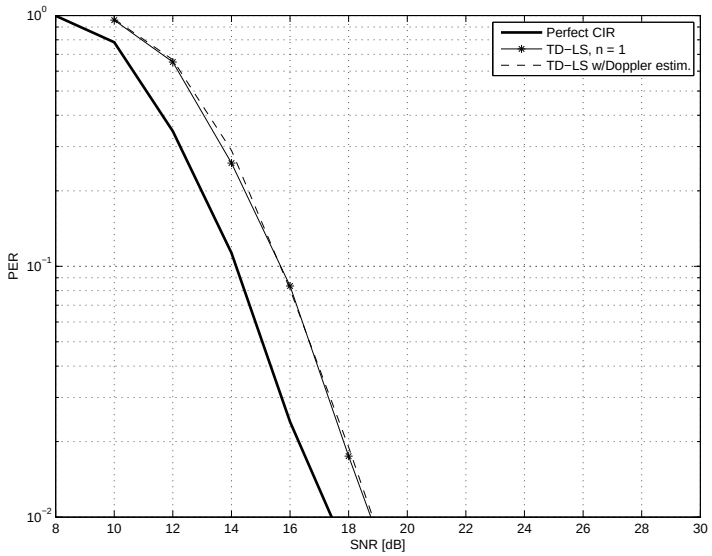

Figure 6.23: PER vs. SNR. 16-QAM 1/2, L=2000B, v = 60 km/h, reduced CE occurrance

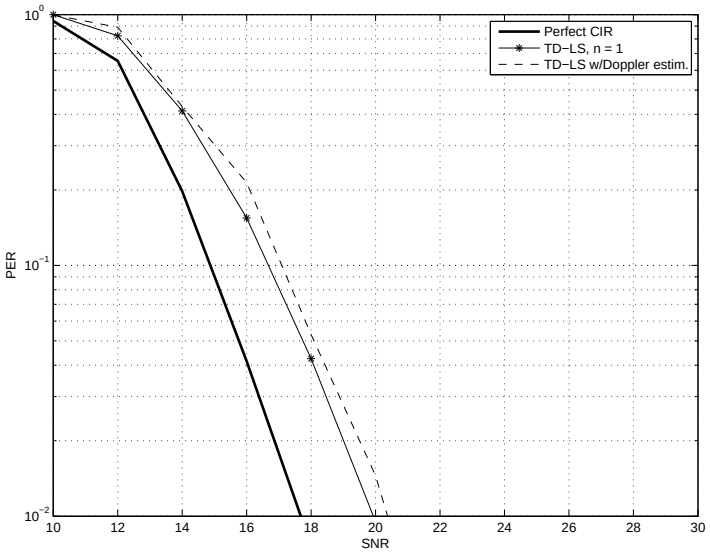

Figure 6.24: PER vs. SNR. 16-QAM 1/2, L=2000B, v = 120 km/h, reduced CE occurrance

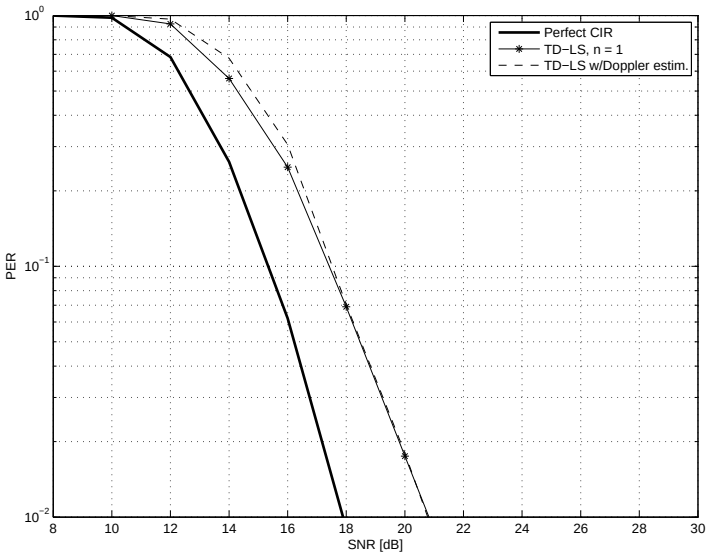

Figure 6.25: PER vs. SNR. 16-QAM 1/2, L=2000B, v = 200 km/h, reduced CE occurrance

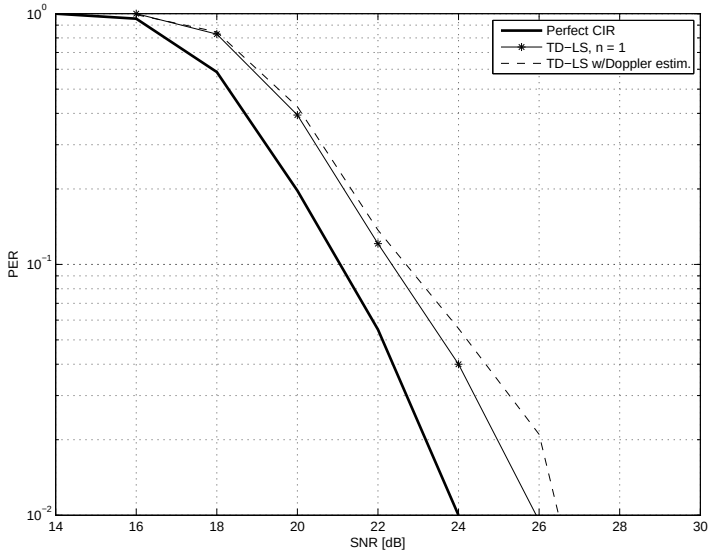

Figure 6.26: PER vs. SNR. 64-QAM 3/4, L=400B, v = 60 km/h, n reduced CE occurrance

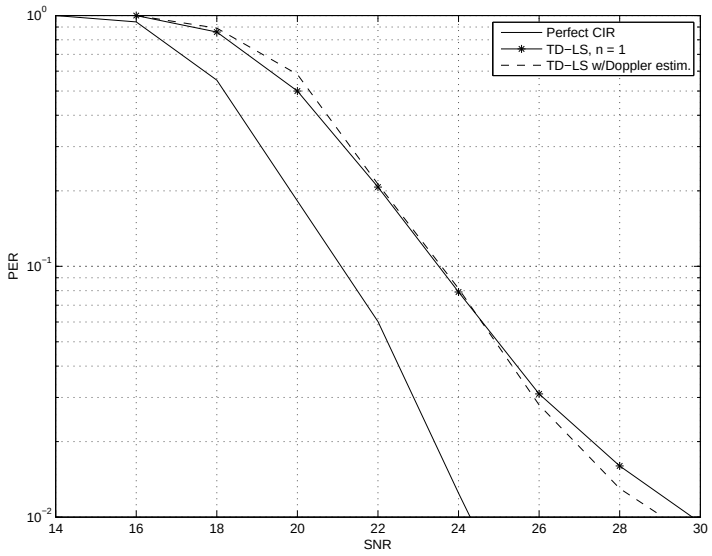

Figure 6.27: PER vs. SNR. 64-QAM 3/4, L=400B, v = 120 km/h, reduced CE occurrance

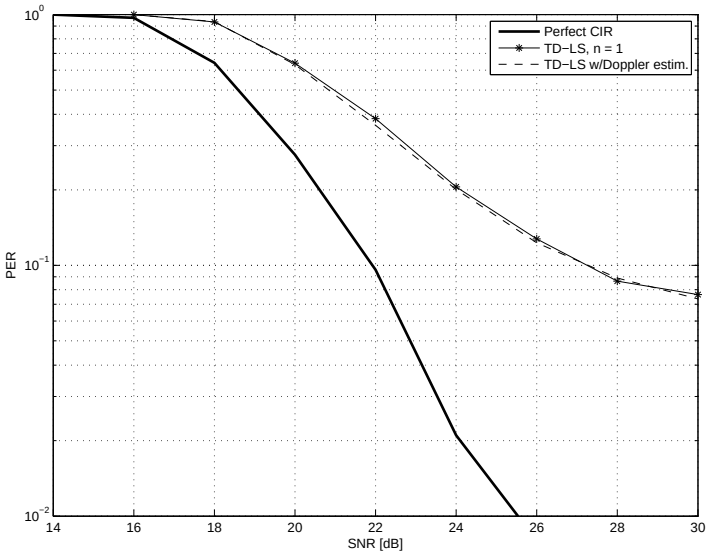

Figure 6.28: PER vs. SNR. 64-QAM 3/4, L=400B, v = 200 km/h, reduced CE occurrance

Chapter 7

Conclusions

In this thesis data decoding-aided channel estimation techniques for OFDM systems in vehicular environment have been studied. The wireless channel in vehicular environment exhibits a time-varying nature due to the relative speed between the transmitter and the receiver, known as Doppler effect. It has been shown that, for IEEE 802.11p systems, the initial channel estimation based on the standard preamble must be updated several times per WLAN packet (each one composed of many OFDM symbols) because of the degradation due to the Doppler effect.

Two different data-decoding aided CE schemes have been proposed:

- an *iterative* Viterbi decoding-aided DD-CE scheme, that make use of the Viterbi decoder to decode the received symbols and reconstruct the transmitter symbols that are used to perform the CE. After the CE has been updated the received data are equalized for a second and final time using the updated CE and finally decoded.

- a *non-iterative* Viterbi decoding-aided DD-CE scheme that is characterized by lower complexity and latency compared to the iterative scheme: the decoded bit stream are used at the same time for both the CE task and as final output bit stream. It results that the Viterbi decoder, that is a very computationally intensive block, is used only once per received symbol.

Simulation results show that the two presented schemes have almost the same performance in most scenarios, and that both are able to track the channel very efficiently for most considered channel and mobility scenarios, as shown by the comparison with the ideally known channel for every received OFDM symbol.

Despite that, two further improvements to the investigated channel tracking algorithms have been evaluated. The first, was motivated by the performance gap still observable compared to the ideal case for very challenging scenarios like high relative speed ($\geq$ 120 Km/h), long WLAN packets ($\geq$ 400 byte), high modulation orders (64-QAM). Linear prediction of the channel estimate has been considered in order to provide a delay-free channel estimation to the equalization instance of the OFDM symbol under focus: the MMSE linear prediction has been analyzed as a term of comparison for the other sub-optimal predictors, being the MMSE predictor practically unfeasible for the considered system due to the high computational requirements and the always increasing memory requirements. The performance gain achievable with the AR(2) predictor has been demonstrated compared to the scheme without predictor and to the scheme featuring an MMSE predictor.

As second improvement to the data decoding-aided DD-CE scheme, the selection of the CE occurrence as a function of the estimated relative speed between transmitter and receiver has been presented. This may be useful in practical portable systems to reduce processing time and/or power consumption. A strategy to select the CE occurrence based on the relative speed between transmitter and receiver and a maximum (set a-priori by the designer) tolerable degradation of the SNR seen at the receiver, due to the Doppler effect, has been presented.

This idea can applied if reliable relative speed estimates are available at the receiver. It could be objected that most vehicular connectivity systems are envisioned to include GPS (satellite global positioning systems) apparatuses that can provide speed information reliably. However, relative speed information is needed so the two terminals should exchange absolute speed information. Besides, the power consumption reduction target would likely be meaningful for portable devices, for which the GPS locator, if present, probably should not be always active. Therefore we deem that baseband techniques for Doppler spread estimation can be appealing for future vehicular connectivity systems. The above considerations motivated the assessment of the state-of-the-art Doppler spread estimation algorithms and their application to vehicular systems. Two different Doppler spread estimators have been analyzed and compared. The Doppler spread estimator based on the autocorrelation function estimation has proven to be the most suitable for IEEE 802.11p.

Finally, the PER vs. SNR simulation results with reduced CE occurrence based on the estimated Doppler spread obtained using the mentioned selected relative speed estimator, show that is possible to limit the SNR performance degradation

within a desired limit (for example, 1 dB) compared to the case where CE tracking is performed once for every received OFDM symbol, by reducing significantly the CE occurrence for a wide range of SNR values (in turn dependent on the estimated relative speed).

Bibliography

[1] N. Benvenuto, G. Cherubini, *Algorithms for Communications Systems and their Applications*, John Wiley & Sons, England, 2002.

[2] A. Goldsmith, *Wireless communications*, Cambridge University Press, 2005.

[3] IEEE P802.11p^{TM}/D9.0, "Part 11: Wireless LAN Medium Access Control (MAC) and Physical Layer (PHY) specifications", Amendment 7: Wireless Access in Vehicular Environments, Sep. 2009.

[4] IEEE 802.11a-1999 Standard, "Part 11: Wireless LAN Medium Access Control (MAC) and Physical Layer (PHY) Specifications: High-speed Physical Layer in the 5 GHz Ban", 1999.

[5] M. A. Ingram, G. Acosta, L. Dong, "Small-Scale Fading Models for the IEEE 802.11p (WAVE/DSRC) Standard", School of Electrical and Computer Engineering Georgia Institute of Technology Atlanta, Sep. 2006.

[6] J. Medbo, "Radio Wave Propagation Characterisitcs at 5 GHz with Modeling Suggestion for HIPERLAN/2", ETSI EP BRAN, Jan. 1998.

[7] J. Medbo, P. Schramm, "Channel Model for HIPERLAN/2 in Different Indoor Scenarios", ETSI EP BRAN, Mar. 1998.

[8] Y. G. Li and L. J. Crimini Jr., "Bounds on the interchannel interference of OFDM in time-varying impairments", IEEE Transactions on Communications, vol. 49, no. 3, Mar. 2001.

[9] L. Wei, C. Ming, S. Cheng, H. Wang, "A complexity reduced blind channel equalization scheme for OFDM systems", IEEE 17th International Symposium on Personal, Indoor and Mobile Radio Communications, 2006.

[10] R. Boloix-Tortosa, F. J. Simois-Tirado, J. J. Murillo-Fuentes, "Blind adaptive channel estimation for OFDM systems", IEEE 10th Workshop on Signal Processing Advances in Wireless Communications, Jun. 2009.

[11] W. Yang, Y. Cai, Y. Xun, "Semi-blind Channel Estimation for OFDM Systems", IEEE 63rd Vehicular Technology Conference, May 2006.

[12] E. G. Larsson, G. Liu, J. Li, G. B. Giannakis, "Joint Symbol Timing and Channel Estimate for OFDM Based WLANs," IEEE Commun. Letters, vol. 5, Aug. 2001.

[13] S. Ohno, G. B. Giannakis, "Optimal training and redundant precoding for block transmissions with application to wireless OFDM", IEEE Transactions on Communications, vol. 50, no. 12, Dec. 2002.

[14] M. Hsieh, C. Wei, "Channel estimation for OFDM systems based on comb-type pilot arrangement in frequency selective fading channels", IEEE Transactions on Consumer Electronics, Feb. 1998.

[15] E. Dall'Anese, A. Assalini, S. Pupolin, "On Reduced-rank Channel Estimation and Prediction for OFDM-based Systems", in Proc. WPMC '07, Jaipur, India, Dec. 2007.

[16] S. Kalyani, K. Giridhar, "Mitigation of Error Propagation in Decision Directed OFDM Channel Tracking Using Generalized M Estimators", IEEE Transactions on Signal Processing, vol. 55, no. 5, May 2007.

[17] M. Siti, A. Assalini, E. Dall'Anese, S. Pupolin, "Low Complexity Decision-Directed Channel Estimation based on a Reliable-Symbol Selection Strategy for OFDM Systems", To Appear: IEEE International Conference on Communications - Workshop on Vehicular Connectivity, May 2010.

[18] H. Abdulhamid, E. Abdel-Raheem and K.E. Tepe, "Channel estimation for 5.9 GHz dedicated short range communications receiver in wireless access vehicular environments", IET Communication, Dec. 2007.

[19] Q. Yuan, C. He, K. Ding, W. Bai, Z. Bu, "Channel Estimation and Equalization for OFDM System with Fast Fading Channels", IEEE 60th Vehicular Technology Conference, 2004.

[20] T. Kella, "Decision-Directed Channel Estimation for Supporting Higher Terminal Velocities in OFDM Based WLANs", IEEE Global Telecommunications Conference, 2003, GLOBECOM 2003.

[21] B. Ozbek, D. Le Ruyet, C. Panazio, "Pilot-Symbol-Aided iterative channel estimation for OFDM-based Systems", Conservatoire National des Arts et Métiers, Aug. 2005.

[22] L. Jarbot, "Combined decoding and channel estimation of OFDM Systems in Mobile Radio Networks", IEEE 47th Vehicular Technology Conference, May 1997.

[23] J. Wee, W. Jeon, Y. Lee, K. Kwon, Y. Cho, "Pilot and Data Aided Channel Estimation for OFDM systems in Rapidly Time-Varying Channels", IEEE 69th Vehicular Technology Conference, 2009. VTC Spring 2009.

[24] E. Dall'Anese, A. Assalini, S. Pupolin, "Enhanced multicarrier radio receiving method for Vehicular Mobile Wideband Channel", Internal report, Oct 2008.

[25] B. Moision, "A Truncation Depth Rule of thumb for Convolutional Codes", Information Theory and Applications Workshop, Jan. 2008.

[26] K. E. Baddour, N. C. Beaulieu, "Autoregressive modelling for Fading Channel simulation", IEEE Transaction on Communications, Jul. 2005.

[27] K. Han, S. Lee, J. Lim, K. Sung, "Channel Estimation for OFDM with Fast Fading Channels by Modified Kalman Filter", IEEE Trans. Consumer Electronics, May 2004.

[28] S. Valle, "Doppler spread measurements for tuning pilot-assisted channel estimation", Proceedings of the 3rd IEEE International Symposium on Signal Processing and Information Technology, 2003. ISSPIT 2003.

[29] O. Mauritz, "A Hybrid Method for Doppler Spread Estimation", VTC 2004-Spring. 2004 IEEE 59th Vehicular Technology Conference, 2004.

[30] L. Qiaoli, C. Wei, X. Tao, L. Biqi, "A Doppler Spread Estimator Design for Mobile OFDM Systems", ICCS 2008. 11th IEEE Singapore International Conference on Communication Systems, 2008.